VERIFICATION OF ESTIMATES OF WATER USE FROM RIVERINE VEGETATION ON THE SABIE RIVER IN THE KRUGER NATIONAL PARK

CS Everson • C Burger • BW Olbrich • MB Gush

WRC Report No 877/1/01

Water Research Commission

Disclaimer

This report emanates from a project financed by the Water Research Commission (WRC) and is approved for publication. Approval does not signify that the contents necessarily reflect the views and policies of the WRC or the members of the project steering committee, nor does mention of trade names or commercial products constitute endorsement or recommendation for use.

Vrywaring

Hierdie verslag spruit voort uit 'n navorsingsprojek wat deur die Waternavorsingskommissie (WNK) gefinansier is en goedgekeur is vir publikasie. Goedkeuring beteken nie noodwendig dat die inhoud die siening en beleid van die WNK of die lede van die projek-loodskomitee weerspieël nie, of dat melding van handelsname of -ware deur die WNK vir gebruik goedgekeur of aanbeveel word nie.

VERIFICATION OF ESTIMATES OF WATER USE FROM RIVERINE VEGETATION ON THE SABIE RIVER IN THE KRUGER NATIONAL PARK

PREPARED BY:
CS Everson; C Burger; BW Olbrich; MB Gush
Environmentek CSIR

Report to the Water Research Commission by the Division of Environmentek, CSIR

OCTOBER 2000

FRONT COVER PHOTO - REG GUSH

PREPARED BY:
CS Everson; C Burger; BW Olbrich; MB Gush
Environmentek CSIR
c/o Department of Agronomy, UNP, Pietermaritzburg, P/Bag X101, Scottsville,3209

Report to the Water Research Commission by the Division of Environmentek, CSIR

WRC REPORT NO : *877/1/01*

ISBN NO : *1 86845 781 8*

CONTENTS

EXECUTIVE SUMMARY

1. MOTIVATION

Expansion of agricultural and forestry activities in catchments west of the Kruger National Park are placing increasing demands on their limited water resources. One of the rivers that has been most affected is the ecologically important Sabie River. Reduced winter base-flows in the river have resulted in increased water stress levels amongst the natural river biota. Consequently, there is an urgent need to manage the water resources within the catchment effectively to ensure the viability of riverine ecosystems.

This report focuses mainly on one aspect of riverine hydrology - evapotranspiration. In many biological systems evapotranspiration is the most important output flux accounting for up to 100% of annual water losses in wetland systems (Linacre 1976). However, accurate estimates of evapotranspiration are notoriously difficult to obtain. Rivers running through semi-arid areas such as the Kruger National Park present a particularly difficult challenge for estimating evapotranspiration, because of the problems associated with advection from the surrounding dry (hotter) areas and the limited fetch within the generally narrow boundaries of the outer banks of the river. In addition, the riverine systems, range from open water or inundated areas, where evapotranspiration is not constrained by water availability, to those where the water table is frequently below the surface and water availability for evapotranspiration is controlled by vegetation factors. As a consequence the evapotranspiration results produced are often inconclusive or conflicting.

In a previous study conducted on the Sabie River (Birkhead *et al* 1997) preliminary estimates of the water use of the reeds and trees were established. Tree transpiration rates were found to be conservative ($\bar{x}$ = 2 mm day^{-1} in summer). By contrast the modelled rates for the reeds consistently averaged more than 15 mm day^{-1} and were considered unrealistically high. The results of the study require verification if water resources within the catchment are to be managed effectively. The aim of the present study was to verify the empirically based transpiration estimates of Birkhead *et. al.* (1997) by using the physically based Bowen ratio technique to estimate evapotranspiration from the Sabie river.

2. PROJECT OBJECTIVES

- To verify preliminary estimates of water use of the trees and reeds on the Sabie River in the Kruger National Park.
- To directly measure reliable, spatially averaged (10^3 to 10^4 m^2) evapotranspiration rates for the two major community types (reeds and forest) using micrometeorological techniques.
- To compare the magnitude of the fluxes both between sites and seasonally, their daily trends and controls and to assess the magnitude of the evaporative losses over a 50km riparian strip.
- To test simple, physically based evapotranspiration models with simple data requirements of value for longer term modelling of the water use of riparian vegetation along the Sabie River and other similar sites.

Although the absolute magnitudes of the results reported are directly relevant only to similar climatic and vegetation types, the processes and controls described may be representative of other major river systems within southern Africa.

3. BACKGROUND

The work for this project (phase II) arose as a direct recommendation from a previous project funded by the Water Research Commission (phase I), which investigated "Developing an Integrated approach to

Predicting the Water Use of Riparian Vegetation", by Birkhead AI, Olbrich BW, James CS & KH Rogers in 1997 (WRC Report No 474/1/97). These authors recommended that further measurements on the water use of reed beds be carried out as the original estimates were not satisfactory. Since reed beds are the dominant vegetation type in the Sabie River, over-estimation of evapotranspiration rates would result in unrealistic values when modelling water use in the Kruger Park. The present project was therefore initiated to determine independent estimates of evapotranspiration from a reed bed and forest community.

4. METHODS

The energy balance Bowen ratio technique was used to estimate evapotranspiration at the reed site. However, the technique could not be used in sites where the reed roots were permanently inundated with water because of insufficient fetch distance and difficulties in building towers.

Since the Bowen ratio technique also has limitations when used over tall tree canopies, the eddy covariance technique was used to measure the latent heat fluxes above the forest canopy.

The data collected from the sites were then substituted into the Penman Monteith equation to calculate actual total evapotranspiration (*ET*).

5. RESULTS

5.1 Reed evapotranspiration

Daily reed evapotranspiration rates (mm day^{-1}) measured during the study period included three summer seasons (1998, 1999 and 2000), two winter periods (1998 and 1999), and the spring of 1999. Strong seasonal trends were exhibited by these data, with mean monthly summer values varying between 4.5 and 7 mm day^{-1} during 1998 and 1999. Mean monthly values in January in 2000 were significantly lower as a result of the high incidence of rain during this year. Maximum evapotranspiration rates of 8-9 mm day^{-1} were often found between December and February. This contrasts with the 12 mm day^{-1} in February reported in the previous study using the dynagauge technique (WRC report 474/1/97).

Evapotranspiration rates from the reeds during the winter months of May and June were noticeably lower, but still averaged about 4 mm day^{-1} in 1999. Evapotranspiration from the reed beds in the Kruger National Park therefore ranged from 4 to 9 mm day^{-1} depending on the season.

As suspected in phase I (Birkhead et al. 1997), the modelled reed values of between 10 and 30 mm day^{-1} were unrealistic and not physically possible, since the values far exceeded the amount of available energy. The reed models developed in phase I should therefore not be used for calculating reed transpiration.

5.2 The use of infra red thermometry to estimate forest evapotranspiration

The use of the infrared technique to estimate evapotranspiration at the forest site was not satisfactory. The infrared data implied that all of the available energy was converted into sensible heat, a very unlikely result in this instance. The Bartholic-Namken-Wiegand method overestimated the equilibrium evaporation rate at all values above 300 Wm^{-2}. Because of the disappointing performance of this technique and the difficulty of routine measurements in the Kruger National Park, it was decided to investigate the technique at a site closer to Pietermaritzburg. The events of the flood, in which all the sensors and data loggers were lost, have prevented this.

5.3 Tree evapotranspiration using the eddy covariance technique

Diurnal evapotranspiration measured with the eddy covariance technique indicated that the tree canopy exhibited very low rates of transpiration during winter (approximately 0.6 mm day^{-1}). One of the problems with this technique is that approximately 200 W m^{-2} of energy are unaccounted for. This may be due to energy in tree trunk storage which was not measured in this study.

5.4 Tree evapotranspiration using the Bowen ratio technique

The results showed that trees transpire freely during winter (up to 2.57 mm day^{-1}), although the maximum rates are limited by the available energy. A striking feature of the summer evapotranspiration data was that the maximum daily rate seldom exceeded 4 mm day^{-1}. Unlike winter, most of the energy (500-700 Wm^{-2}) was utilized in the early morning to drive the evapotranspiration process. At mid-day this trend was reversed, when approximately 300-600 Wm^{-2} was partitioned into heating the air. The main differences between the summer and the winter energy balances were: (i) the magnitude of the fluxes and (ii) the time at which the partitioning between the latent and sensible flux changes from being predominantly latent heat to principally sensible heat.

There were no strong seasonal trends in the tree evapotranspiration data with winter values being similar to summer values. The mean daily evapotranspiration for the winter and summer was 2.62 and 2.23 mm respectively. The lower incidence of cloud cover and rain in winter resulted in the marginally higher evapotranspiration rate in winter. The results of this study were higher than those recorded in phase I (1 mm day^{-1} in winter).

Both studies have shown that the evapotranspiration from the tree community was surprisingly low, especially considering the high atmospheric demand experienced in the KNP and the freely available supply of water to the trees. A possible explanation is that the transpiration per unit leaf area declines in mature trees that have extensive flow paths from the roots through long branches to the leaves. The corollary, that young trees will have significantly higher water requirements, now has particular relevance, due to the removal of most of the mature forest during the February 2000 floods. The post flood succession of the riparian forest now offers a unique opportunity to investigate this hypothesis.

5.5 Comparison of trees and reeds

Comparisons of simultaneous evapotranspiration rates from the reeds and forest communities in the KNP showed that the daily water use of the reeds was consistently higher than in the forest community. During the study period the forest community used 36% less water that the reed community (2.5 mm day^{-1} versus 3.9 mm day^{-1} respectively).

6. MODELLING REED AND TREE EVAPOTRANSPIRATION

The estimates of actual evapotranspiration obtained in this study were used to develop canopy specific models of the Penman-Monteith equation that could be used for the reeds and trees. A very close agreement was found in the reed site between the measured (Bowen ratio evapotranspiration) and the simulated Penman-Monteith evapotranspiration in summer with totals of 176.7 mm and 178 mm respectively. Good relationships were also found between the autumn and spring Bowen ration evapotranspiration data and the Penman-Monteith estimates. However, a poor relationship was measured during winter, possibly due to the underestimation of the simulated net radiation and soil heat flux density.

7. LOW FLOW VERIFICATION STUDIES

The results of the vegetation cover analysis showed that the forests (38%) and reeds (22%) were the dominant vegetation types accounting for 60 % of the area. Open water, rock and sand accounted for a further 28%. These data were used to scale up the evapotranspiration data for a 55 km section of the Sabie between the Kruger and Lower Sabie weirs. Comparisons of the total evaporation losses during the low flow period attributed to vegetation (0.32 m^3 s^{-1})

and gauging losses (0.35 $m^3 s^{-1}$) showed good agreement, and added validity to the evapotranspiration data.

8. CONCLUSIONS

The main objective of the verification of previous transpiration measurements from reeds and trees in the Sabie River was achieved using the Bowen ratio energy balance technique. The results have shown that the previously high evapotranspiration rates attributed to reeds were unfounded. These reed evapotranspiration models should therefore not be used to model consumptive water use of the vegetation.

Evapotranspiration from the tree site was consistent with the previous research where conservative tree transpiration rates were found. However, the absolute daily evapotranspiration rates were higher in this study (3.2 mm day^{-1}) when compared with the previous study (1.7 mm day^{-1}).

Canopy specific models for the reeds and trees have been developed through an understanding of the energy balance of each community and its relationship to the well-known Penman-Monteith approach, providing a more accurate calculation of the water requirements of similar riparian vegetation in southern Africa.

Verification of the evapotranspiration estimates of this study was achieved by comparing the Bowen ratio estimates with transmission losses estimated through gauging studies. The gauging data were consistent with the evapotranspiration data collected in this project, confirming the validity of the evapotranspiration data.

9. EXTENT TO WHICH CONTRACT OBJECTIVES HAVE BEEN MET

Project Objective:

- *To verify preliminary estimates of water use of the trees and reeds on the Sabie River in the Kruger National Park.*

Verification of previous transpiration measurements from reeds and trees in the Sabie River was successfully achieved using the Bowen ratio energy balance technique.

- *To directly measure reliable, spatially averaged (10^3 -10^4 m^2) evapotranspiration rates for the two major community types (reeds and forest) using micrometeorological techniques.*

Good seasonal data were obtained from the reed site. Tree data were obtained only for the winter and spring periods. High river levels and the February 2000 floods prevented the collection of summer tree data.

- *Compare the magnitude of the fluxes both between sites and seasonally, their daily trends and controls and to assess the magnitude of the evaporative losses over a 50 km riparian strip.*

Low flow verification studies confirmed the spatially averaged estimates of the consumptive water use of the riparian vegetation along a 55 km stretch of the Sabie River.

- *To test simple, physically based evapotranspiration models with simple data requirements of value for longer term modelling of the water use of riparian vegetation along the Sabie River and other similar sites.*

In terms of modelling the latent heat flux in the Sabie River and other similar environments, either the Priestley-Taylor or Penman-Monteith methods yield the best results. The use of canopy and seasonal specific surface resistances and modelled available energy from relationships determined in this study, provides a model that yields excellent results yet is simple to use.

10. RECOMMENDATIONS FOR FURTHER RESEARCH

1. Further research is required on the physiological and physical processes that underlie the conservative water use of the forests growing along the Sabie River. This research should determine the extent to

which these conservative rates are applicable to other indigenous riparian systems in South Africa, since some hydrological models, such as ACRU, depend on a crop factor approach to determine the water use of different plant communities. The data from this project are inconsistent with popular beliefs that indigenous riparian communities are high water users. For example, the future development of the BLINKS riparian vegetation model is to encourage links with the ACRU model, so that meaningful hydrological scenarios can be used to predict the response of the riparian vegetation (Mackenzie et al 1999). This will be dependent on accurate predictions of the consumptive water use of the vegetation.

2. Both the phase I and II projects have highlighted the difficulties in obtaining routine measurements of evapotranspiration from mixed tree canopies in riverine situations. There is an urgent need to find a technique that will overcome these problems if progress is to be made in the area of evaporative research in riparian communities. Recent investigations have demonstrated the potential use of scintillometry to measure spatially averaged sensible heat fluxes over path lengths that range from 50 m to several kilometres. A scintillometer measures the intensity fluctuations of visible or infrared radiation after propagation over the plant canopy of interest. In contrast to local measurements, scintillometers provide path-averaged results. The temporal resolution achievable is one order of magnitude higher than that of point measurements. Due to the spatial averaging, extended experimental areas can be representatively characterised with a single instrument. Future research should test the feasibility of using this technique in riverine areas.

3. For practical reasons the reed measurements of this project were carried out on communities growing on elevated sand banks. There is still a need to characterise the evapotranspiration of permanently inundated reeds, which represent a large proportion of vegetation growing along the banks of South African rivers. Scintillometry would provide an alternative solution to the problems faced when working with conventional techniques. The use of infrared thermometry should also be investigated as a cheaper solution.

4. A possible reason suggested for the low consumptive water use of the trees is that the transpiration rate per unit of leaf area declines as a result of the extensive pathways water must follow from the roots through long branches to the leaves. The corollary, that young actively growing trees will have significantly higher water requirements, now has particular relevance, due to the removal of most of the mature forest during the February 2000 floods. The post flood succession of the riparian forest now offers a unique opportunity to investigate this hypothesis.

5. A major threat to the Sabie river ecosystem is through the replacement of indigenous vegetation by alien invasives. The manner in which these invasives invade the river ecosystem following the floods needs to be researched. A key question must be the impact that these fast growing and hence highly water efficient plants, must have on the delicate balance between the indigenous riparian plants and the soil and ground water reserves.

6. Water resources development and management require an understanding of basic hydrologic processes and simulation at the catchment scale (thousands to tens of thousands of square kilometres). Recent advances in computer hardware and software and GIS/spatial analysis software have allowed large area simulation to become feasible. The information on the evapotranspiration of the dominant indigenous vegetation collected in this study will ultimately provide modellers with important inputs and data for the verification of these models. It is recommended that a workshop be held (outside the scope of this project), on how to further interpret the research in terms of the "ecological reserve", by bringing all the results on the impact of the water use of vegetation together, and by developing a link to the operational management of rivers.

11. CAPACITY BUILDING

The research field of micrometeorology is currently in a crisis with very few new researchers entering the discipline. Mrs Jarmain (nee Burger) is the only new young female researcher to be recruited into this field in recent years. As the use of the open path eddy covariance represented a new research approach not used in South Africa before, it is clear that new capacity was imparted to both the junior and senior researchers. It must be recognised that neither previously disadvantaged students, nor other students are entering this field. Capacity building in the future must focus on attracting promising young scientists into hydrology and micrometeorology and building the skills that are needed for the research and management of South Africa's scarce water resources.

ACKNOWLEDGEMENTS

THE RESEARCH IN THIS PROJECT WAS FUNDED BY THE WATER RESEARCH COMMISSION, FOR WHOSE ASSISTANCE WE ARE SINCERELY GRATEFUL.

We wish to acknowledge valuable contributions made by members of the steering committee:

Mr DS van der Merwe	Water Research Commission (Chairman)
Dr SA Mitchell	Water Research Commission
Mrs CM Smit	Water Research Commission (Secretary)
Prof C. Breen	Institute for Natural Resources
Dr C. Brown	Southern Waters
Prof J O'Keeffe	Rhodes University
Dr H MacKay	Dept. of Water Affairs and Forestry
Prof KH Rogers	University of the Witwatersrand
Dr A Deacon	South African National Parks
Dr Harry Biggs	South African National Parks
Dr DF Scott	CSIR Environmentek

Our thanks are also extended to the staff of the South African National Parks at Skukuza, in particular Nick Zambatis, Harry Biggs, Andrew Deacon and Beukes Enslin for logistical support and Mr Samuel Nkuna, Parks Ranger, who braved many swollen streams to enable us to reach our equipment.

Technical support from David Mpanga was greatly appreciated.

LIST OF SYMBOLS

$\bar{x}$	Average evapotranspiration		mm/day
$\bar{w}$	Average vertical wind velocity		m s^{-1}
$\overline{\rho_a}$	Mean density of air		kgm^{-3}
$\bar{s}$	Mean entity per unit mass of the fluid		
β	Bowen ratio		Unitless
ρ	Density of air		kg m^{-3}
φ	Elevation angle of the sun		Degrees
θ	Kelvin temperature	273	K
ε	Ratio of the molecular mass of water to that of dry air		Unitless
λ	Specific latent heat of vaporization	2450	kJ kg^{-1}
γ	Thermodynamic psychrometer constant		kPa K^{-1}
Δ	Slope of the saturation water vapour pressure *vs.*		
γ^*	Apparent psychrometer constant		kPa K^{-1}
ρ_a	Density of air		kg m^{-3}
ρ_a'	Density of air departure from the mean		kg m^{-3}
λE	Latent heat flux density		W m^{-2}
δq	Measured specific humidity profile difference		kPa
Δq	Specific humidity difference		kPa
α_s	Crop reflection coefficient (albedo)		Unitless
δT	Measured air temperature profile difference		°C or K
ΔT	Temperature difference		°C or K
Δz	Difference in height		m
δz	Measured separation difference		m
A	Altitude		m
a_i	Calibration coefficients for the Li-6262		
BET	Bowen ratio evapotranspiration		mm
c	Intercept		
c_i	Regression coefficient		
C_p	Specific heat capacity of air at constant pressure		J kg^{-1} K^{-1}
C_s	Mole fractions for CO_2 or H_2O		µmol mol^{-1}
c_s	Speed of sound in air		ms^{-1}
c_w	Specific heat capacity of water		J kg^{-1} K^{-1}
d	Solar declination angle		Degrees
d	Zero plane displacement		m
de	True profile water vapour pressure difference		kPa
DOY	Day of year		Day
dT	True profile temperature difference		°C or K
e	Water vapour pressure of water in air		kPa
E	Water vapour flux		Wm^{-2}
e_a	Atmospheric water vapour pressure		kPa
	emittance at air temperature under clear skies		W m^{-2}
	emittance at air temperature		W m^{-2}
e_s	Saturated water vapour pressure		kPa

$e_s(T_a)$	Saturated vapour pressure at air temperature		kPa
$e_s(T_c)$	Saturated vapour pressure at canopy temperature		kPa
ET	Actual evapotranspiration		mm
ET_o	Potential or reference Penman-Monteith evapotranspiration		mm
F	Mean vertical flux		Wm^{-2}
g	Acceleration due to gravity		ms^{-1}
G	Soil heat flux density		$W\ m^{-2}$
G_s	Simulated soil heat flux density		$W\ m^{-2}$
Gsim	Simulated soil heat flux density		Wm^{-2}
H	Average canopy height		m
H	Sensible heat flux density		$W\ m^{-2}$
j	Day of year		Unitless
k	Von Karmans constant		0.41
k_h	Diffusivity coefficient for sensible heat transfer		$m^2\ s^{-1}$
k_v	Diffusivity coefficient for latent heat transfer		$m^2\ s^{-1}$
k_w	Diffusivity coefficient for latent heat transfer		$m^2\ s^{-1}$
l	Latitude at a site		Degrees
L	Longitude of site		Degrees
LAI	Leaf area index		
L_c	Longitude correction		Degrees
LE	Latent heat flux density		Wm^{-2}
L_{ni}	Atmospheric radiant emittance minus the crop		
L_{nic}	Atmospheric radiant emittance minus the crop under clear skies		
L_s	Longitude of the standard meridian		Degrees
m	Slope		
M_w	Molecular mass of water	0.18	$kg\ mol^{-1}$
P	Atmospheric pressure		kPa
PMET	Penman-Monteith evapotranspiration		mm
P_o	Sea level pressure		kPa
q	specific humidity		kPa
R	Universal gas constant	8.3143×10^{-3}	$kJ\ mol^{-1}\ K^{-1}$
r^2	Coefficient of determination		
r_a	Aerodynamic resistance		$s\ m^{-1}$
r_{ac}	Corrected aerodynamic resistance		ms^{-1}
r_c	Canopy resistance		$s\ m^{-1}$
R_n	Net irradiance		$W\ m^{-2}$
R_{ns}	Simulated net irradiance		$W\ m^{-2}$
R_o	Potential net irradiance		$W\ m^{-2}$
R_s	Solar irradiance		$W\ m^{-2}$
r_v	Combined canopy and aerodynamic resistance to water		sm^{-1}
s	Entity per unit mass of the fluid		
s'	Entity per unit mass of the fluid departure from the mean		
T	air temperature		°C
t	Clock time		h
t	Equation of time		day
T	Transpiration rate		ℓ/day
T_a	Air temperature		°C or K
T_{air}	Air temperature		°C

T_c	Canopy temperature	°C
To	Calibration temperature for the LI-6262	°C
t_o	Time of solar noon	h
u	Windspeed	m s^{-1}
u_z	Windspeed at height z	ms^{-1}
u_{zu}	Windspeed at height z_u	m s^{-1}
	vapour	s m^{-1}
V_c	Analogue signal from Li-6262 at 10 Hz for either CO_2 or H_2O	
VPD	Mean daytime vapour pressure deficit	kPa
w	Vertical wind velocity	ms^{-1}
w'	Vertical wind velocity departure from the mean	ms^{-1}
z	Vertical height interval	m
z_o	Roughness length	m
z_{oh}	Roughness length for heat and water vapour transfer	m
z_{om}	Roughness length for momentum transfer	m
z_{ps}	Relative phreatic surface elevation	m
z_t	Height of air temperature and humidity measurement	m
z_u	Height of windspeed measurement	m

1. INTRODUCTION

Increasing agricultural and forestry activities in catchments west of the Kruger National Park are placing increasing demands on their limited water resources. As a result the flow regimes of these eastward flowing rivers have been negatively affected and a number have changed from perennial to seasonal.

The historically perennial Sabie River has also been affected, and the reduced winter base-flows are resulting in increased stress levels amongst the natural river biota. Consequently, there is an urgent need to manage the water resources within the catchment effectively to ensure the viability of riverine ecosystems.

The Sabie River in the Kruger National Park is the focus of an integrated research thrust funded under the Kruger National Park Rivers Research Programme. This river was selected because of its ecological importance, and the potential impacts that further flow modifications could have on the riparian vegetation and related ecosystems.

This report focuses mainly on one aspect of riverine hydrology evapotranspiration. In many biological systems evapotranspiration is the most important output flux accounting for up to 100% of annual water losses in wetland systems (Linacre 1976). Accurate estimates of this flux are required for a variety of climatological, hydrological and ecological problems, yet are notoriously difficult to obtain. Rivers running through semi-arid areas present a particularly difficult challenge for estimating evapotranspiration, because of the problems associated with advection from the surrounding dry (hotter) areas and the limited fetch within the generally narrow boundaries of the outer banks of the river. In addition there are numerous possibilities for the structure of riverine systems, ranging from open water or inundated areas, where evaporation is not constrained by water availability, to those where the water table is frequently below the surface and water availability for evapotranspiration is controlled by vegetation factors. As a consequence the results produced are often inconclusive or conflicting (Unland *et al.* 1998).

In a previous study conducted on the Sabie River (Birkhead *et al.* 1997) preliminary estimates of the water use of the reeds and trees were established. The results of this study require verification as the tree transpiration rates were found to be conservative ($\bar{x}$ = 2 mm day^{-1} in summer). By contrast the modelled rates for the reeds consistently averaged more than 15 mm day^{-1} and were considered unrealistically high.

1.1 Project Objectives

> *The primary objective of this project was to verify preliminary estimates of water use of the trees and reeds on the Sabie River in the Kruger National Park.*

Secondary objectives were:

- To directly measure reliable, spatially averaged (10^3-10^4m^{-2}) evapotranspiration rates for the two major community types (reeds and forest) using micrometeorological techniques;
- To compare the magnitude of the fluxes both between sites and seasonally, their daily trends and controls and to assess the magnitude of the evaporative losses over a 50km riparian strip; and
- To test simple, physically based evapotranspiration models with simple data requirements of value for longer term modelling of the water use of riparian vegetation along the Sabie River and other similar sites.

Although the absolute magnitudes of the results reported are directly relevant only to similar climatic and vegetation types, the processes and controls described may be representative of other major river systems within southern Africa.

1.2 Background

The work for this project (phase II) arose as a direct recommendation from a previous project funded by the Water Research Commission, which investigated "Developing an Integrated approach to Predicting the Water Use of Riparian Vegetation", by Birkhead AI, Olbrich BW, James CS & Rogers KH in 1997 (WRC Report No 474/1/97). A précis of the executive summary of this report is given below for those not familiar with this report.

Seven major rivers rise west of the Kruger National Park (KNP) in catchment areas subjected to large-scale afforestation and increasing agricultural activity. This is causing a reduction in streamflow, and a number of rivers have changed from perennial to seasonal. Concerns for the impacts of these streamflow reductions on the ecological functioning of the riverine ecosystems within the Kruger National Park led to the formation of the multidisciplinary KNP Rivers Research Programme. The programme was initiated to establish the ecological water requirements of the rivers flowing through the KNP, so that they may be given due consideration in the planning and management of future resource developments (Birkhead *et al.* 1997). Because of the national importance of the Kruger National Park to biodiversity and tourism, and the international boundary with Mozambique, adequate water must be supplied to meet the evaporative demands of the riparian vegetation and for international obligations to South Africa's neighbours. With this in mind the specific objective of the initial project (phase I) was to

> *Develop the means to predict transpiration by riparian vegetation under different river flow and meteorological conditions for the Sabie River in the Kruger National Park.*

Three quantitative models were developed and integrated to describe the various components of the riparian water balance. The supply of water was addressed in a river hydraulics model describing surface flow in the river. Subsurface flow in the alluvial bank zone adjacent to the river and availability of soil water for transpiration was modelled in a bank storage dynamics model, and a transpiration model accounted for the consumptive water use by riparian vegetation. It is the improvement of the latter which is the focus of the present study.

The transpiration component of the riparian water balance was modelled empirically in order to develop a model whose input data requirements were easily satisfied. Thus, a simple regression modelling approach was used. As a result, two models were developed, one for riparian trees and the other for the abundant reed species, *Phragmites mauritianus*.

1.2.1 Transpiration by trees (Phase I)

The strategy used to model the transpiration by trees in phase I was to first concentrate data collection at a single site (Nerina) and a single species (*Ficus sycomorus*) over a two year period and compare its transpiration rates to other trees (*Berchemia zeyheri, Diospyros mespiliformis, Trichilia emetica* and *Spirostachys africana*) at the site during four intensive water use sampling surveys. Further research was also conducted to determine whether there were significant differences between the dominant riparian species in a survey of transpiration rates along the Sabie River. This survey also included the species *Combretum erythrophyllum, Acacia robusta, Breonadia salicina* and *Syzigium guineense*.

The species comparison revealed that there were no significant differences in transpiration between the various riparian tree species, suggesting that in the riparian habitat, the absolute transpiration rate depended more on tree size than the species concerned. Transpiration from the trees was found to be low, averaging only 2.3 mm day^{-1} in summer, and only 1.34 mm day^{-1} in winter. These conservative rates were attributed to the obstructed hydraulic architecture of the older trees. The generalised transpiration model developed for the *F. sycomorus* trees and *P. mauritianus* reeds is given by:

$$T = c_1 LAI + c_2 (1 - e^{-VPD}) + c_3 z_{ps} + c_4 \qquad (1.1)$$

Where

T	is the transpiration rate (litres day^{-1})
$c_1 \ldots c_4$	are the regression coefficients
LAI	is the leaf area index (unit less)
VPD	is the mean daytime vapour pressure deficit (kPa)
z_{ps}	is the relative phreatic surface elevation (m)

A good fit against observed tree transpiration data was obtained using this model (r^2=0.78). Although this model requires only one meteorological parameter (VPD), it does require LAI and phreatic surface level data, which are not easily obtainable.

1.2.2 Transpiration by reeds (Phase I)

Transpiration measurements from the reeds during phase I were made during three periods (one in wet summer season and two at the end of the dry season) ranging from 9 to 23 days in duration. During each survey 16 reeds were sampled using heat balance technology (dynagauge) (Birkhead *et al* 1997). The individual measurements were scaled-up using the leaf area index of the canopy. The absolute transpiration rates measured were high averaging 12 mm day^{-1} in summer and 7 mm day^{-1} in winter. Age class (young and mature) and seasonally (winter and summer) dependent regression coefficients were developed from the data for Equation 1. The modelled rates for the period January 1994 to June 1994 consistently averaged more than 15 mm day^{-1} (maximum of 24 mm day^{-1}) and were considered unrealistically high. A research recommendation arising from phase I was therefore for further measurements on the water use of reed beds, as the original estimates using the heat balance technique on individual reeds were not considered satisfactory. It was also suggested that the reed models be validated and verified, as reeds are the dominant vegetation type in the Sabie River. With this background, the present project was initiated, where a more integrative technique such as the Bowen ratio would be used to derive independent estimates of evapotranspiration from a reed bed community.

1.3 Definitions

Evaporation in this report is defined as "the physical process by which a liquid is transferred to the gaseous state." The evaporation of water into the atmosphere occurs from water bodies such as oceans, lakes and rivers, from soils, and from wet vegetation. Most water evaporated at leaf surfaces is water that has passed through the vascular system of the plant, exiting into the surrounding air, primarily through stomata. Evaporation of water that has passed through the plant is called transpiration. Direct evaporation from the soil and from plants occurs simultaneously in nature, and there is no easy way to distinguish the water vapour produced through the two processes. Therefore the term evapotranspiration is used to describe the total process of water transfer into the atmosphere from vegetated land surfaces. In this report the stem steady state heat balance and heat pulse velocity techniques only measure water passing through the plant (transpiration), whereas the Bowen ratio energy balance technique includes both plant and soil evaporation (i.e. evapotranspiration). Another concept widely used in the study of evaporation and evapotranspiration is that of potential evapotranspiration. Potential evapotranspiration is the evaporation from an extended surface of a short green crop that fully shades the ground, exerts little or negligible resistance to the flow of water, and is always well supplied with water. Potential evaporation cannot exceed open water evaporation under the same weather conditions. The preceding definitions are after Rosenberg *et al.* (1983).

2. THE STUDY SITES

The Sabie River has been identified as the most natural but imminently threatened perennial river flowing through the Kruger National Park (KNP) (Birkhead *et al.* 1997). The Sabie River drains a 7096 km^2 catchment in the Mpumalanga Province, South Africa and Mozambique. This river is characterised by a wide fringe of riparian vegetation colonising the riverbanks, where more than 130 indigenous species of trees and shrubs occur. This vegetation is important to the survival of the many animal species, which are dependant on this habitat for food and refuge. The viability of the riverine system is in turn dependent on sufficient water supply from the headwater catchments that are being severely impacted by changing land use. Winter base flows are supplied by the dolomitic aquifers in the mountainous areas in the west (Broadhurst *et al.* 1997).

2.1 The reed study site.

Reeds are one of the dominant vegetation types in the Sabie River system. The reed *Phragmites mauritianus* plays an important role in the river system by stabilizing interfluvial sand banks and providing fodder to elephants and buffalo.

The requirements of a suitable reed bed for the application of the Bowen ratio equipment were the following:

1. The reed community (*Phragmites mauritianus*) should be as extensive as possible to allow maximum 'fetch' for the equilibrium of water vapour over the canopy.
2. The reeds should be homogenous in extent and riparian in nature.
3. The site should be easily accessible.

During June 1997 an airborne survey of the reed beds was conducted along the Sabie River within the Kruger National Park. This survey showed that there were few suitable sites that met the above criteria. The site eventually selected was near the confluence of the Sand, Sabie and Muthlumuvi Rivers (Figure 2.1). The Bowen ratio system was sited in the centre of the reed community (Figure 2.2). The fetch at the site was generally in excess of 100 m metres in all directions. The site was situated on a sand bar about 1.5 m above the low flow level of the river. This site represents a mixed anastomosing channel type according to the classification of Heritage *et al.* 1995.

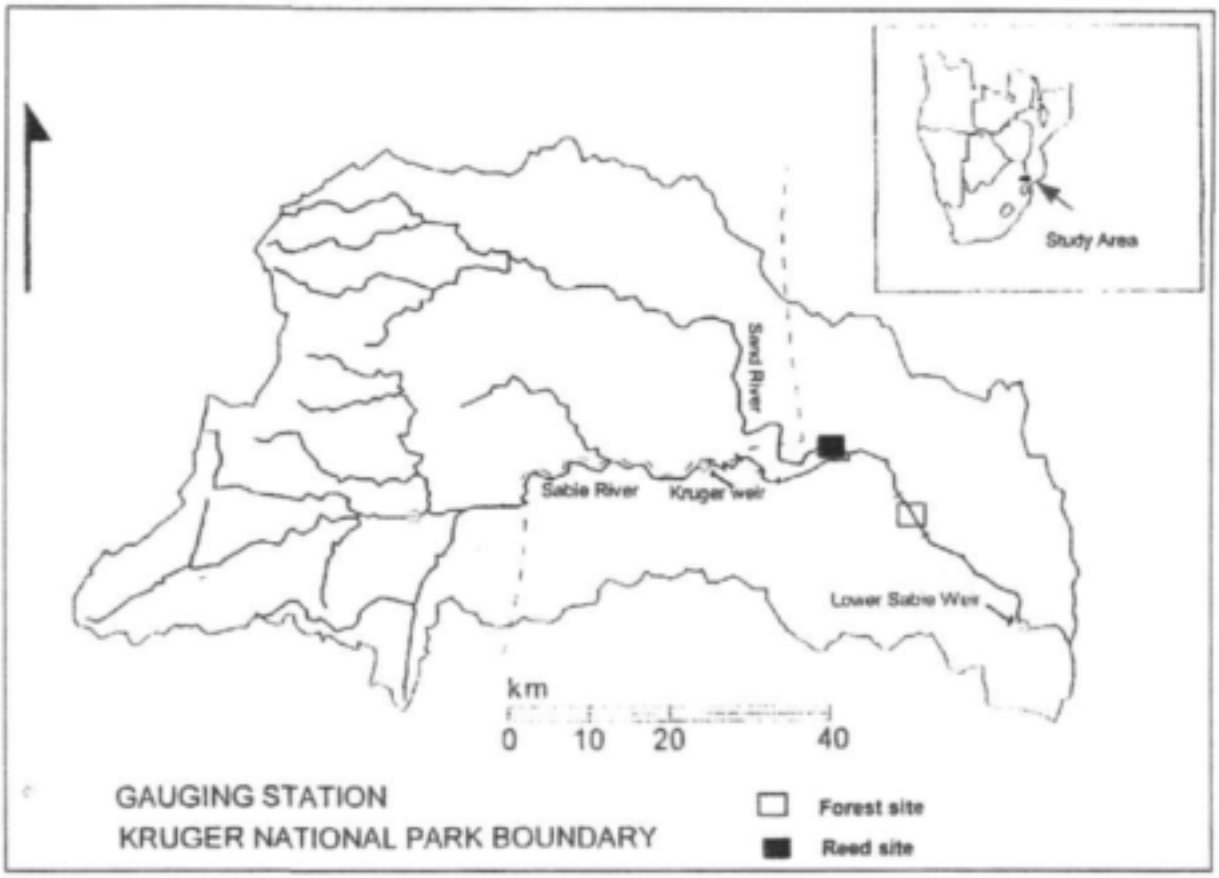

Figure 2.1: The location of the Reed and Forest study sites in the Kruger National Park

2.2 The tree study site

A broad patch of forest about 17 km downstream from Skukuza was selected for the tree evaporation study (Figure 2.3). The site was selected because of the good fetch conditions and accessibility from the road. The trees at the site were approximately 17 m high and the riparian tree, *Breonadia salicia* that establishes in bedrock cracks was common. Other large trees included *Nuxia oppostifolia, Ficus sycomorus, Combretum erythrophyllum,* while *Ziziphus mucronata* and *Dichrostachys cinerea* formed a dense shrub cover on channel banks beneath the open canopy tree layer (Figure 2.4).

Figure 2.2: The reed study site showing the extensive areas of *Phragmites mauritianus* during summer. The Muthlumuvi bridge can be seen in the background.

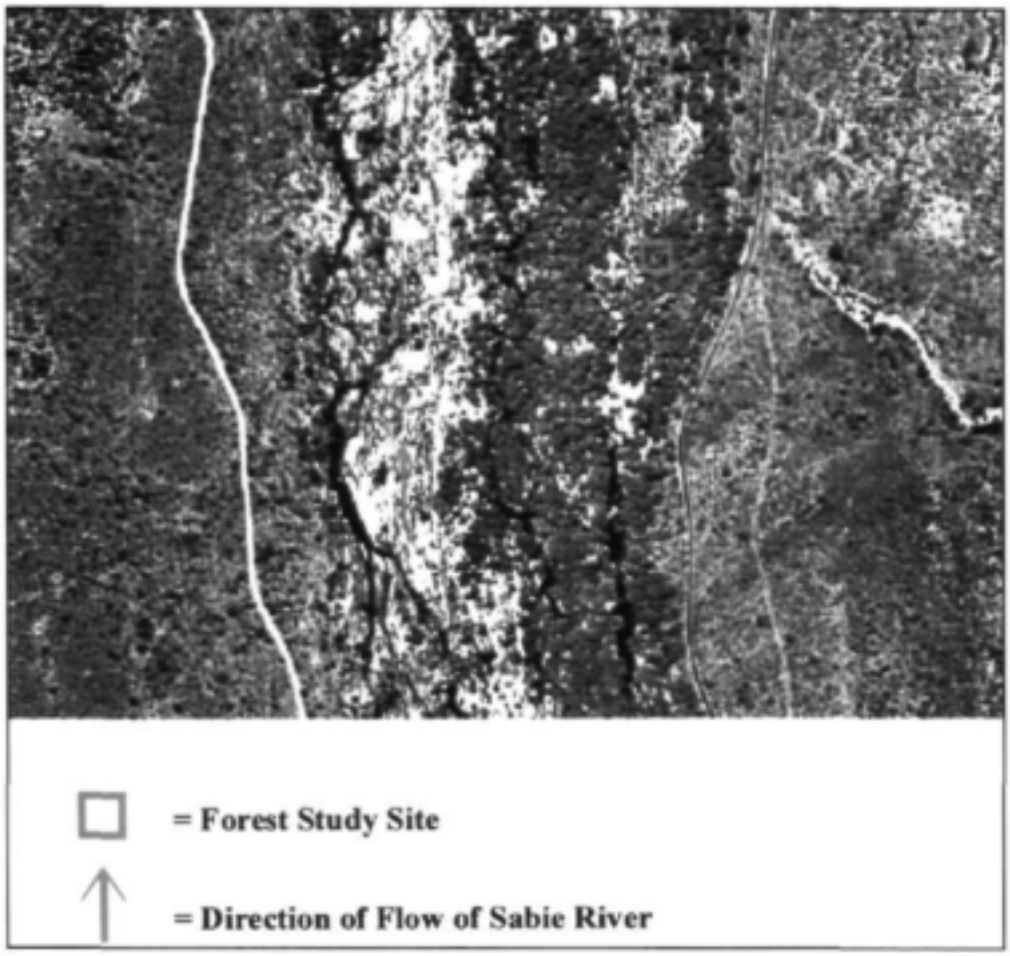

Figure 2.3: An aerial view of the typical forest at the tree site on the Sabie River in the Kruger National Park. Scale: 1 cm = approx 100 m

Figure 2.4: A view of the forest canopy from the tree tower

3. METHODS AND MATERIALS

3.1 Bowen ratio energy balance technique

3.1.1 Background and theory

The energy balance method requires knowledge of the factors contributing to the thermal balance at the evaporating surface. The energy balance equation may be written as:

$$R_n = H + \lambda E + G \quad \text{.......(3.1)}$$

where H is the sensible heat flux, E is the evaporation rate, λ is the latent heat of vaporization (J kg^{-1}), R_n is the net (all wave) radiation (Wm^{-2}), and G is the soil heat flux.

To permit the determination of evapotranspiration using Equation (3.1) the relationship established by Bowen (1926.), the Bowen ratio, β, can be used:

$$\beta = \frac{H}{\lambda E} \quad \text{.......(3.2)}$$

The Bowen ratio may also be expressed in terms of the temperature (T) and specific humidity (q) gradients where z is the vertical height interval:

$$\frac{\partial T}{\partial z} \quad and \quad \frac{\partial q}{\partial z}$$

Using appropriate transfer coefficients K_h and K_w:

$$\beta = \frac{H}{\lambda E} = \frac{\rho C_p K_h \frac{\partial T}{\partial z}}{\frac{\lambda \rho \varepsilon K_w}{P} \frac{\partial q}{\partial z}} = \gamma \frac{\Delta T}{\Delta q} \quad \text{.......(3.3)}$$

since K_h and K_w are assumed equal.

In general, K_h and K_w are not known. However, under specific conditions they can be assumed to be equal and the ratio of H to λE, is used to partition available energy at the surface into sensible and latent heat flux. Equation (3.3) shows that β values are derived from measuring differences (Δ) in air temperature and vapour pressure over the same vertical height interval (Δz) and the thermodynamic value of the psychrometric constant $\gamma = \frac{C_p P}{\lambda \varepsilon}$ where C_p is the specific heat of air at constant pressure.

From Equations (3.1) and (3.3) β and ($R_n - G$) values are used to compute the latent heat flux from:

$$\lambda E = \frac{(R_n - G)}{(1+\beta)} \qquad \text{(3.4)}$$

The sensible heat flux is calculated from:

$$H = (R_n - G)(1 + \beta) \qquad \text{(3.5)}$$

β can be estimated from Equation (3.3), by measuring the air temperature and vapour pressure gradients above the canopy.

3.1.2 Bowen ratio instrumentation

A diagrammatic representation of the Bowen ratio instrumentation is shown in Figure 3.1. A dewpoint hygrometer measured the dewpoint temperature (°C) of the air drawn into the system through inlet tubes situated at 0.5 m and 1.5 m above the reed canopy surface. The dewpoint temperature was used to estimate the vapour pressure (kPa) of the air (e_a).

The air temperature at 0.5 m and 1.5 m, and the air temperature difference between 0.5 and 1.5 m were measured using two bare type E-thermocouples, each with a parallel combination of 76 µm diameter thermocouples. This combination functioned even if one thermocouple was damaged.

Net radiation was measured with a Q*6 REBS net radiometer mounted 1.5m above the canopy surface. The heat flux into the soil (G) was measured with Middleton soil heat flux plates and soil averaging thermocouples.

Measurements of wind speed, wind direction, precipitation, air temperature, relative humidity and incoming solar radiation were recorded 2 m above the reed canopy surface.

The weather station instruments, linked to the CR21X, recorded the following measurements:

i) Rain using a Rimco tipping bucket raingauge (0.2 mm tip).
ii) Solar radiation measured with a Kipp solarimeter.
iii) Wind speed measured at a height of 2.0 m above the canopy with a Met-One cup anemometer.
iv) Wind direction using a Met-One wind direction sensor.
v) Temperature and relative humidity were measured with a PC207 temperature and humidity probe.

All sensors were averaged or totalled at 20-minute intervals. The entire system at the reed site is shown in Figure 3.2.

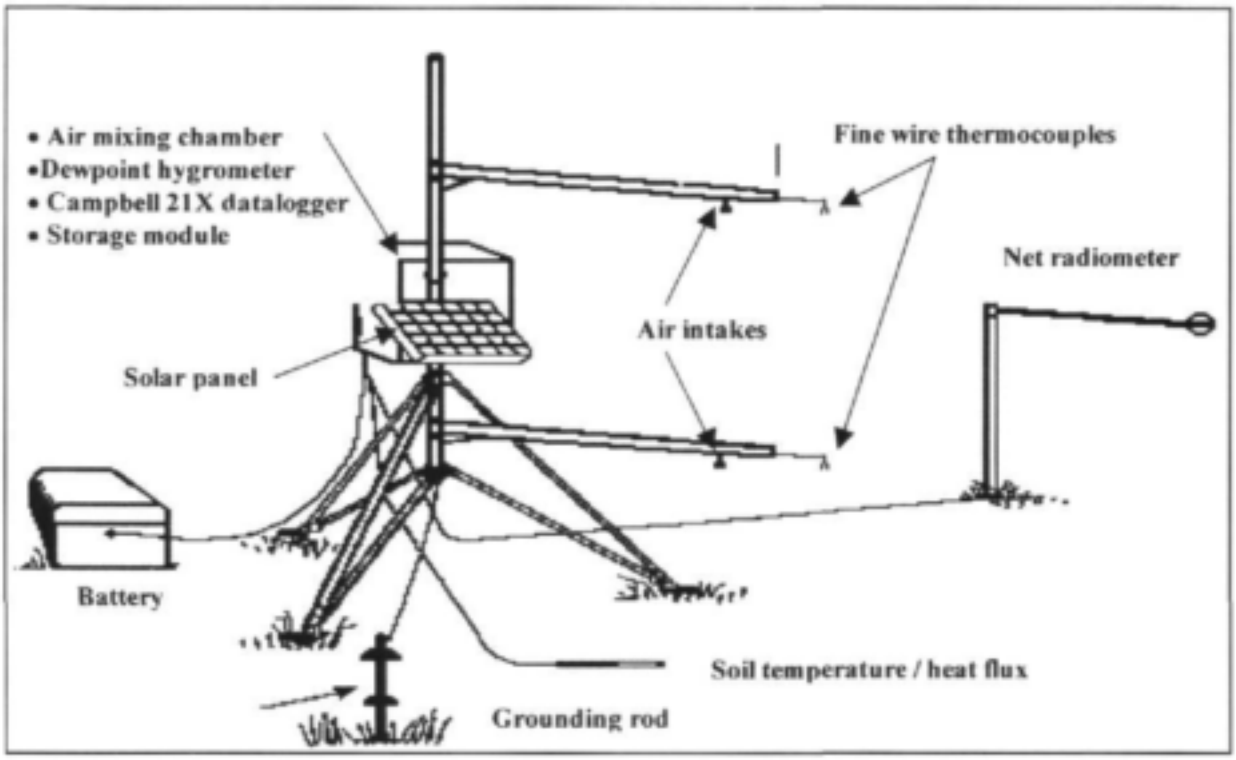

Figure 3.1: A diagrammatic representation of the Bowen ratio system

Figure 3.2: The Bowen ratio system and automatic weather station at the reed site in the Kruger National Park during summer.

3.1.3 Data processing

The Bowen ratio energy balance data collected were passed through an exacting set of data rejection criteria to test for their reliability. The primary exclusions being to ignore data when observations were beyond instrumental accuracy of the Bowen ratio system as a whole or the individual sensors involved in the system. Accordingly, observations of the Bowen ratio for which the absolute value of the vapour pressure and temperature difference between the two measurement levels de and dT, were less than 0.01 kPa and 0.006 °C respectively, were excluded, as were observations for which the Bowen ratio was close to -1, specifically for the range $|1+\beta| < 0.75$.

3.2 Eddy covariance technique

3.2.1 Introduction

The energy balance Bowen ratio technique has traditionally been used over uniform agricultural crops on homogeneous terrain. However, this method has limitations when used over tall tree canopies. The increased turbulence associated with these aerodynamically rough surfaces results in small temperature and vapour pressure gradients. As the resolution of current Bowen ratio energy balance systems is not sufficient to resolve these small differences, the separation distance between the sensors must be increased. This significantly increases the amount of fetch required.

With recent advances in the development of sonic anemometers, the eddy covariance technique (ECT) is rapidly becoming the standard for the measurement of energy and mass fluxes above vegetation. Flux measurements have been successfully carried out over many different canopy surfaces such as forests, grasslands, agricultural fields, oceans, and deserts. However, long term studies using the ECT raise special demands on the measuring system concerning durability, software reliability, data capacity and power requirements.

3.2.2 Theory

In fully turbulent flow the mean vertical flux F of an entity s per unit mass of the fluid is given by

$$F = \overline{\rho_a w s} \qquad (3.6)$$

where ρ_a is the density of air, w the vertical wind velocity, and the over bar denotes the average value during a time period of suitable length.

In the surface boundary layer all atmospheric entities exhibit short-period fluctuations about their mean value. Therefore, the instantaneous values of w, s, and ρ_a can be expressed by:

$$w = \overline{w} + w', \qquad s = \overline{s} + s', \qquad \rho_a = \overline{\rho_a} + \rho_a' \quad \text{.......... ....(3.7)}$$

where the prime symbol denotes an instantaneous departure from the mean. These expressions can be substituted into Equation (3.6) and if we neglect the very small fluctuations in density, the mean vertical flux F reduces to:

$$F = \overline{\rho_a w s} + \overline{\rho_a w' s'} \quad \text{......................................(3.8)}$$

or by writing ρ_a for $_a$

$$F = \rho_a \overline{w s} + \rho_a \overline{w' s'} \quad \text{...(3.9)}$$

The first term on the right-hand side of Equation (3.9) represents the flux due to the mean vertical flow or mass transfer. The second term represents flux due to eddying motion or eddy flux. The mass transfer term may arise from a convergence or divergence of air due to sloping surface. For a sufficiently long period of time over horizontally uniform terrain the total quantity of ascending air is approximately equal to the quantity descending and the mean value of the vertical velocity will be negligible. Therefore, Equation (3.9) reduces to

$$F \approx \rho_a \overline{w' s'} \quad \text{...(3.10)}$$

Based on the above equation, the sensible heat flux (H) and water vapour flux (E) can be expressed as:

$$H = \rho_a C_p \overline{w' T'} \quad \text{...(3.11)}$$

and

$$E = \frac{\varepsilon}{P} \rho_a \overline{w' e'_a} \quad \text{...(3.12)}$$

where w', T', and e_a' are the instantaneous departures from the mean horizontal velocity, air temperature and vapour pressure; and ε is the ratio of molecular weights of water vapour and air and P is the atmospheric pressure.

3.2.3 Eddy covariance instrumentation

Figure 3.3 is a schematic representation of the eddy covariance system and shows the main components of the instrumentation. Analogue signals from the infra-red gas analyser (IRGA) are passed to the 3-axis sonic anemometer which uses an analogue-to-digital converter to digitize the signals (at 10 Hz). The u, v and w components of the wind and the speed of sound (from which the sonic virtual temperature is derived) are available at a rate of 10 Hz at the serial output of the anemometer. The digitized signals from the IRGA are combined with the wind speed information and sent to the serial port of the data collection unit (DCU). Up to five analogue signals can be input into the DCU in this manner and combined with the turbulence data.

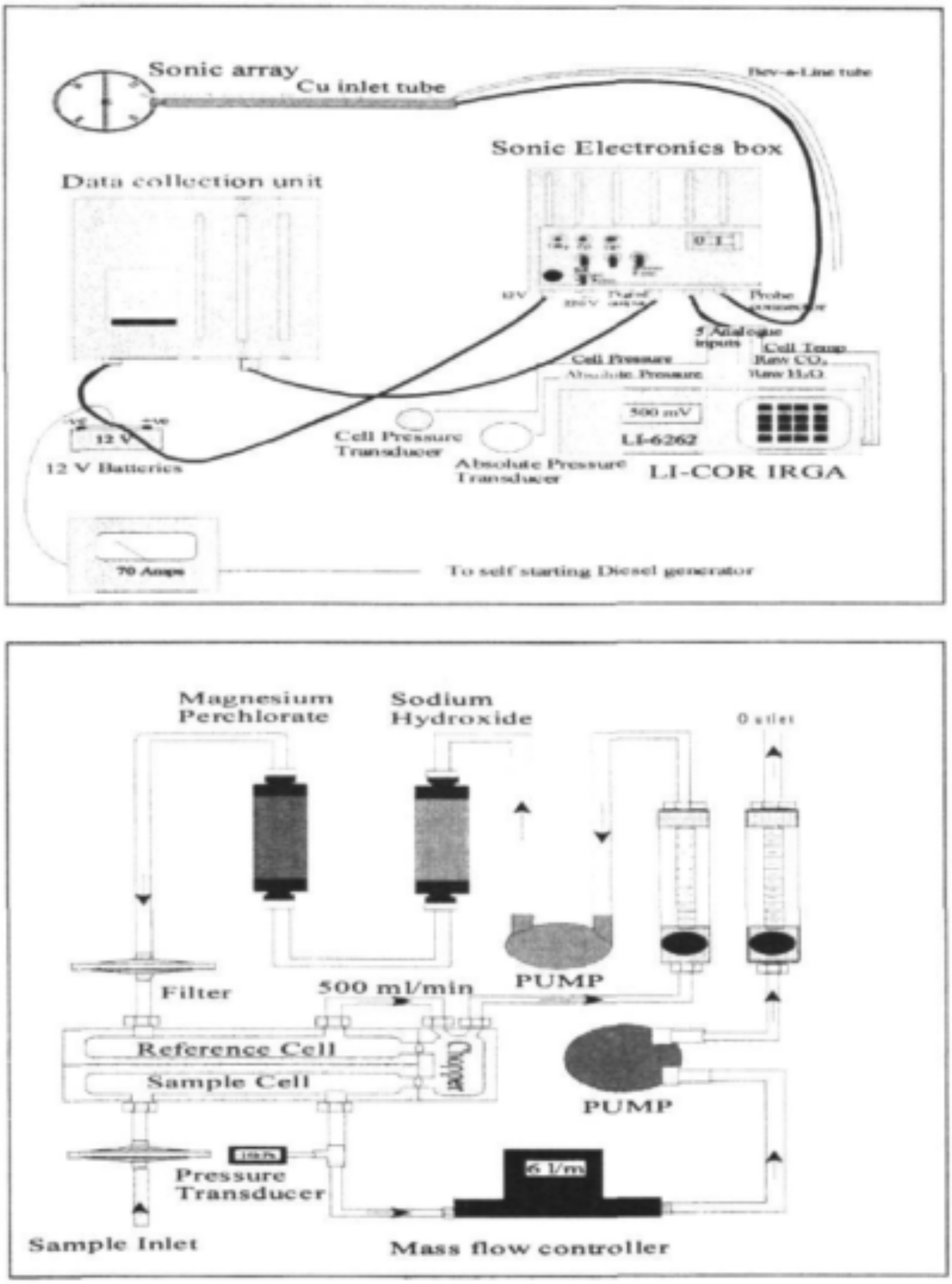

Figure 3.3: A diagrammatic representation of the major components of the eddy covariance system

3.2.3.1 Sonic anemometer

The speed of sampling for eddy covariance estimates is normally 10 Hz (i.e. 10 samples per second). For such rapid measurements conventional anemometers are unsuitable and the more recently developed sonic anemometers have become accepted as the standard instrument. In this study wind and temperature were measured with a 3-axis sonic anemometer (Applied Technologies, Boulder, Colorado) pointed into the prevailing wind direction. The instrument is waterproof and can operate in wind speeds up to 10 m s^{-1}. The instrument is based on the principal that sound travels faster from an emitter to a receiver in the direction of the wind and conversely more slowly against the wind. With three sets of emitters and receivers orientated in the x, y, and z directions, it is possible to determine simultaneously the three orthogonal components of the wind velocity.

One of the assumptions of the eddy covariance theory is that the wind sensors are mounted on a perfectly flat experimental site. However, in most practical situations such conditions do not exist. The influence of sensor tilt or terrain irregularities can contaminate the computation of the flux covariance by causing an apparent mean vertical velocity. This problem is overcome with the three-dimensional sonic anemometer, which rotates the co-ordinate system of the three wind velocity components, making the vertical, and lateral velocity components equal to zero.

This enables computation of the turbulent fluxes perpendicular to the streamlines. Generally it is adequate to perform only a two-dimensional rotation.

The virtual temperature is obtained from the transit time of the ultrasonic pulses (Kaimal and Businger, 1963; Kaimal and Gaynor, 1991) using the relation:

$$c_s = 403\ T_{air}\left(1+0.32\frac{e}{P}\right) \quad\text{...(3.13)}$$

where c_s is the speed of sound in air, T_{air} is absolute temperature, e is the vapour pressure of water in air and P is the absolute atmospheric pressure. A sonic temperature (T) is defined as

$$T = c_s^{\ 2} = T_{air}\left(1+0.32\frac{e}{P}\right) \quad\text{...(3.14)}$$

According to Stull (1988), the sonic temperature is close to the virtual temperature or potential temperature

$$\theta = T_{air}\left(1+0.38\frac{e}{P}\right) \quad\text{...(3.15)}$$

Using the sonic virtual temperature for the calculation of sensible heat flux will be adequate under most conditions.

3.2.3.2 Measurements of vapour pressure and CO_2 concentration

3.2.3.2.1 Infra red gas analysis

The concentrations of water vapour and CO_2 were measured by a LI-6262 infrared gas analyser (LI-COR, Lincoln Nebraska, USA). This is a differential analyser that compares the absorption of infrared light by water and CO_2 in two different chambers. Here the analyser was used in absolute mode, i.e. the reference chamber was purged of both water and CO_2. The quoted response time is 0.1s. This is the time taken for the analyser to respond to 95% of a one timestep change in gas concentration. However, a more useful indicator of the analysers response time is the cut-off frequency, i.e. the frequency at which the indicated amplitude of a sinusoidal oscillation in gas concentration is 0.707 of the real amplitude. This is 5 Hz for the LI-COR 6262.

The signals for the vapour pressure and CO_2 concentration can be output in a variety of units (analogue voltage, analogue current, or ASCII) by serial communication. However, for fast response (a requirement of the ECT) the raw signals for the carbon dioxide and water vapour mixing ratio had to be used. The mole fractions of water and carbon dioxide therefore had to be calculated in the developed software.

The following formulae were used to calculate the CO_2 and H_2O mole fractions (μmol mol^{-1}):

For H_2O $$C_S = \left[a_1\left(V_c\frac{P_o}{P}\right) + a_2\left(V_c\frac{P_o}{P}\right)^2 + a_3\left(V_c\frac{P_o}{P}\right)^3\right]\left(\frac{T+273}{T_o+273}\right) \quad (3.16)$$

For CO_2

$$C_s = \left[a_1\left(V_c\frac{P_o}{P}\right) + a_2\left(V_c\frac{P_o}{P}\right)^2 + a_3\left(V_c\frac{P_o}{P}\right)^3 + a_4\left(V_c\frac{P_o}{P}\right)^4 + a_5\left(V_c\frac{P_o}{P}\right)^5\right]\left(\frac{T+273}{T_o+273}\right) \quad (3.17)$$

where a_1, a_2 etc are the calibration coefficients for the LI-6262, V_c the analogue signal from LI-6262 at 10 Hz for either CO_2 or H_2O, P_0 standard pressure (101.3 kPa), P vacuum in the sample cell, T_0 calibration temperature for the LI-6262, and T is the Celsius temperature of the sample cell.

Flowing a known gas concentration through the analyser performed the calibration of carbon dioxide. Water vapour calibrations were performed using a Campbell Scientific 21X data logger and a General Eastern Dew Point Hygrometer. Zero points were established using magnesium perchlorate and soda lime to purge water and carbon dioxide respectively. This was done every morning prior to starting measurements. Calibrations were performed at the same flow rates as measurements so that pressure differences were maintained equal during both calibration and operation mode.

Figure 3.3 depicts the layout of the system with air being drawn through the analyser by having a pump at the end of the sampling line. The air was brought to the analyser through 1 m of copper tubing at the intake followed by a 10 m length of 6.5 mm OD Bev-a-Line tubing (high density polyethylene). The inner diameter of the tubing was 4 mm. The intake was placed as close as possible to the centre of the sonic, without disturbing the sonic signals. The air was sucked by a double diaphragm pump when run from the 12 V battery system. The flow rate of 6.0 ℓ min^{-1} was kept constant by a mass flow controller (Tylon General, Torrance CA). Due to the high flow rate, the vacuum created inside the cell of the analyser was about -16 kPa below atmospheric pressure and the concentration was automatically corrected using a pressure transducer at the inlet of the LI-6262. A second transducer monitored the ambient changes in atmospheric pressure. Tube configuration affects the flow rate, pressure drop and the lag time between the sonic and IRGA sensors. The effects of these on the measurements are discussed in the results section.

3.2.3.3 The power supply

The 12 V battery system enables experiments to be carried out at remote sites. Two 110 Ah batteries are charged by a self-starting Diesel generator. The system was designed to automatically start when the battery voltage drops to 11.9 V. A 70 Amp battery charger was able to recharge the batteries within 30 minutes. The generator automatically shuts off when the batteries are recharged (13 V). The generator was placed 50 m downwind from the system.

3.2.3.4 The data collection system

The Applied technologies data collection unit (DCU) is a system designed for a 386 SX computer operating at 25 MHZ. Its low power requirements and small size make it an ideal computer for high performance in a battery operated environment. Internal to the DCU is the data acquisition software. The raw and processed data are written to a 150 MB Bernoulli platter. Changes to the analogue gain and offset constants, running mean sample number, boom orientation and calibration coefficients for the gas analyser are accomplished by editing a setup file on the Bernoulli disk.

The software was designed for flux measurements and performed the following calculations in near real time:

- preset time averages such as 5 minutes, 30 minutes, etc.
- means of wind vectors
- variances of wind vector combinations
- standard deviation of wind direction
- vector averaged wind speed and wind direction.

If all the inputs are available, it can also calculate the following:

- mixing ratio
- water vapour pressure
- air density
- specific heat at constant pressure
- heat of vaporization
- friction velocity (relates to the effectiveness of turbulent exchange over the surface).
- vertical fluxes of sensible and latent heat.
- CO_2 flux.

To handle non-horizontal mean wind fields over inclined terrain, a 3-D coordinate rotation of the covariance matrix into the mean wind vector was applied to wind data.

For misaligned sensors a trend removal can be used to correct the turbulent fluxes. In practice, a running mean was removed from the data using a recursive digital filter with a user selectable time constant.

An example of the raw data for a one second interval and processed output data for a single half hour interval are shown in Tables 3.1 and 3.2. Both the raw and processed data are sent to the storage disk as binary outputs. The software then performs spectral analysis of the data. These binary data files are converted to ASCII data by running a programme back at the office.

Table 3.1:

One second of raw data output from the eddy covariance system. U, V, W are the three orthogonal wind components (m s^{-1}) and T, the virtual or sonic temperature (°C). The analogue inputs (0-4.095 Volts) are: (a) Raw carbon dioxide signal from LI-6262; (b) Raw water vapour signal from LI-6262; (c) LI-6262 signal for the sample cell temperature; (d) Input from absolute pressure sensor and (e) Input from vacuum pressure sensor

U-00.10	V-39.36	W-00.05	T 05.64	a 0912	b 1041	c 1111	d 0869	e 1490
U-00.08	V-39.39	W-00.10	T 05.60	a 0910	b 1042	c 1111	d 0869	e 1482
U-00.11	V-39.34	W-00.09	T 05.65	a 0910	b 1041	c 1109	d 0868	e 1479
U-00.12	V-39.32	W-00.06	T 05.64	a 0909	b 1041	c 1111	d 0870	e 1487
U-00.13	V-39.33	W-00.13	T 05.52	a 0908	b 1042	c 1111	d 0870	e 1472
U-00.13	V-39.30	W-00.18	T 05.55	a 0907	b 1042	c 1111	d 0869	e 1492
U-00.17	V-39.28	W-00.15	T 05.48	a 0908	b 1041	c 1110	d 0869	e 1476
U-00.18	V-39.25	W-00.07	T 05.55	a 0909	b 1040	c 1110	d 0869	e 1488
U-00.19	V-39.16	W-00.10	T 05.56	a 0909	b 1038	c 1111	d 0869	e 1487
U-00.17	V-39.08	W-00.11	T 05.57	a 0908	b 1037	c 1110	d 0868	e 1477

Table 3.2:

An example of a half hour period of the processed data from the Eddy covariance system

TABLE OF MEANS

Mean[U]	=	3.26089
Mean[V]	=	-0.36825
Mean[W]	=	-0.49929
Mean[T]	=	19.21950
Mean[Pc]	=	15.67710
Mean[VP]	=	0.57567
Mean[S]	=	3.64420
Mean[CO2]	=	178.98617
Mean[H2O]	=	6.57305
Mean[t]	=	24.26134
Mean[P]	=	87.58997

TABLE OF COVARIANCES

		Departure from Mean	Departure from Running Mean
CVAR[UU]	=	4.00561	4.03785
CVAR[UV]	=	-0.30586	-0.18980
CVAR[UW]	=	-1.28063	-0.82692
CVAR[UT]	=	-0.76320	-0.61847
CVAR[UPc]	=	0.04241	0.05223
CVAR[UVP]	=	-0.04137	-0.02961
CVAR[US]	=	3.76746	3.44261
CVAR[UCO2]	=	0.37670	0.69296
CVAR[UH2O]	=	-0.47664	-0.33497
CVAR[VV]	=	2.37043	2.19137
CVAR[VW]	=	0.24366	0.07112
CVAR[VT]	=	0.12330	0.06604
CVAR[VPc]	=	-0.00267	0.00414
CVAR[VVP]	=	0.00296	0.00096
CVAR[VS]	=	-0.53932	-0.54273
CVAR[VCO2]	=	-0.02888	0.09755
CVAR[VH2O]	=	0.03394	0.01281
CVAR[WW]	=	1.32565	0.99781
CVAR[WT]	=	0.32462	0.20424
CVAR[WPc]	=	-0.02068	-0.01402
CVAR[WVP]	=	0.01616	0.00948
CVAR[WS]	=	-1.31903	-1.25729
CVAR[WCO2]	=	-0.20675	-0.15084
CVAR[WH2O]	=	0.18561	0.10862
CVAR[TT]	=	0.50354	0.36278
CVAR[TPc]	=	-0.01299	-0.02002
CVAR[TVP]	=	0.02417	0.01521
CVAR[TS]	=	-0.79949	-0.61813
CVAR[TCO2]	=	0.02139	-0.22747
CVAR[TH2O]	=	0.28234	0.17384
CVAR[PcPc]	=	0.00607	0.00561
CVAR[PcVP]	=	-0.00100	-0.00133
CVAR[PcS]	=	0.04407	0.04953
CVAR[PcCO2]	=	0.08966	0.07601
CVAR[PcH2O]	=	-0.01068	-0.01481
CVAR[VPVP]	=	0.00177	0.00113
CVAR[VPS]	=	-0.04273	-0.02950
CVAR[VPCO2]	=	-0.00214	-0.01505
CVAR[VPH2O]	=	0.02051	0.01292

```
CVAR[     SS] =    3.86484                        3.54100
CVAR[   SCO2] =    0.40174                        0.63439
CVAR[   SH2O] =   -0.49196                       -0.33472
CVAR[CO2CO2] =    1.62953                        1.20263
CVAR[CO2H2O] =   -0.00235                       -0.16000
CVAR[H2OH2O] =    0.23862                        0.14791
```

```
                           Theta = -6.44313 deg
Phi                                          =    -8.65104 deg
Vector Averaged Wind Speed                   =     3.28162 m/s
Wind Direction                               =    -6.44313 deg
Standard Deviation of Wind Direction         =    25.54987
Mix Ratio                                    =     0.00411
Vapor_Press                                  =     0.57567 kPa
Air Density                                  =  1023.61003 g/m3
Specific Heat of Dry Air at Constant Pressure =        1.01360 W*s/(g*K)
Heat of Vaporization                         =  2443.89767 W*s/g
Friction Velocity                            =     0.90935 m/s
Flux of Momentum                             =   846.44375 g/(m*s2)
Flux of Sensible Heat                        =  -211.90110 W/m2
Flux of Latent Heat                          =  -168.41686 W/m2
Flux of Carbon Dioxide                       =    -0.15084 uMol/(Mol*m*s)
Flux of Water Vapor                          =    -0.06891 g/(m2*s)
```

3.2.3.4.1 Determination of the lag time

The establishment of the lag time is crucial to the integrity of the data. The co-variances (fluxes) cannot be maximized if the lag time is not correct. The effect of the tube configuration and flow rate on the lag time, were determined by measuring the raw milli-volt output of the LI-6262 to 5 s step changes in vapour pressure concentration. The data were logged (CR21X) at 0.1 s intervals. The lag time calculated was 2.2 s.

3.2.3.5 Construction and installation of the eddy covariance tower

Approval for the erection of a mast required an environmental management plan and permission from the Department of Environment Affairs and the Kruger National Park. Permission for the construction of the 2 m^3 concrete base for a specially designed mast, was granted in September 1998 (Figure 3.4). The trees at the site are approximately 17 m high and the mast had been designed to raise the sonic anemometer to 25 m (i.e. about 8 m above the canopy). This is illustrated in Figure 3.5.

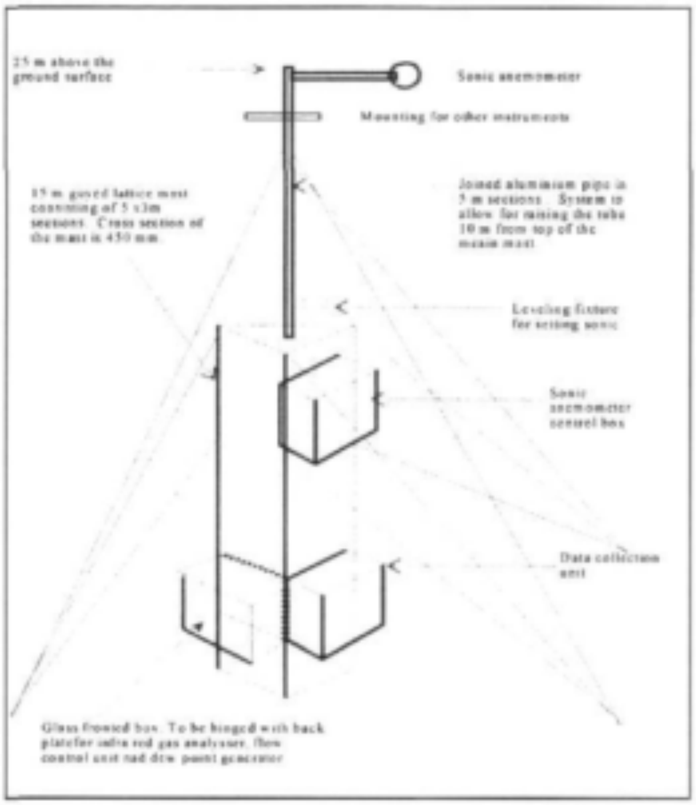

Figure 3.4: A schematic representation of the Eddy Covariance mast

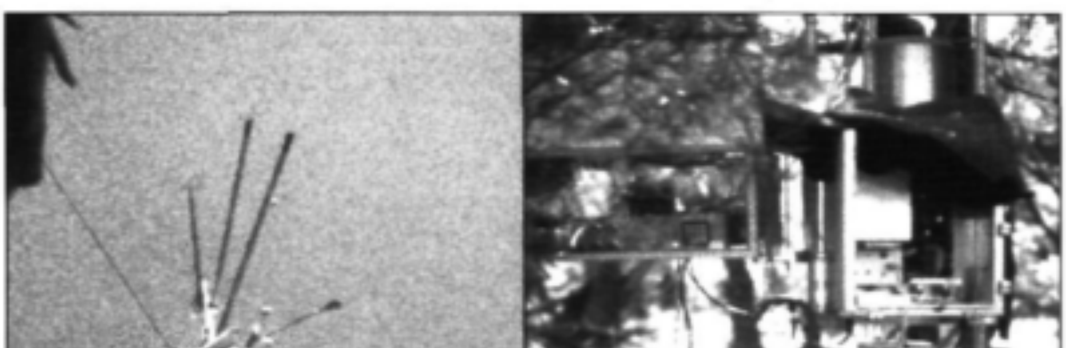

Figure 3.5: The eddy covariance mast at the forest site

3.3 The use of canopy temperatures to monitor evapotranspiration

During the study the project team planned to determine the evapotranspiration from a "wet" site, where the reed roots were permanently inundated with water. It soon became apparent that the Bowen ratio energy balance approach could not be used since:

1. At these sites, there was insufficient fetch distance.
2. The changing water levels and deep water made it very difficult to build suitable towers.
3. Safe access to the sites would be difficult without building major structures such as walkways etc.

For these reasons an alternative technique was sought which could be used to measure evapotranspiration which was independent of fetch and which did not need to be placed on towers above the canopy. The technique selected was the remote sensing of canopy temperatures with infrared thermometers, in combination with surface energy balance models.

Evaporation from a surface is a component of the partitioning of energy received by that surface. This process can be described by the familiar energy balance equation with expanded sensible and latent heat terms, as

$$R_n + G = \rho C_p \frac{(T_c - T_a)}{r_a} + \frac{\rho C_p}{\gamma} \frac{[e_s(T_c - e_a)]}{r_a + r_c} \quad \text{....... .... 3.18}$$

where R_n is the net radiation (Wm^{-2}), G the soil heat flux (Wm^{-2}), C_p the volumetric heat capacity of air (Jkg^{-1} °C^{-1}), T_c the canopy temperature (°C), r_a the aerodynamic resistance (sm^{-1}), γ the psychrometric constant, $e_s(T_c)$ the saturated vapour pressure at T_c (kPa), e_a the actual vapour pressure (kPa), and r_c the canopy resistance. This form of the energy balance equation has often been cited, but the difficulty of measuring canopy temperature led to other approaches that decouple Equation (3.18) from a direct surface temperature measurement.

With the development of thermal infrared thermometers that are accurate and easily used it is now possible to use surface energy balance models to estimate evaporation. These approaches have ranged from the manipulation of Equation (3.18) to the use of empirical coefficients for deriving daily evaporation from midday canopy temperatures. Although these approaches have been proposed, only limited evaluations have been suggested.

The energy balance of a surface given in Equation (3.18) (Monteith, 1973), can be rewritten as

$$\lambda E = R_n + G - \frac{\rho C_p}{\gamma} \frac{(T_c - T_a)}{r_a} \quad \text{.......................................(3.19)}$$

where λE is the latent heat of vaporization (Jkg^{-1}). In this method, we calculated r_a from

$$r_a = [\ln (z-d)/z_0]^2 / k^2 u \quad \text{... ....(3.20)}$$

with z being the height (m) of observation of air temperature, wind speed, and vapour pressure above the canopy, d the displacement height (m), z_0 the roughness length (m), k von Karmans constant (0.4), and u the windspeed (ms^{-1}). Following Monteith's (1973) correction for stability, we corrected the aerodynamic resistance as

$$r_{ac} = r_a \left(1 - \frac{ln(z-d) g (T_c - T_a)}{Tu^2} \right) \quad \text{..............................(3.21)}$$

where g is the acceleration due to gravity and T the absolute temperature (K). Bartholic, Namken and Wiegand (1972), rearranged Equation (3.18) to obtain the following:

$$E = \frac{R_n + G}{1 + \gamma \frac{(T_a - T_c)}{[e_s(T_a) - e_s(T_c)]}} \quad \text{..(3.22)}$$

This approximation sets the surface and air at the saturation vapour pressure that limits the equation to potential evapotranspiration from an infinitely wet surface.

Canopy temperatures were measured at both the reed and forest site, together with net radiation, soil heat flux and windspeed. The measurements were made at 20-minute intervals.

3.4 The use of the Penman-Monteith equation in the estimation of actual evapotranspiration

3.4.1 Derivation of the Penman-Monteith equation

The Penman-Monteith reference evapotranspiration (Campbell, undated) is given by

$$ET_o = \Delta(R_n - G)/[\lambda(\Delta + \gamma^*)] + \gamma^* M_w (e_s - e_a)/[R\theta r_v (\Delta + \gamma^*)] \quad \text{..............} (3.23)$$

with ET_o as the potential evaporation rate (mm/s), R_n the net irradiance (kW m^2), G the soil heat flux density (kW m^{-2}), M_w the molecular mass of water (0.018 kg mol^{-1}), R the gas constant (8.31 x 10^{-3} kJ mol^{-1} K^{-1}), θ the Kelvin temperature (293 K), $(e_s - e_a)$ the vapour pressure deficit of the air (kPa), λ the latent heat of vaporization of water (2450 kJ kg^{-1}), r_v the combined resistance for vapour (s m^{-1}), Δ the slope of the saturation water vapour pressure function (Pa °C^{-1}) and γ^* the apparent psychrometer constant (Pa °C^{-1}).

The net irradiance, R_n, is the sum of the net solar irradiance and the net long-wave irradiance and is approximated as

$$R_n = a_s R_s + L_{ni} \quad \text{..............} (3.24)$$

where a_s is the absorptivity of the crop, R_s is the measured solar irradiance measured by the datalogger and L_{ni} is the atmospheric radiant emittance minus the crop emittance at air temperature. Under clear skies, L_{ni} (kW m^{-2}) is given by

$$L_{nic} = 0.0003T_a - 0.107 \quad \text{..............} (3.25)$$

with T_a as the air temperature (°C). Under cloudy skies L_{ni} approaches zero. Cloudiness is estimated from the ratio of measured to potential solar irradiance during daylight hours (R_s/R_o). A cloudiness function, $f(R_s/R_o)$ is computed

$$f(R_s/R_o) = 1 - 1/[1+0.034\exp(7.9R_s/R_o)] \quad \text{..............} (3.26)$$

The net isothermal long-wave irradiance (L_{ni}) is then calculated as

$$L_{ni} = f(R_s/R_o)L_{nic} \quad \text{..............} (3.27)$$

The cloudiness function (*Eq. 3.26*) requires the computation of the potential solar irradiance on a horizontal surface outside the earth's atmosphere, R_o

$$R_o = 1.36\sin\varphi \quad \text{..............} (3.28)$$

where *1.36* (kW m^{-2}) is the solar constant, and φ the elevation angle of the sun

$$\sin \varphi \quad = \quad \cos\ d \cos l + \sin d \sin l\ \cos[15(t-t_o)] \quad (3.29)$$

where d is the solar declination angle, l the latitude at the site, t the local time and t_o the time of solar noon. $Sin\ d$ is approximated using the polynomial

$$\sin d \quad = -0.37726-0.10564j+1.2458j^2-0.75478j^3+0.13627j^4-0.00572j^5 \quad (3.30)$$

where j is the day of the year (DOY) divided by 100 (DOY/100) and d is the declination. The cosine of d is computed from the trigonometric identity

$$\cos d \quad = \quad (1-\sin^2 d)^{0.5} \quad (3.31)$$

The time t is the datalogger local time less half the time increment from the last ET_o computation. The time of solar noon, t_o, is given by

$$t_o \ = \ 12.5-L_c-t_e \quad (3.32)$$

with L_c the longitude correction and t_e the "equation of time". The longitude correction is calculated by determining the difference between the longitude of the site and the longitude of the standard meridian. The longitude correction is given as

$$L_c \ = \ (L_s-L)/15 \quad (3.33)$$

The "equation of time" is an additional correction to the time of solar noon that depends on the day of year. Two equations are used to calculate t_e - one for the first half of the year (for DOY < 180, where j = DOY/100)

$$t_e = -0.04056-0.74503j+0.08823j^2+2.0515j^3-1.8111j^4+0.42832j^5 \quad (3.34)$$

and one for the second half of the year (for DOY > 180, where j = (DOY-180)/100)

$$t_e = -0.05039-0.33954j+0.04084j^2+1.8928j^3-1.7619j^4+0.4224j^5 \quad (3.35)$$

Evapotranspiration occurs mainly during daytime hours when the net irradiance is the main driving force of the evapotranspiration process. The soil heat flux density can be estimated as a fraction of the net irradiance. For a complete canopy cover, G is assumed to be approximately 10 % of the net irradiance

$$G \quad = \quad 0.1R_n \quad (3.36)$$

During the night $R_s \ = \ 0$ and G is assumed to be 50 % of the net irradiance

$$G \quad = \quad 0.5R_n \quad (3.37)$$

The slope of the saturation vapour pressure function ($Pa\ {}^{\circ}C^{-1}$) depends on air temperature, yielding

$$\Delta = 45.3+2.97T_a+0.0549T_a^2+0.00223T_a^3 \quad (3.38)$$

with T_a the average air temperature (°C).

The apparent psychrometer constant γ^* is calculated as

$$\gamma^* = \gamma (r_v/r_a) \quad (3.39)$$

where γ *is* the thermodynamic psychrometer constant, r_v the combined aerodynamic and canopy resistance to water vapour and r_a the convective resistance for heat transfer. The vapour resistance is computed as

$$r_v = r_a+r_c \quad (3.40)$$

where the canopy resistance is 70 s m^{-1} for a reference crop.

The aerodynamic resistance (r_a) is given by

$$r_a = \ln[z_u \cdot d/z_{om}]\ln[z_t \cdot d/z_{oh}]/k^2u_z \quad (3.41)$$

with k the Von Karman constant (0.41), z_u the height of the anemometer above the soil surface and z_t the height of the temperature and humidity sensor above the soil surface. For clipped grass the zeroplane displacement (d), roughness length for momentum transfer (z_{om}) and heat and water vapour transfer (z_{oh}) are

$$d = 0.67h \quad (3.42)$$

$$z_{om} = 0.12h \quad (3.43)$$

$$z_{oh} = 0.1z_o \quad (3.44)$$

where h is the average canopy height.

Ignoring the psychrometer constant's weak temperature dependence and taking the pressure dependence into account, the ratio between the atmospheric pressure and sea level pressure (P/P_o) is

$$P/P_o = \exp(-A/8500) \quad (3.45)$$

where A is the altitude (m).

The Kelvin temperature is set as 293 K, yielding a constant value of $M_w/R\theta$.

The saturated (e_s) and actual (e_a) water vapour pressures are computed from the air temperature and relative humidity measurements (Campbell, undated; Monteith and Unsworth, 1990).

3.4.2 The application of the Penman-Monteith equation to canopy specific conditions in the calculation of actual evapotranspiration

In general, the Penman-Monteith evapotranspiration equation is applied to calculate reference evaporation. The Penman-Monteith evapotranspiration equation can be applied to calculate potential and actual evaporation.

In the evapotranspiration experiment conducted in the Kruger National Park, the Penman-Monteith equation (Equation (3.23)) has been applied to canopy specific conditions, where actual total evaporation (ET) was calculated. Canopy specific reflection coefficients (α_s) were used in the simulation of the net irradiance (R_{ns}) (Equation (3.24)). The soil heat flux density (G_s) was calculated as a fraction of the simulated net irradiance. A combined resistance (r_v) was calculated from the aerodynamic resistance to vapour transfer (r_a) and the canopy resistance (r_c). The aerodynamic resistance was calculated as a function of the zero-plane displacement height (d), roughness length for momentum transfer (z_{om}) and roughness length for heat and vapour pressure transfer (z_{oh}). The aerodynamic resistance is a function of the height of the windspeed measurement (z_u), the average canopy height (h), the zero plane displacement (d), the roughness length for momentum (z_{om}) and heat and vapour transfer (z_{oh}), Von Karman's constant (k) and the windspeed at height z_u (u_{zu}) (Monteith and Unsworth, 1990; Campbell, undated).

The canopy resistance (r_c) was back-calculated (utilizing the Penman-Monteith equation and the actual Bowen ratio total evapotranspiration), providing average 20 minute r_c estimates over the different seasons for the different canopies. The generalised canopy resistances were then used in the canopy-specific Penman-Monteith total evaporation calculation.

4. RESULTS

4.1 General meteorological conditions during the study period.

The observations provided by the automatic weather station at the reed site show clearly that the Kruger Park has a very hot and humid climate. Daily averages of temperature, incoming solar radiation, vapour pressure and daily rainfall for 1998 and 1999 are shown in Figures 4.1 and 4.2 respectively. The daily totals of incoming radiation range from 21 MJ day^{-1} during summer (December, Figure 4.1) to about 10 MJ day^{-1} during winter (June, Figure 4.2), with the occasional cloudy days having much less than this. These high radiation levels are reflected in the average daily temperatures, which in summer average about 26°C, with maximums regularly in the upper 30's and minima seldom below 20°C. Even during winter, average air temperatures seldom dropped below 15°C. Vapour pressures were high (2.5-3.0 kPa) in summer and low (1.0-1.5 kPa) in winter, showing the typical hot humid summer days and warm dry days in winter. The high rainfall events in December and January 1998/99 (194 mm) that caused the flooding of the reed site in January, is clearly evident in the rainfall graphs.

4.2 Reed evapotranspiration

4.2.1 Energy budget

4.2.1.1 Summer

The energy balance of two typical summer days data collected during December 1997 are shown in Figure 4.3. The first day (DOY 338, 4 December) was intermittently cloudy while the second day (DOY 339, 5 December) was cloudless. On both days the net radiation was high, peaking at approximately 800 Wm^{-2} between 13h00 and 14h00. The diurnal net radiation on the cloudy day was characterised by a jagged curve due to alternating high and low values caused by the shading effect of the intermittent cloud cover. The net radiation on the clear day was characterised by a bell shaped curve, which is typical of a sunny cloudless day. Most of the radiant energy at this time of the year was partitioned into the latent heat of evaporation (350-400 Wm^{-2}), with the balance going almost equally into sensible heat and soil heat flux (± 200 Wm^{-2} each). It is interesting to note that on the clear sunny day the evapotranspiration rate peaked early at 10h30 and then declined slowly until 18h00, dropping rapidly at sunset. These data suggest that on these days the reeds were unable to transpire at potential evaporation rates, in spite of their access to the ground water. The total evapotranspiration for the cloudy and sunny day was 2.6 and 5.2 mm day^{-1} respectively.

Figure 4.4 shows a 14-day period of the net radiation and latent heat flux. These data show that the evapotranspiration seldom exceeds 500 Wm^{-2}. The effect of cold weather fronts on reducing evapotranspiration is apparent from DOY 329-335 where values of the latent heat flux density were seldom above 200 Wm^{-2}. This translates into an evapotranspiration rate of < 1.5 mm day^{-1}.

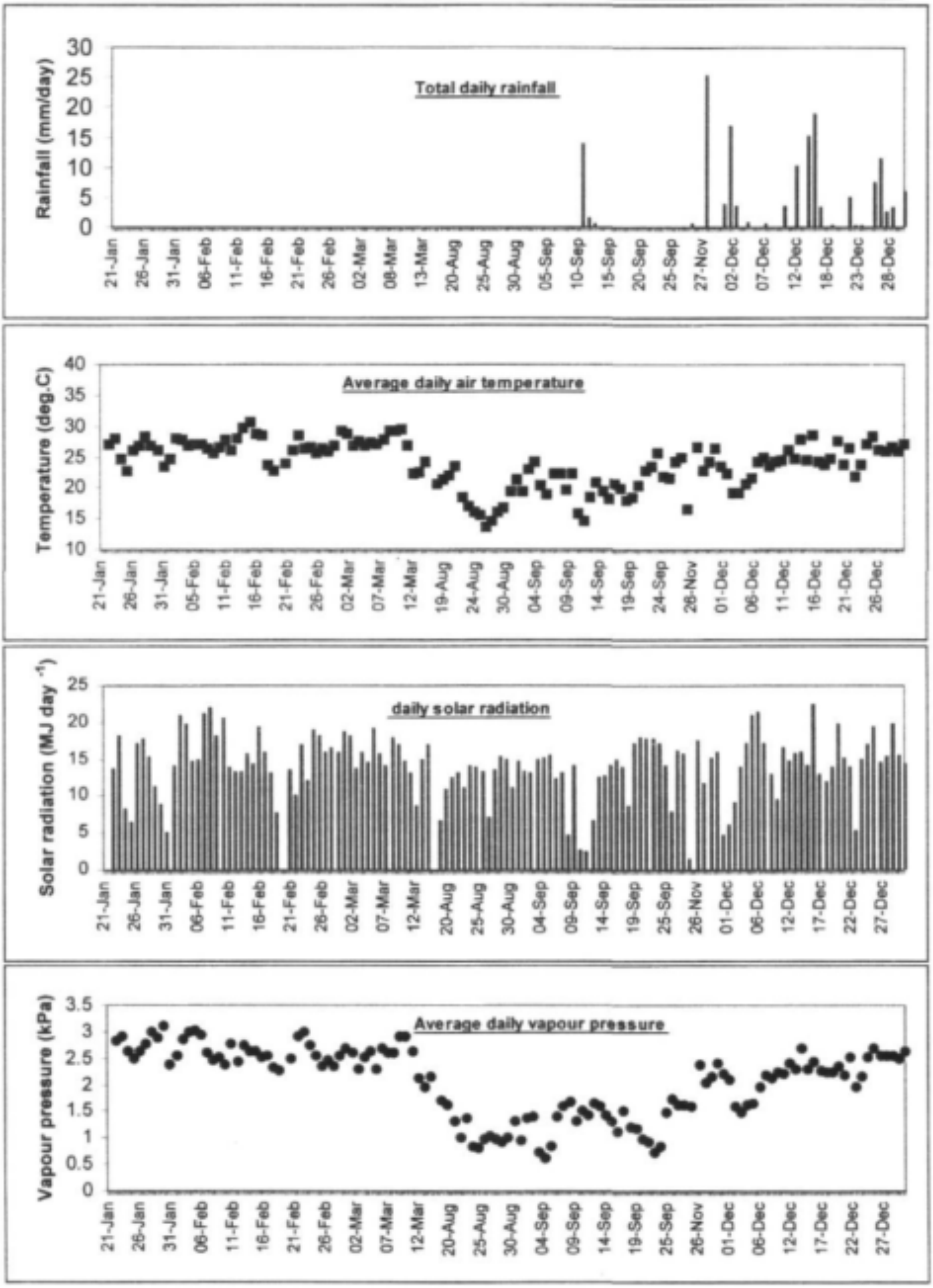

Figure 4.1: The annual variation in temperature, solar radiation, rainfall and vapour pressure at the reed study site during 1998. Note: periods of missing data were from 17 April to 17 August & 1 October to 26 November Between 1 January and 10 July the raingauge was faulty.

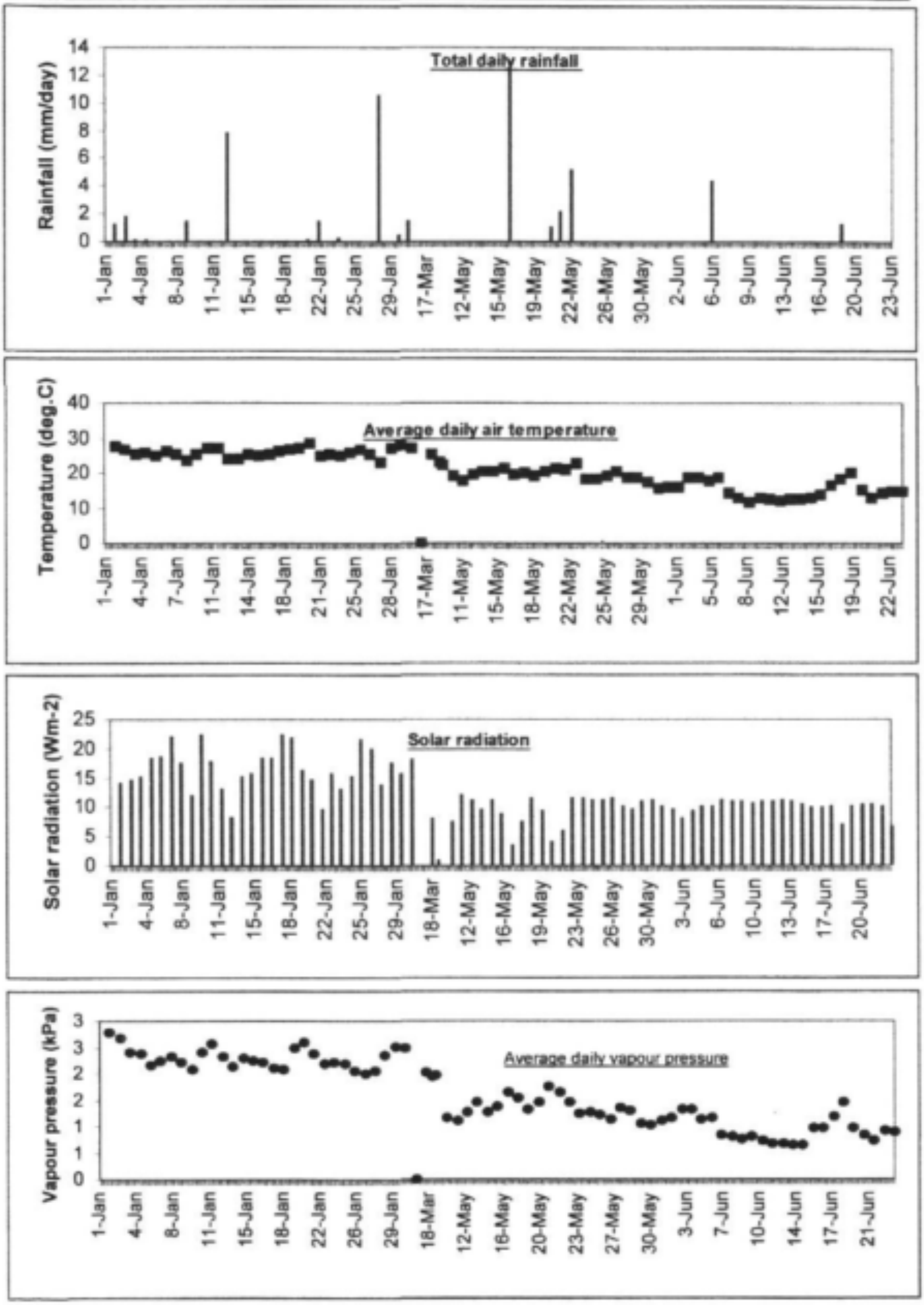

Figure 4.2: The annual variation in temperature, solar radiation, rainfall and vapour pressure at the reed study site during 1999. Note: periods of missing data were from 1 Feb. to 13 March & 19 March to 9 May.

Figure 4 3: The energy balance above the reeds on a cloudy (DOY 338) and a clear day (DOY 339) in December 1997. Legend: Rn=Net radiation, G=soil heat, LE=Latent heat & H=Sensible heat.

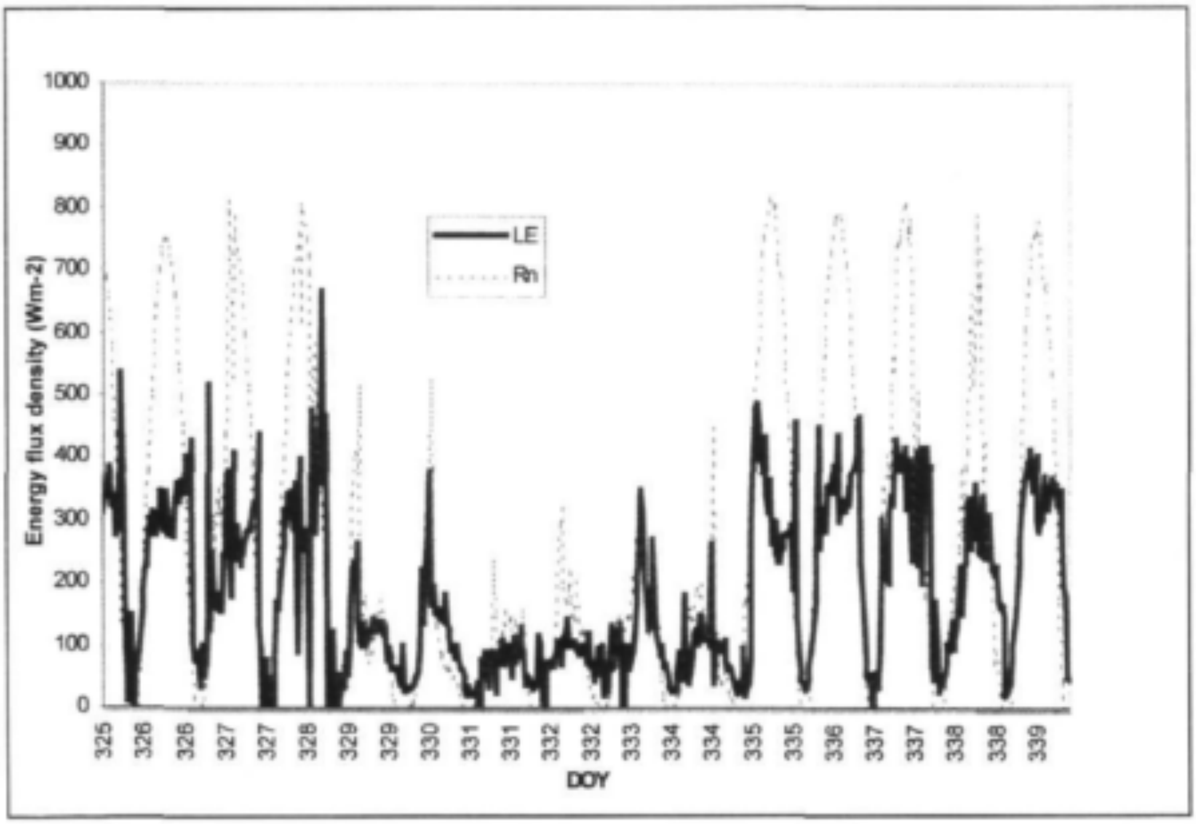

Figure 4. 4: The daily trend in the latent heat flux density and net radiation in the KNP at the reed site for 14 days in summer (October to November). Rn=Net radiation, LE=Latent

4.2.1.2 *Winter*

The energy balance for a typical day in winter shows that the amount of available energy (net radiation minus soil heat flux) for driving evapotranspiration is much less than in summer. At this time of the year maximum net radiation varies between 500 and 600 Wm^{-2} and soil heat flux 100 – 140 Wm^{-2}, leaving only 400-450 Wm^{-2} for partitioning into sensible and latent heat (Figure 4.5). In the early and late part of the day most of this remaining energy goes into the sensible heat flux, while during the period between 09h00 and 14h00 most of the partitioned energy was used in driving the latent heat flux. In spite of sunny cloudless days in winter, evapotranspiration at this time was generally < 3 mm day^{-1} (Figure 4.6). These low values can be attributed to the lower available energy and dry conditions experienced during winter. The LE values occasionally exceeded the net radiation (10h40 to 12h00) suggesting advection from the surrounding hotter and drier vegetation.

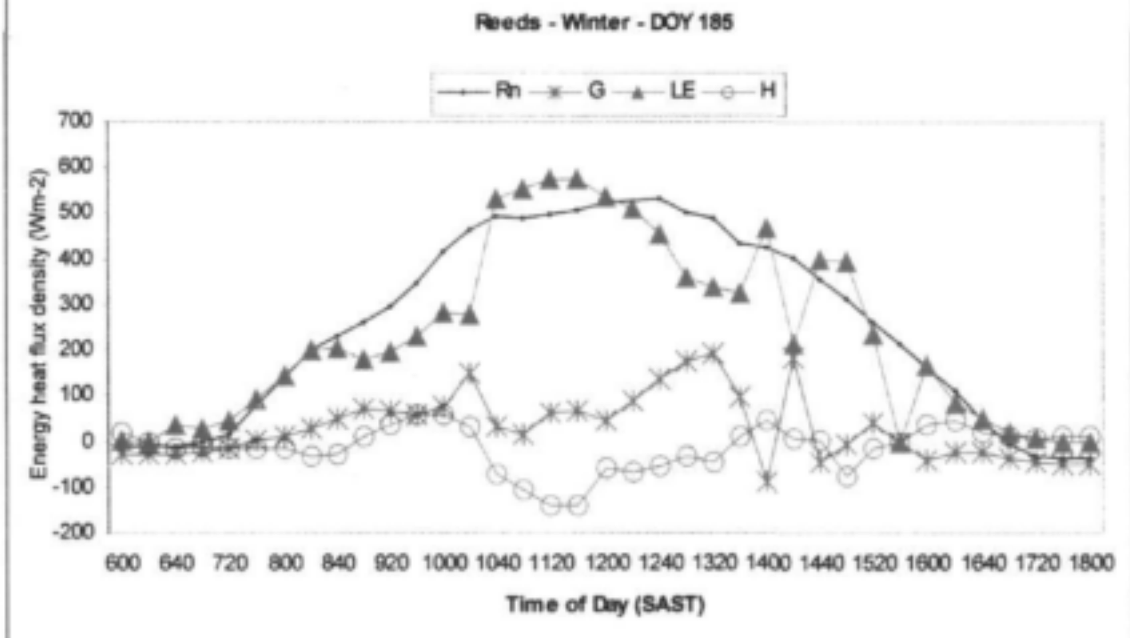

Figure 4 5: The energy balance of the reed community during winter (August 1998). Rn=Net radiation, G=soil heat, LE=Latent heat & H=Sensible heat

4.2.2 The annual cycle of evapotranspiration from the reed community

Daily reed evapotranspiration rates (mm day^{-1}) of data collected for the entire study period are shown in Figure 4.6. This data set includes three summer seasons (1998, 1999 and 2000), two winter periods (1998 and 1999), and the spring of 1999. All the months of the year with the exception of April (missing data) are represented within this data set. The means and standard errors are shown for each month. Strong seasonal trends are exhibited by these data, with mean monthly summer values varying between 4.5 and 7 mm day^{-1} during 1998 and 1999. Mean monthly values in January in 2000 were significantly lower as a result of the high incidence of rain during this year. Maximum evapotranspiration rates of 8-9 mm day^{-1} were often found between December and February.

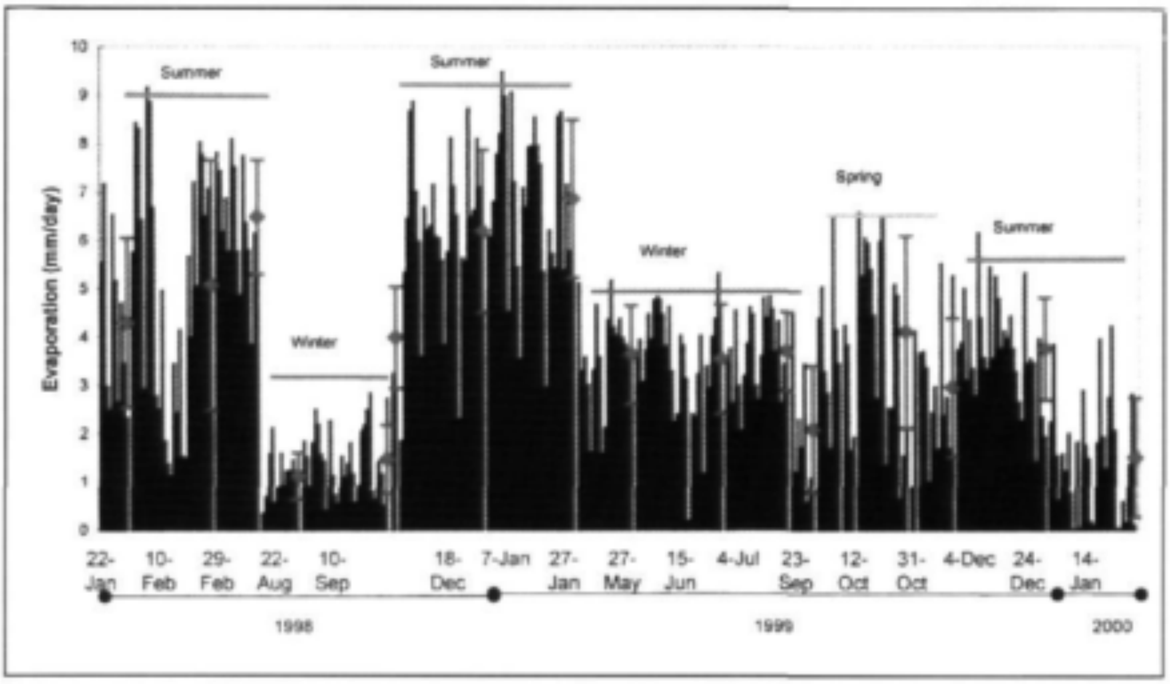

Figure 4.6: Daily estimates of evapotranspiration from the reed community showing the seasonal cycle of evapotranspiration in the KNP.

Evapotranspiration rates from the reeds during the winter months of May to August were noticeably lower, but still averaged about 4 mm day^{-1} in 1999. Besides the lower available energy this time of the year, two further factors contribute to reducing evapotranspiration: namely, lack of access to water (low water table), and heavy grazing of the reeds by elephants during August.

Evapotranspiration from the reed beds in the Kruger National Park ranged from 4 to 9 mm day^{-1} depending on the season. This contrasts with the 12 mm day^{-1} in February and 7 mm day^{-1} in September reported in the previous study (WRC report 474/1/97). These values were not considered high considering the high evaporative demand and free access to water at the Nerina site. The data presented here have shown that the dynagauge data were almost double the Bowen ratio estimates for evapotranspiration for corresponding periods.

A difficult problem faced when using the dynagauge technique is that of scaling-up from individual plants to whole canopies. In the previous study two options were considered. The first was scaling up using the daily water use per reed data. This required population density estimates of the reed beds and was considered impractical. The second and preferred method was to use a linear relationship between leaf area index and transpiration to scale up the transpiration to the entire canopy. It is likely that this approach may have led to the high values eventually produced by the reed model as recent studies have shown that this relationship is curvilinear rather than linear, reaching an asymptote of transpiration around a LAI of six (Baldocchi and Meyers 1998). As suspected in phase I (Birkhead *et al.* 1997), the modelled reed values of between 10 and 30 mm day^{-1} were unrealistic and not physically possible, since the values far exceeded the amount of available energy. The reed models developed in phase I should therefore not be used for calculating reed transpiration.

4.3 Tree evapotranspiration

4.3.1 Eddy correlation technique

The measurement of tree evapotranspiration using the eddy correlation technique was hampered by continual technical and logistical problems preventing the collection of reliable data. These problems included:

- The breakdown of the LI-6262 infrared gas analyzer in November 1999.
- The very high river levels of the Sabie River preventing access to the tower during the summer months.
- Power problems to the equipment.
- "Spiking" of the signal from the sonic anemometer causing erroneous wind data due to electronic problems with the signal processing.

Other difficulties associated with working in the riparian forest included:

- Limited fetch.
- The high biodiversity and complex structure, which necessitated the use of techniques which sample within the boundary layer above the canopy.
- The high tree canopy which requires the construction of tall towers.
- Difficult access through the water exacerbated by the presence of dangerous animals such as crocodiles.

The entire study site and R750 000.00 worth of equipment were destroyed by the February 2000 floods. The loss of all equipment, structures and data storage modules represented a major set back to the project.

4.3.1.1 Tree evapotranspiration using the eddy correlation technique

The diurnal course of evapotranspiration measured on two days in July 1999 is presented in Figure 4.7. These data showed that the latent heat of evapotranspiration was low, reaching maximum values of between 100 and 125 Wm^{-2} at midday. The sensible heat flux was much higher with maximum values between 200 and 225 Wm^{-2} on DOY 203 and 204 respectively. These data, although limited, do show very low rates of transpiration from the tree canopy during winter (approximately 0.6 mm day^{-1}). Approximately 200 Wm^{-2}

of energy is unaccounted for. A possible reason for this lack of closure could be the energy attributed to tree trunk storage, which was not measured in this study.

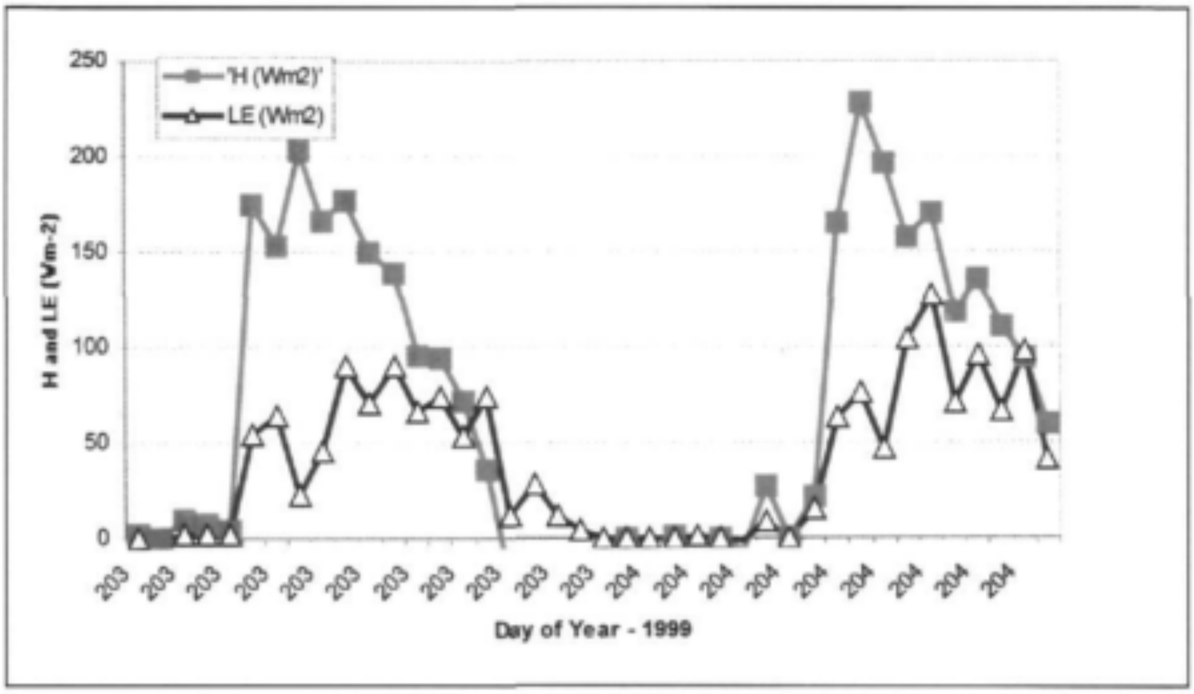

Figure 4.7: Latent and sensible heat flux density during DOY 203 and 204 at the forest site, measured using the EC system

4.3.2 Tree evapotranspiration using the Infra-red thermometry technique

A comparison of the Bartholic-Namken-Wiegand method (BNW) (Bartholic, Namken, Wiegand, 1972), against the net radiation and equilibrium rate for a representative day in summer are shown in Figure 4.8. The results show that the BNW model is strongly coupled to the net radiation (Figure 4.8). The model overestimates the equilibrium rate at all values above 300 Wm^{-2}. The infrared data imply that all of the available energy is converted into sensible heat, a very unlikely result in this instance. Because of the disappointing performance of this technique and the difficulty of routine measurements in the Kruger National Park, it was decided to investigate the technique at a site closer to Pietermaritzburg. The events of the flood, in which all the sensors and data loggers were lost, have prevented this.

4.3.3 The Bowen ratio energy balance technique at the forest site

Because of the practical and technical difficulties experienced with the eddy correlation equipment at the forest site a Bowen ratio system was installed on the forest tower in 1999. The rationale was to obtain continuous estimates of the forest evapotranspiration, which could also be used for direct comparisons with the reed site. However the eddy correlation data could not be verified against the Bowen ratio estimates because of the problems encountered with the eddy correlation technique.

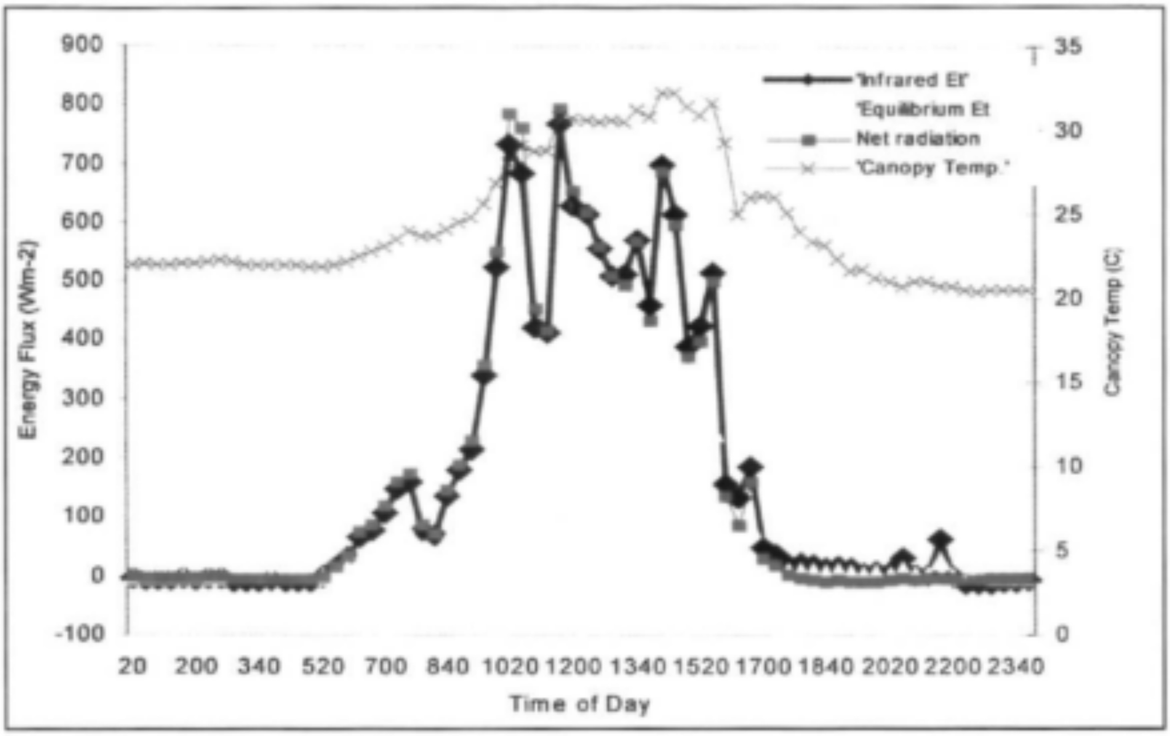

Figure 4.8: The diurnal course of evapotranspiration on the 24th of November, at the Forest site using the BNW method and the equilibrium evapotranspiration rate.

4.3.3.1 The energy balance

4.3.3.1.1 Winter (DOY 183)

The diurnal pattern of the energy balance for a typical winter day at the forest site is shown in Figure 4.9. From approximately mid-morning until 14h00, the latent heat flux followed the net radiation and accounted for most of the energy (300 Wm^{-2}) (Figure 4.9). After 14h00, most of the energy was partitioned into heating the air (250 – 300 Wm^{-2}). Very little energy entered the soil during the day (<20 Wm^{-2}). The total evapotranspiration on this day was 2.57 mm day^{-1}. The results suggest that trees still transpire freely during winter, although the maximum rates are limited by the available energy.

4.3.3.1.2 Summer (DOY 289)

During summer the energy balance above the tree canopy is clearly different from that during winter (Figure 4.10). By 08h00 most of the energy (500-700 Wm^{-2}) is already used to drive the evapotranspiration process (the latent heat flux). At mid-day this trend is reversed, when approximately 300-600 Wm^{-2} is partitioned into heating the air. The main differences between the summer and the winter energy balances are: (i) the magnitude of the fluxes and (ii) the time at which the partitioning between the latent and sensible flux changes from being predominantly latent heat to principally sensible heat. On this day, 3.2 mm was evaporated. As DOY 289 (16 October) is still spring, one would expect evapotranspiration rates to exceed 3.2 mm day^{-1} during mid-summer, when there is more available energy (longer day lengths and solar altitudes) and available water (increasing water tables). However, increasing cloud cover may compensate for these expected increases. It was unfortunate that we were unable to obtain mid-summer values to test these possibilities.

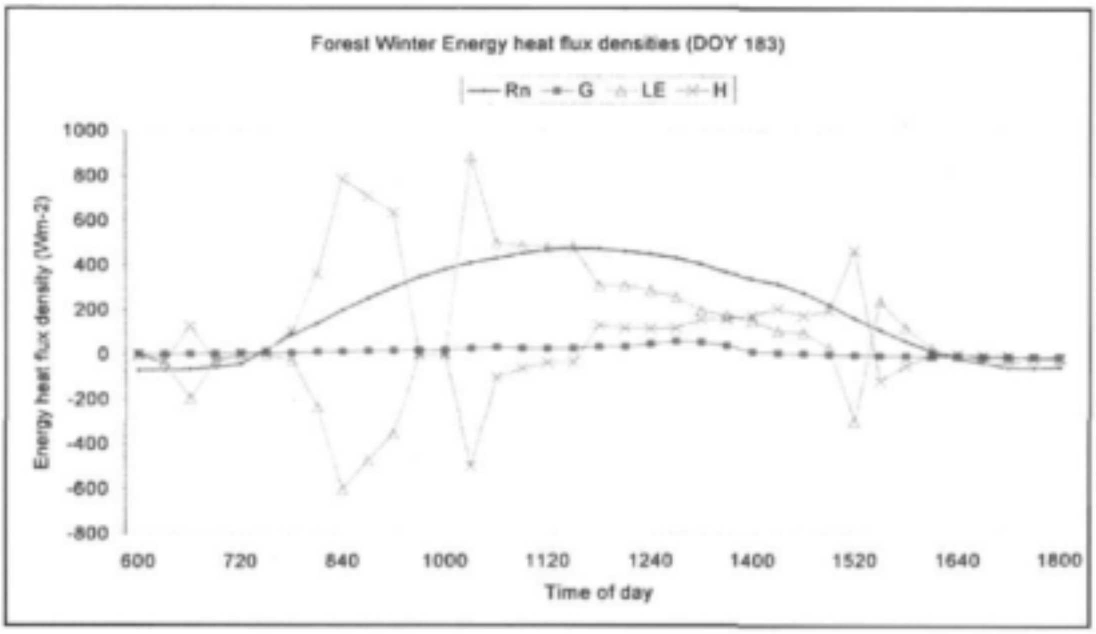

Figure 4.9: Energy flux densities during winter at the Forest site (DOY 183, 2 July). Note: reversing gradients due to the high turbulence above the forest causes large negative LE values.

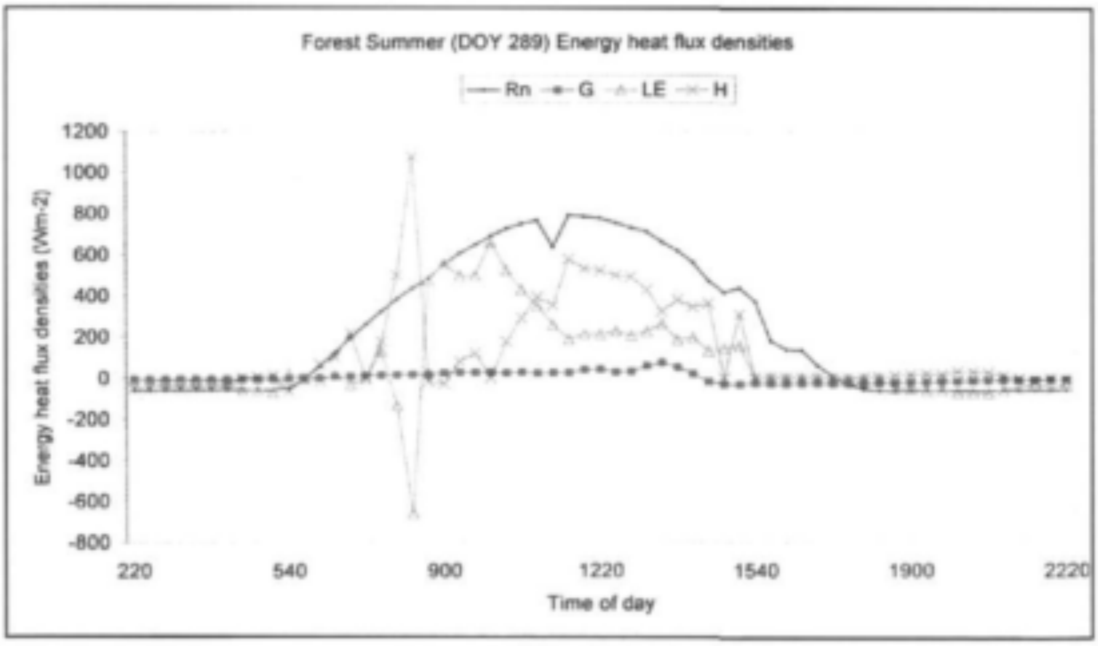

Figure 4.10: Energy flux densities at the forest site during summer (DOY 289, 16 October) Note: reversing gradients due to the high turbulence above the forest causes large negative LE values.

4.3.3.2 Daily trends in the tree evapotranspiration

The daily evapotranspiration rates recorded from June to July (DOY 175-203), September to November (DOY 267 to 316) and 6 days in February 2000 illustrated the high variability in the daily evapotranspiration rates brought about by daily changes in meteorological conditions (Figure 4.11). A striking feature of these data is that the maximum daily rate seldom exceeded 4 mm day^{-1}. Also noticeable was that there were no strong seasonal trends in the data, winter values being similar to summer values. The lower incidence of cloud cover and rain in winter results in the average evapotranspiration rate being higher in winter than in summer. For example, the total evapotranspiration for 24 days in winter (June & July: DOY 176 to 200) was 65 mm compared to 56 mm for a similar length summer period (October & November: DOY 267 to 291). The mean daily evapotranspiration for the winter and summer was 2.62 and 2.23 mm respectively. The results of this study are therefore similar to those obtained in phase I, where very low evapotranspiration rates were recorded. The daily evapotranspiration results of this study were, however, higher than for corresponding periods of transpiration measured during phase I (see Figure 4.12). For example, mean July transpiration measured for all the trees at the Nerina site was approximately 1 mm day^{-1} compared with the 2.62 mm day^{-1} in this study. This is not surprising as the HPV technique only measures transpiration and includes errors due to vegetation not sampled (i.e. the herbaceous layer and multi-stemmed plants). The Bowen ratio estimates, if in error, would be lower than absolute estimates, as the technique does not account for the possibility of additional energy being advected from the surrounding hotter and drier areas.

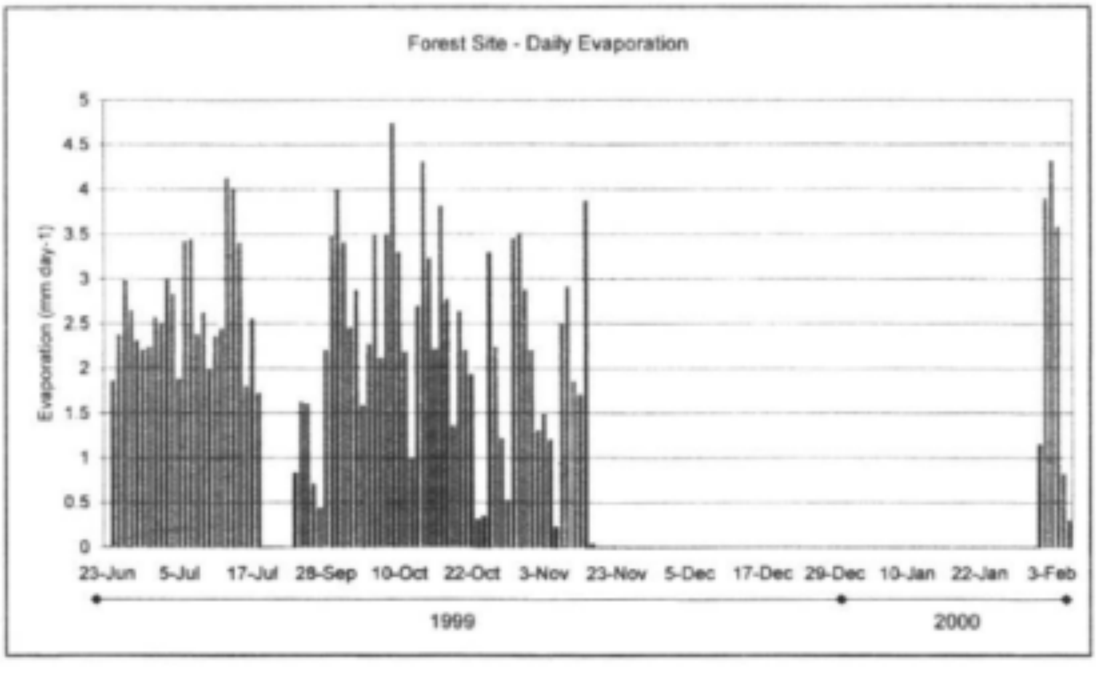

Figure 401: Daily evapotranspiration at the forest site measured by the BREB system. Gaps in data represent periods when no data were collected due to high river levels or technical problems.

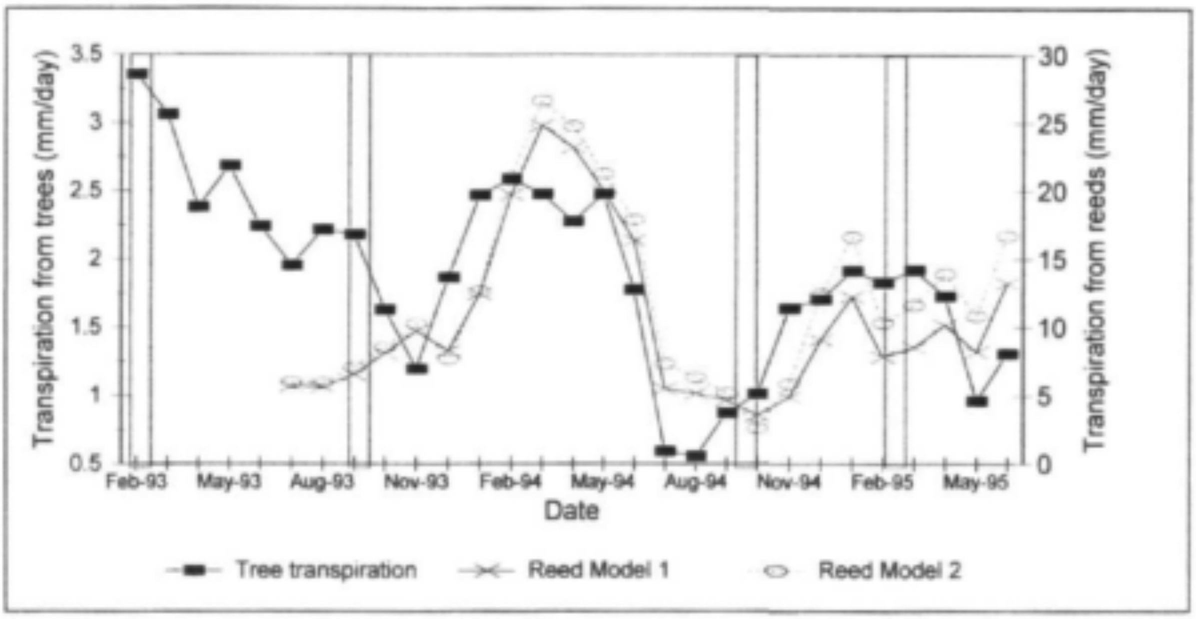

Figure 4.12: Tree and reed evapotranspiration as measured using the model developed during Phase I

What both studies have shown is that the evapotranspiration from of the riparian community is surprisingly low, especially considering the high atmospheric demand experienced in the KNP and the freely available supply of water to the trees. A possible explanation, as mentioned in the previous report, is that the transpiration per unit leaf area declines with age as a consequence of the extensive flow paths water must follow in passing from the root through long branches to the leaves. The corollary, that young trees will have significantly higher water requirements, now has particular relevance, due to the removal of most of the mature forest during the February 2000 floods. The post flood succession of the riparian forest now offers a unique opportunity to investigate this hypothesis.

4.4 Comparison of tree and reed evapotranspiration

Comparisons of simultaneous evapotranspiration rates from the reeds and forest communities in the KNP showed that the daily water use of the reeds was consistently higher than in the forest community (Figure 4.13). During this period the forest community used 36% less water that the reed community (2.5 mm day^{-1} versus 3.9 mm day^{-1} respectively).

4.4.1 Winter

Average evapotranspiration values for each 20 minute period during winter (DOY 177-199) and summer (DOY 268-306) were used to plot diurnal evapotranspiration curves for the reed and forest sites (Figure 4.14). The results showed significant diurnal differences in evapotranspiration between seasons.

In winter, the forest and reed evapotranspiration patterns were very similar from sunrise until 12h00, but after midday, evapotranspiration from the reeds was at a higher rate than the forest until sunset. This resulted in an average daily evapotranspiration rate of 3.46 mm day^{-1} for reeds, and 2.99 mm day^{-1} for the forest, equating to a difference of 0.47 mm day^{-1} for this winter period. This compared well with the 3.9 and 2.5 mm day^{-1} calculated earlier on during the 38 day winter period.

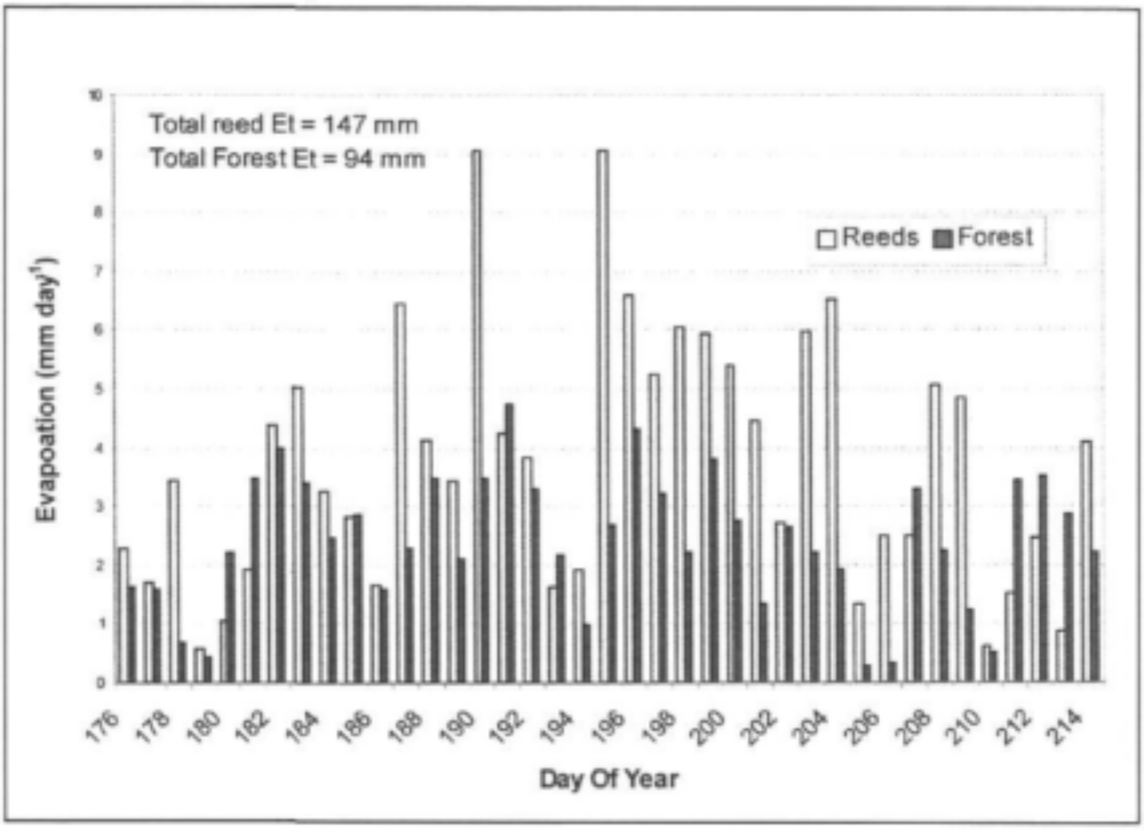

Figure 4.13: Daily forest and reed evapotranspiration as measured over a 38-day period in winter (25 June to 3 August) with two Bowen ratio energy balance systems.

4.4.2 Summer

The summer curves were very different from the winter curves, with the reed evapotranspiration exceeding the forest evapotranspiration during the entire day (Figure 4.15). Daily averages of 4.8 mm day^{-1} and 3.1 mm day^{-1} were calculated at the reed and forest sites respectively. This is approximately 1 mm day^{-1} higher than during winter for the reeds and 0.6 mm day^{-1} higher for the forest site. Thus the reed evapotranspiration exceeded the forest evapotranspiration during both summer and winter.

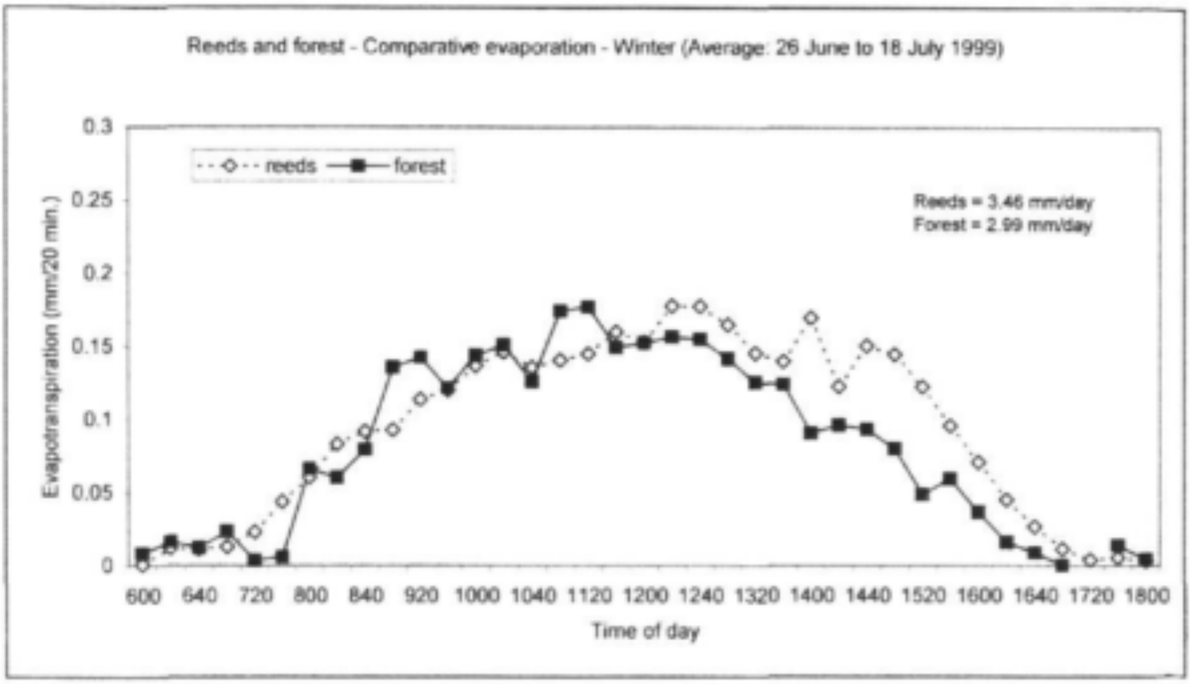

Figure 4.14 Reed and forest evapotranspiration during winter

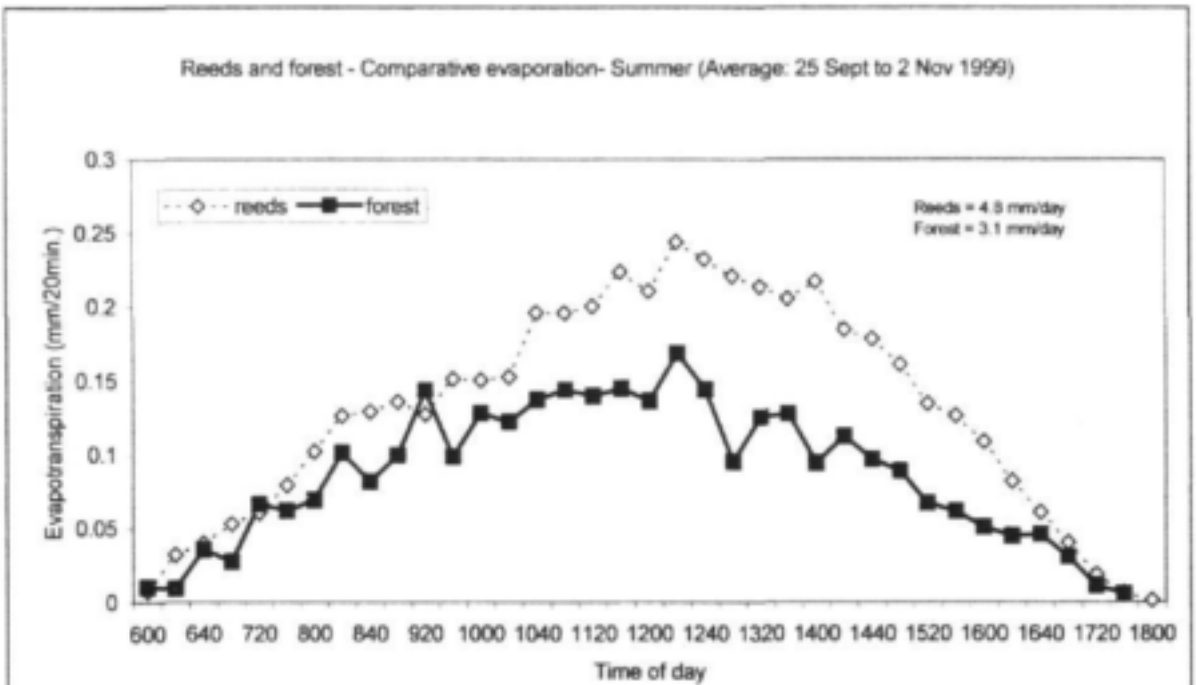

Figure 4.15: Reed and forest evapotranspiration during summer

5. MODELLING REED AND TREE EVAPOTRANSPIRATION

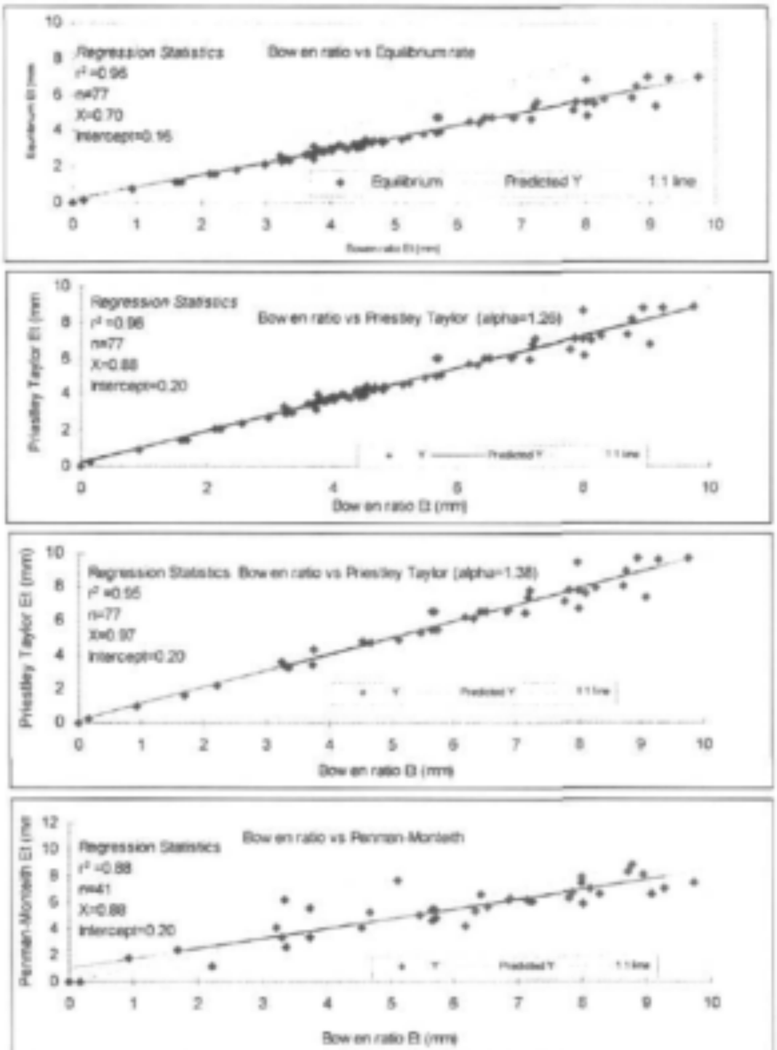

Figure 5.1 The relationship between the Bowen ratio, equilibrium and Priestley Taylor evapotranspiration rates.

Since the data of this study have shown the original reed transpiration model to be unreliable, it became essential to use the estimates of actual evapotranspiration obtained in this study to develop a new reed evapotranspiration model. The data presented in Figure 5.1 show a comparison of the Bowen ratio evapotranspiration with the equilibrium, Priestley-Taylor and Penman-Monteith formulations. The equilibrium rate consistently under estimated the evapotranspiration (see slope and 1:1 line), whereas both the Priestly-Taylor and Penman-Monteith equations provided a better fit against the measured evapotranspiration estimates. The best relationship was found using an alpha of 1.38 instead of 1.26 in the Priestley Taylor equation. The r^2 was 0.95 with a coefficient of x of 0.97 (n=77).

Since the Penman-Monteith equation is becoming widely accepted as the best technique for modelling evapotranspiration it was decided to develop canopy specific models of the Penman-Monteith equation that could be used for the reeds and trees.

Attempts were made to compare reed and modelled open water evaporation. However, we could not justify a direct comparison of open water and reed evaporation, as no direct measurements of the open water evaporation were made. Accurate calculations for the open water evaporation would require detailed information on the available energy, windspeed and albedo of the water in the river near the reed study site. None of these measurements were made and they would therefore have to be guessed. This should form an area for future research.

5.1 *Total evapotranspiration comparison as simulated by canopy specific Penman-Monteith equations*

In order to simulate the total evapotranspiration accurately with the canopy specific Penman-Monteith equation, the various components of the equation need to be calculated accurately. The available energy flux density is the main contributor to the evapotranspiration process as calculated from the simulated net radiation, (R_{ns}) and the soil heat flux density (G_s), calculated as a fraction of the simulated net radiation.

5.1.1 Simulation of the net radiation

The net radiation required in the Penman-Monteith equation, is only available from research sites, whereas the solar radiation is normally obtainable from automatic weather stations. The net radiation required for this study was simulated from the solar radiation and a canopy specific seasonal reflection coefficient (albedo). The reflection coefficient is simply a parameter, which must be input into the net radiation model. The net radiation was modelled successively by incrementing the albedo from 1, 5, 10 and 20% to determine the best value of the reflection coefficient to input into the model. The reflection coefficient that gave a slope (coefficient of x) closest to unity was judged to be the best value for parameterising the model.

The net radiation was simulated from the measured radiation (R_s) and a seasonal, canopy specific reflection coefficient (α_s) (Section 3.4). The relationship between the 20 minute measured (R_n) and simulated net radiation flux densities (R_{ns}), revealed the most suitable reflection coefficient to be used, and the accuracy of the simulation (Tables 5.1 and 5.2).

Statistically significant relationships were found between the measured and simulated net radiation during the period studied, with slopes approaching 1 and coefficients of determination (r^2) exceeding 0.99 (Tables 5.1 and 5.2, Figure 5.2). The maximum daytime net radiation values (noon values) are generally underestimated in the simulation and the minimum daytime net radiation values (sunset to sunrise), overestimated (Figure 5.3). The linear relationship ($y = mx + c$) between the measured and simulated net radiation indicates an increased slope ($m \rightarrow 1$), with a decreased reflection coefficient (Tables 5.1 and 5.2).

Table 5.1:

Statistical information on the relationship between the measured (x) and simulated (y) net radiation, using different reflection coefficients (α_s) at the reed site.

MONTH	REFLECTION COEFFICIENTS			
	$\alpha_s = 0.2$	$\alpha_s = 0.1$	$\alpha_s = 0.05$	$\alpha_s = 0.01$
January (whole month)	$\alpha_s = 0.2$ $y = 0.7396x + 16.953$ $r^2 = 0.9905$	$\alpha_s = 0.1$ $y = 0.832x + 19.076$ $r^2 = 0.9905$	$\alpha_s = 0.05$ $y = 0.8782x + 20.138$ $r^2 = 0.9905$	$\alpha_s = 0.01$ $y = 0.9152x + 20.987$ $r^2 = 0.9905$
May (whole month)	$\alpha_s = 0.2$ $y = 0.653x + 13.259$ $r^2 = 0.9907$	$\alpha_s = 0.1$ $y = 0.7346x + 14.923$ $r^2 = 0.9907$	$\alpha_s = 0.05$ $y = 0.7754x + 15.755$ $r^2 = 0.9907$	$\alpha_s = 0.01$ $y = 0.8081x + 16.421$ $r^2 = 0.9907$
June (whole month)	$\alpha_s = 0.2$ $y = 0.6439x + 14.601$ $r^2 = 0.9913$	$\alpha_s = 0.1$ $y = 0.7244x + 16.435$ $r^2 = 0.9913$	$\alpha_s = 0.05$ $y = 0.7646x + 17.352$ $r^2 = 0.9913$	$\alpha_s = 0.01$ $y = 0.7968x + 18.086$ $r^2 = 0.9913$
September		$\alpha_s = 0.1$ $y = 0.772x + 17.7$ $r^2 = 0.9936$	$\alpha_s = 0.01$ $y = 0.8492x + 19.475$ $r^2 = 0.9936$	$\alpha_s = 0.005$ $y = 0.8535x + 19.574$ $r^2 = 0.9936$
October (whole month)	$\alpha_s = 0.2$ $y = 0.6936x + 17.998$ $r^2 = 0.993$	$\alpha_s = 0.1$ $y = 0.7803x + 20.254$ $r^2 = 0.993$	$\alpha_s = 0.05$ $y = 0.8236x + 21.352$ $r^2 = 0.993$	$\alpha_s = 0.01$ $y = 0.8583x + 22.285$ $r^2 = 0.993$
November (DOY 305 - sunny)	$\alpha_s = 0.2$ $y = 0.6727x + 18.808$ $r^2 = 0.997$	$\alpha_s = 0.1$ $y = 0.7568x + 21.165$ $r^2 = 0.997$	$\alpha_s = 0.05$ $y = 0.7988x + 22.343$ $r^2 = 0.997$	$\alpha_s = 0.01$ $y = 0.8325x + 23.287$ $r^2 = 0.997$
December (whole month)		$\alpha_s = 0.1$ $y = 0.8078x + 17.307$ $r^2 = 0.9954$		$\alpha_s = 0.01$ $y = 0.8886x + 19.041$ $r^2 = 0.9954$

Table 5.2:

Statistical information (r^2 = coefficient of determination,) on the relationship between the measured (x) and simulated (y) net radiation, using different reflection coefficients (α_s) at the forest site.

YEAR	MONTH	REFLECTION COEFFICIENTS		
		$\alpha_s = 0.1$	$\alpha_s = 0.05$	$\alpha_s = 0.01$
1999	June	$\alpha_s = 0.1$ $y = 0.7281x + 44.765$ $r^2 = 0.9249$	$\alpha_s = 0.05$ $y = 0.7686x + 47.256$ $r^2 = 0.9249$	$\alpha_s = 0.01$ $y = 0.8009x + 49.249$ $r^2 = 0.9249$
	July	$\alpha_s = 0.1$ $y = 0.7034x + 39.275$ $r^2 = 0.9077$	$\alpha_s = 0.05$ $y = 0.7425x + 41.46$ $r^2 = 0.9077$	$\alpha_s = 0.01$ $y = 0.7738x + 43.208$ $r^2 = 0.9077$
1999	September	$\alpha_s = 0.1$ $y = 0.7764x + 29.552$ $r^2 = 0.923$	$\alpha_s = 0.05$ $y = 0.8195x + 31.197$ $r^2 = 0.923$	$\alpha_s = 0.01$ $y = 0.854x + 32.512$ $r^2 = 0.923$
	October	$\alpha_s = 0.1$ $y = 0.7495x + 34.476$ $r^2 = 0.9129$	$\alpha_s = 0.05$ $y = 0.7911x + 36.394$ $r^2 = 0.9129$	$\alpha_s = 0.01$ $y = 0.8244x + 37.929$ $r^2 = 0.9129$

The reflection coefficients (1%) used in the simulation of net radiation during the whole period at both the reed and forest sites (Tables 5.1 and 5.2), are low, since the range of shortwave reflectivity for vegetation is generally between 10-30% of solar radiation (Rosenberg *et al.*, 1983 and Monteith, 1976). For example, sugarcane, which is similar in physiognomic structure to *Phragmites*, has reflection coefficients in the order of 22% (McGlinchey and Inman-Bamber, 1996). Shortwave reflectivity for forests range between 11-15%, forests acting as a diffuse reflector, thereby reducing the reflectivity. Low reflection coefficients suggest a well-watered, dark green canopy with low canopy and aerodynamic resistances. The reed site had access to water for most of the year suggesting a low canopy resistance.

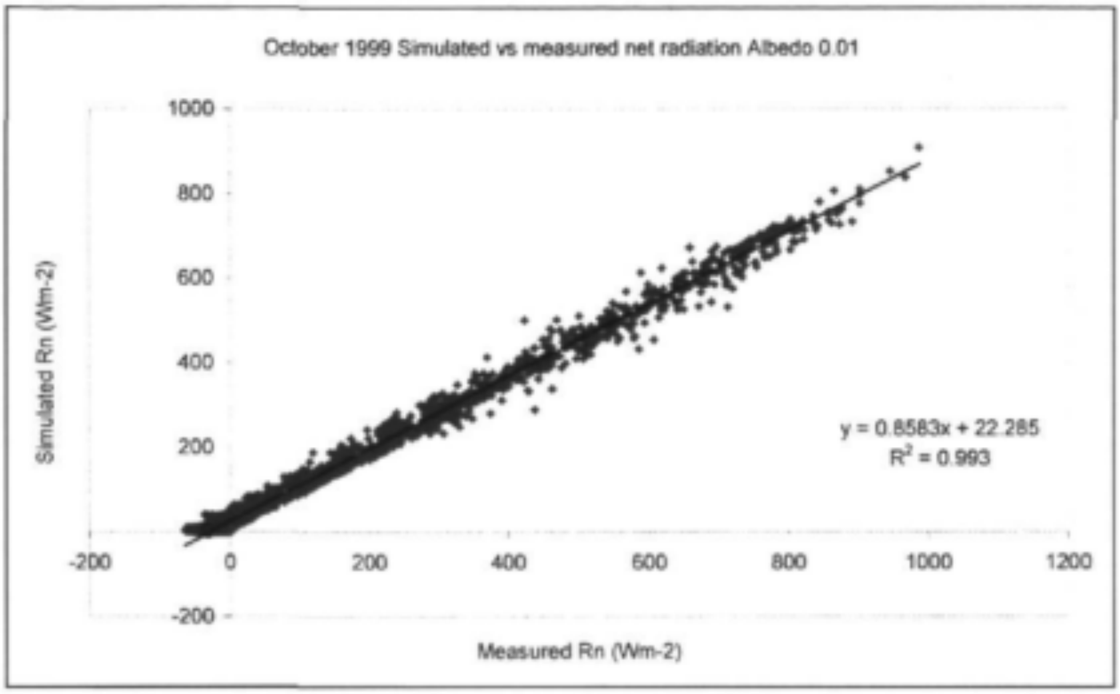

Figure 5.2: Measured *vs.* simulated net radiation at the reed site during October 1999 ($\alpha_s = 0.01$)

However, the statistically significant relationships ($m \rightarrow 1$, $r^2 > 0.99$) found between the measured and simulated net radiation have demonstrated that the net radiation can be modelled accurately utilizing the measured solar radiation and a reflection coefficient of 1%.

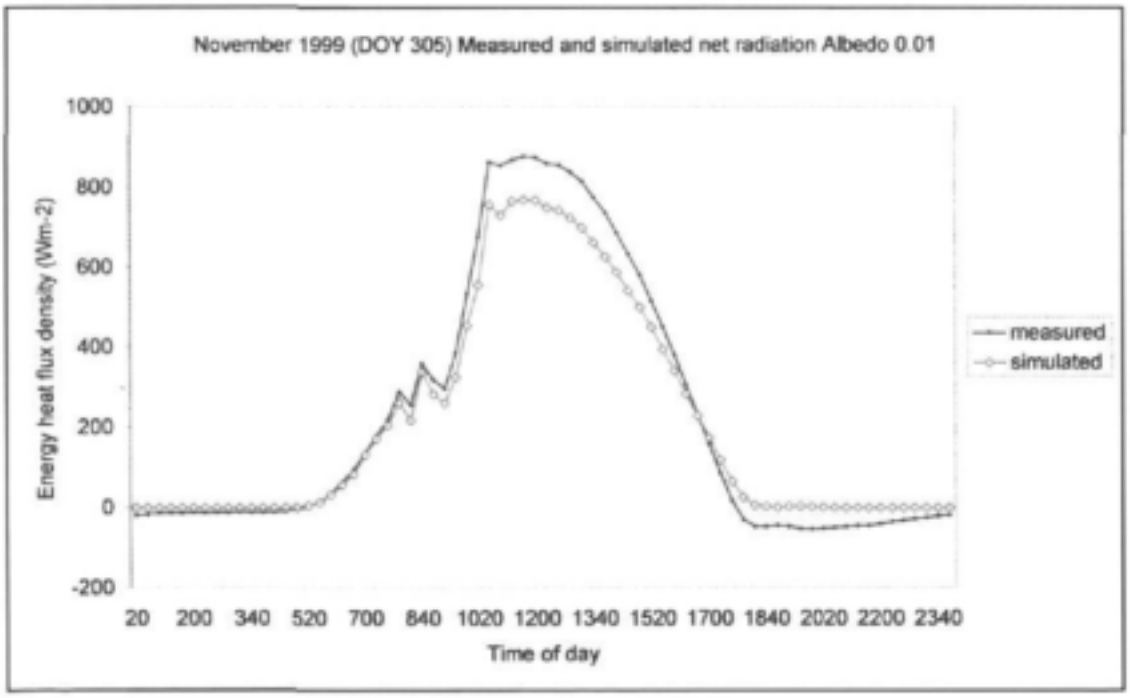

Figure 5.3: Diurnal change of the net radiation measured with a net radiometer, and simulated from solar radiation and a reflection coefficient of 0.01.

5.1.2 *Calculation of the soil heat flux density (Gs) from the simulated net radiation (Rns)*

The soil heat flux density (G) reduces or increases the energy flux density available (R_n - G) for partitioning between the sensible and latent heat flux densities. The soil heat flux density (G_s) was calculated as a fraction of the simulated net radiation (R_{ns}). The accuracy of the calculated soil heat flux density was dependent on (i) the accuracy to which the net radiation was simulated and (ii) the degree to which a linear relationship between the soil heat flux density and the net radiation existed.
Simple linear relationships were found between the soil heat flux density (G) and the net radiation (R_n) for the reed site during summer (January, December). These relationships were derived from typical soil heat flux density to net radiation ratios (G:R_n) (%) (Table 5.3, Figure 5.4). During summer, the soil heat flux density accounted for approximately 8-12 % of the net radiation at the reed site (Table 5.3). This resulted from high leaf area indices and subsequent soil shading. The soil heat flux density was estimated as 10 % of the net radiation. Statistically significant relationships were found between the measured and simulated soil heat flux density (m = 0.97, r^2 = 0.855; m = 0.65, r^2 = 0.8865). The degree to which the soil was shaded by the vegetation, determined the soil heat flux density and the ratio between the soil heat flux density and net radiation. The soil heat flux density is inversely proportional to the amount of direct soil shading. At the reed site, higher leaf area indices during summer resulted in lower soil heat flux densities and subsequently lower G:R_n ratios, compared to winter time, when the reeds were grazed down heavily, and higher soil heat flux densities and G:R_n ratios existed.

During winter, the relationships between the soil heat flux density and net radiation were more complex at the reed site. A large diurnal variation in the soil heat flux density occurred at the reed site (Figure 5.5).

During spring and winter, the soil heat flux density at the reed site contributed significantly to the energy balance and accounted for between 13 and 22% of the net radiation at the reed site, leaving little energy available for partitioning between the sensible and latent heat flux densities (Table 5.3, Figure 5.6a). Little energy was available for evapotranspiration at this site during winter and spring and low evapotranspiration rates were expected (compared to summer). During winter, the soil heat flux density at the reed site was not as dependent on the net radiation as one would expect, and did not closely follow the diurnal curve of net radiation (Figure 5.5). During the period from sunrise until mid-day, the soil heat flux density followed the net radiation reasonably well, but after mid-day, there was a lot of variation in the soil heat flux density. One would therefore expect (i) a non-linear relationship between soil heat flux density and net radiation, or (ii) two relationships – one from sunrise until mid-day and another from mid-day until sunset, to yield a better r^2 than a simple linear relationship. The high variability in the soil heat flux density during winter was probably due to the large spatial variation in the soil heat flux density as a result of differential shading of the two sensors at the lower winter sun angles. The soil heat flux density was simulated as 15 % of the simulated net radiation during spring, and 20 % during winter. The G to R_n ratios calculated as linear relationships, had therefore much lower r^2 values compared to summer (Table 5.3). The relationship between the simulated and measured net radiation was not highly significant (m = 0.54 to 0.84, r^2 = 0.7174 to 0.8545) (Figure 5.6b).

Table 5.3:

Statistical information on the relationship between G (y) and Rn (x) at the reed site, and the relationship between the simulated (y) and measured (x) soil heat flux densities

YEAR	MONTH	STATISTICAL RELATIONSHIPS BETWEEN G And R_n	G: R_n (%)	SIMULATED (y) vs MEASURED (x) SOIL HEAT FLUX DENSITY	COMMENT
1999	January	y = 0.0803x – 16.455 r^2 = 0.855	8.0	y = 0.9706x + 20.58 r^2 = 0.841	Use G:R_n as 10 % in simulation
	May	y = 0.2037x – 34.234 r^2 = 0.6534	20.4		Doesn't follow smooth Rn curve – a lot of spikes
	June	y = 0.2153x – 27.548 r^2 = 0.7217	21.5	y = 0.5433x + 23.685 r^2 = 0.7174 (20 %) y = 0.6791x + 29.606 r^2 = 0.7174 (25 %) y = 1.0865x + 47.37 r^2 = 0.7174 (40 %)	DOY 167 to 168 (20, 25 and 40 %)
		y = 0.2162 x – 25.76 r^2 = 0.7436	21.6	y = 1.1585x + 46.086 r^2 = 0.7437 y = 0.5793x + 23.043 r^2 = 0.7437 y = 0.8689x + 34.565 r^2 = 0.7437	DOY 168 (40, 20 and 30 %)
	September	y = 0.1413x – 16.433 r^2 = 0.8627	14.1	y = 1.0396x + 23.808 r^2 = 0.8717 (20 %) y = 0.7797x + 17.856 r^2 = 0.8717 (15 %)	Simulation with 15 and 20 % ratios
	October (DOY 288-299)	y = 0.132x – 21.762 r^2 = 0.8683	13.2	y = 1.0254x + 33.845 r^2 = 0.8626 (18 %) y = 0.8545x + 28.204 r^2 = 0.8626 (15 %)	Using different G:R_n ratios – 18 and 15 % Still two equations – morning, afternoon might be better OR Non-linear relationship
1998	December	y = 0.1199x – 21.054 r^2 = 0.8894	11.99	y = 0.6591x + 17.512 r^2 = 0.8856	Use G:R_n as 10 % in simulation
	Winter		20		
	Spring		15		
	Summer		10		

During Spring (September, October) at the forest site, the soil heat flux density followed the increasing trend of the net radiation until midday, after which the soil heat flux density quality became negative, once the net radiation started to decrease. This diurnal pattern made a simple $G{:}R_n$ relationship difficult to obtain (Figure 5.7). This meant that during the period from sunrise to midday, the soil heat flux density reduced the energy flux density available for partitioning between H and λE, but after midday, increased the available energy flux density. A simple linear relationship was calculated between the soil heat flux density and the net radiation for the sunrise-to-midday period (Table 5.4), and applied to the whole day. A $G{:}R_n$ ratio of 4 % was used in the simulation of the soil heat flux density. Statistically significant relationships were subsequently found between the measured and simulated soil heat flux density (m = 0.8286, $r^2 = 0.934$; m = 1.0894, $r^2 = 0.9719$) (Table 5.4).

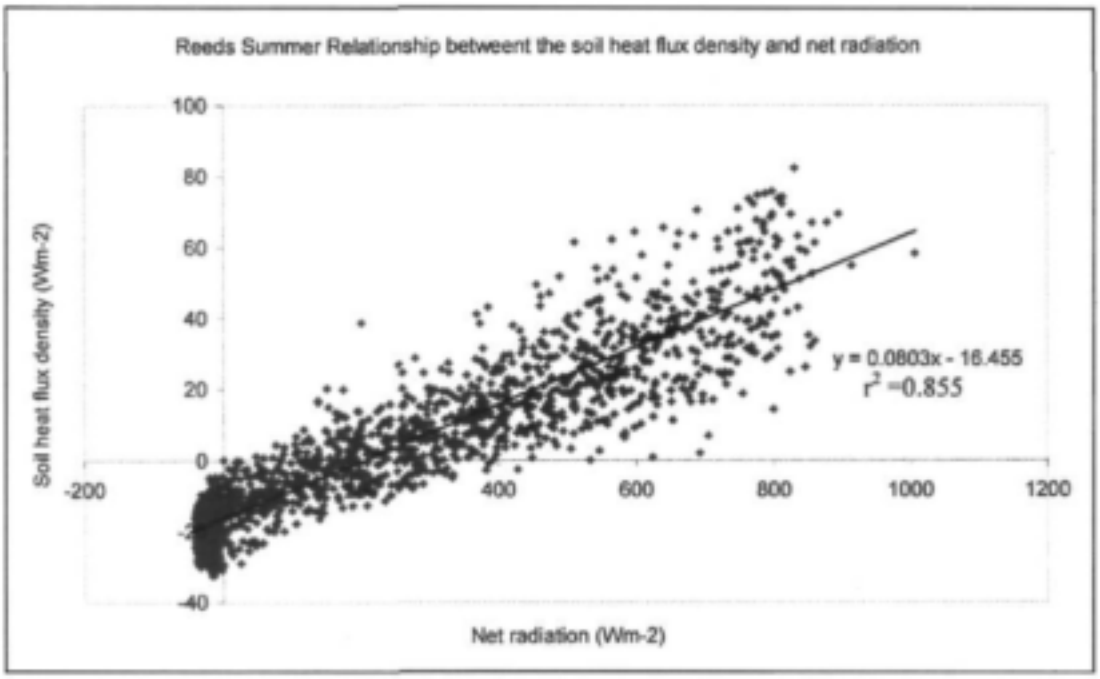

Figure 5.4: Relationship between the soil heat flux density and net radiation at the reed site during summer

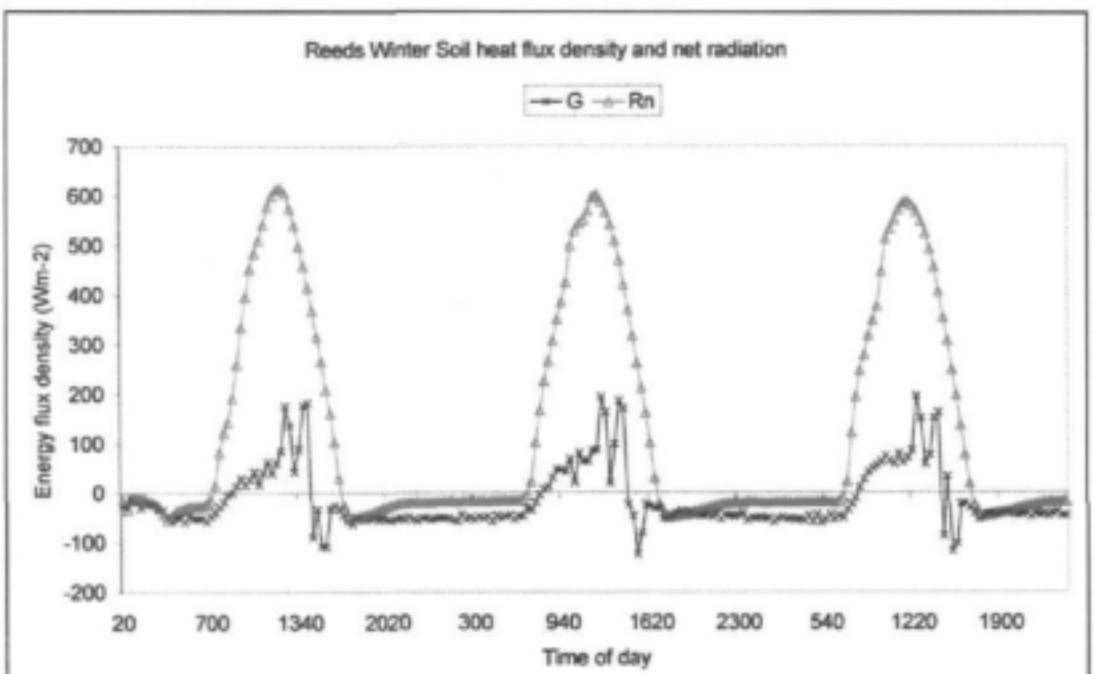

Figure 5.5: Diurnal variation in the net radiation and soil heat flux density during winter at the reed site

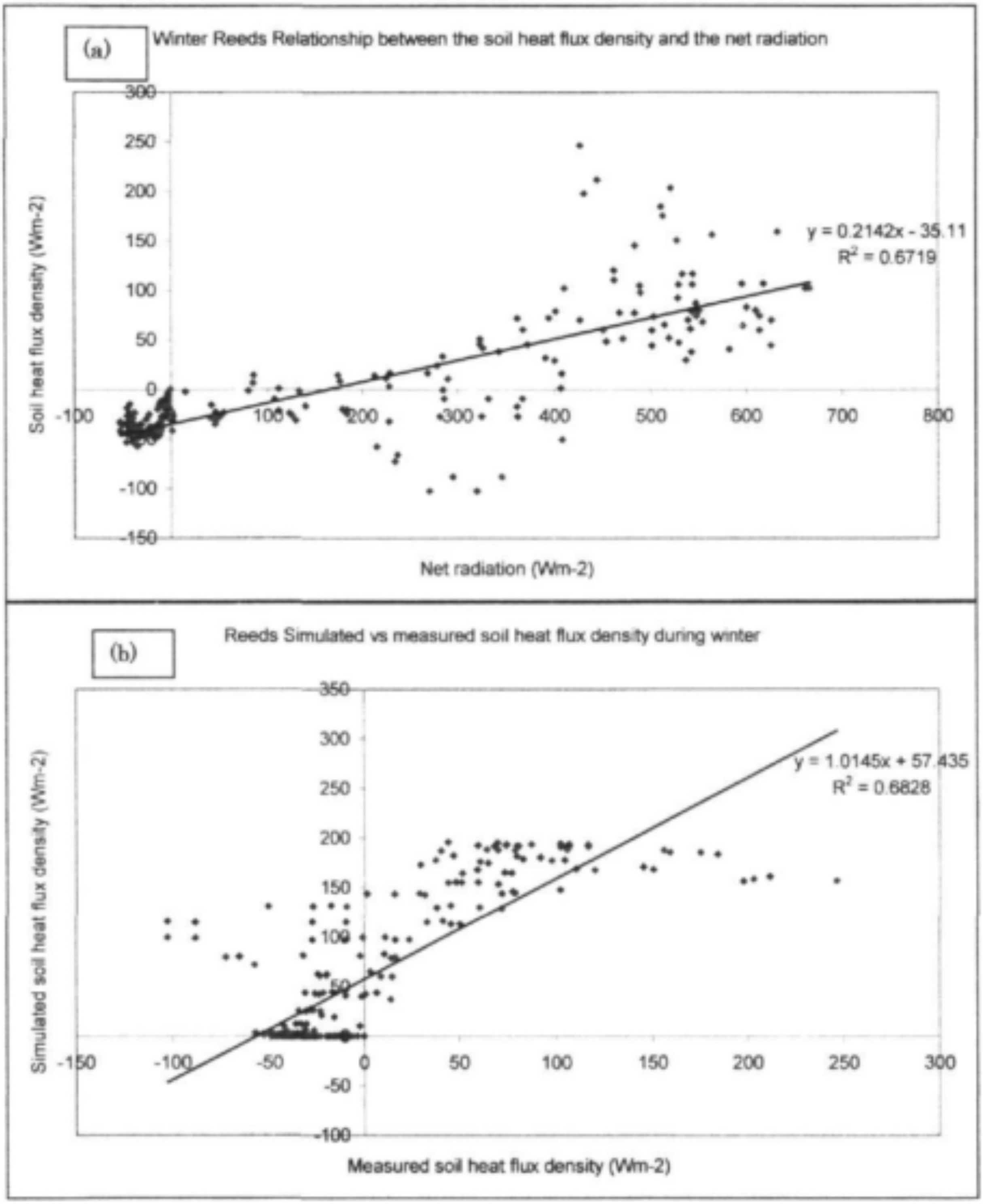

Figure 5.6: Relationship between (a) the soil heat flux density (y) and the net radiation (x), and (b) the relationship between the simulated (y) and measured (x) soil heat flux density during winter at the reed site

Table 5.4:

Statistical information on the relationship between the soil heat flux density (y) and net radiation (x) at the forest site

YEAR	MONTH	G: Rn	G: Rn (%)	SIMULATED (y) *vs* MEASURED (x) SOIL HEAT FLUX DENSITY	COMMENT
1999	September (DOY 268)	$y = 0.039x - 0.0905$ $r^2 = 0.9346$	3.9	$y = 0.8286x + 1.5154$ $r^2 = 0.934$	Sunrise to midday values Use 4 % in simulation
	October (DOY 284)	$y = 0.0313x + 3.4617$ $r^2 = 0.9659$	3	$y = 1.0894x - 1.6746$ $r^2 = 0.9719$	Sunrise to midday Use 4 % in simulation
	Summer		4		

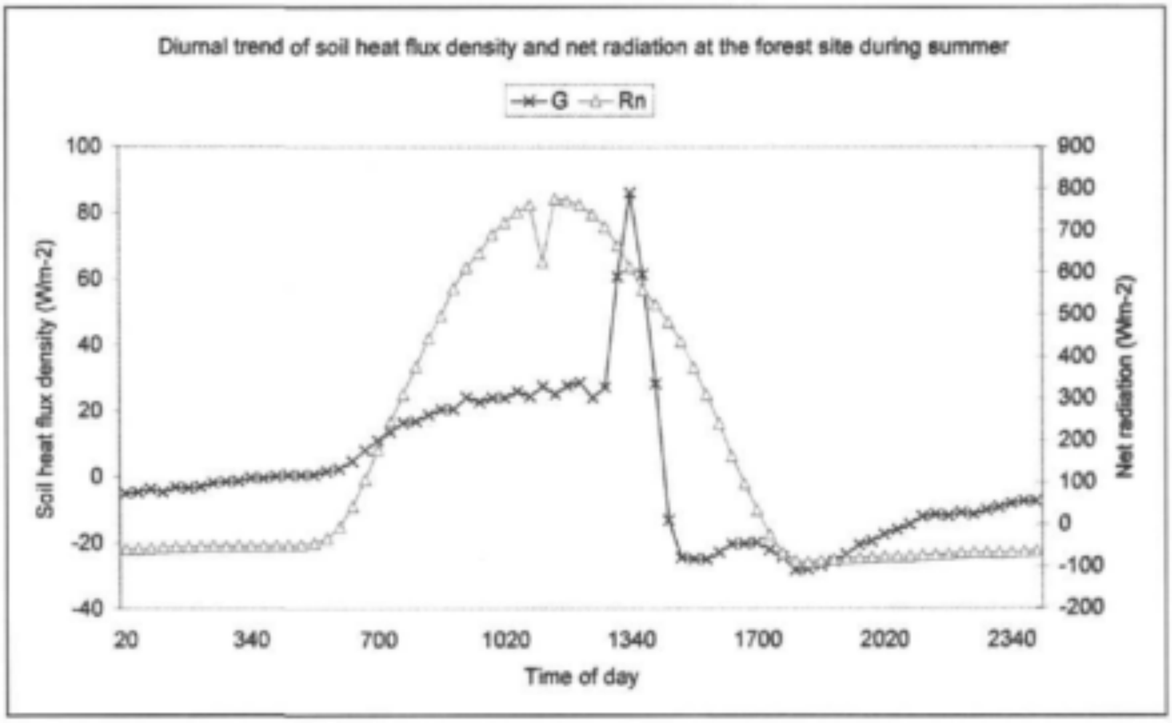

Figure 5.7: Diurnal trend of the soil heat flux density and net radiation during summer at the forest site

Using the above relationships between the soil heat flux density and net radiation, it was possible to model soil heat flux densities and available energy values for input into the canopy-specific Penman-Monteith equations. This approach was considered more accurate than the generally accepted procedure of reducing the net radiation by 10% to obtain the available energy.

5.1.3 Total canopy specific Penman-Monteith evapotranspiration

The Penman-Monteith equation has been successfully applied to estimate evapotranspiration from different crops (Slabbers, 1977; McGlinchey and Inman-Bamber, 1996) and from forests (Calder, 1977; Everson, 1995). Although the Penman-Monteith equation is complex, it is extremely flexible and widely applicable, particularly in modelling studies where it is necessary to predict the water balance of plant communities under different conditions. The Penman-Monteith equation requires detailed climatic data (net radiation, air temperature, water vapour pressure and windspeed) and aerodynamic and canopy resistance data (not easily available), possibly limiting the use of this equation primarily to research applications. It is possible to estimate net radiation from data collected from an automatic weather station. The aerodynamic resistance (r_a) is calculated from knowledge of average canopy height and windspeed. The canopy resistance (r_c) is not easily obtained and therefore canopy specific studies are required to understand how it varies on a seasonal basis. The canopy resistance can be obtained, by back calculating the canopy resistance in the Penman-Monteith equation, using the Bowen ratio evapotranspiration estimates. The canopy resistance can also be obtained by varying the canopy resistance in the Penman-Monteith equation, to establish the best linear relationship between the Bowen ratio and the Penman-Monteith evapotranspiration estimates. The canopy resistance essentially allows for the difference between the potential and the actual evapotranspiration from canopies.

Statistically significant linear relationships were found between the 20 minute measured (Bowen ratio) and simulated (canopy specific Penman-Monteith) total evapotranspiration estimates at the reed site during summer. During December and January (summer), a canopy resistance of 50 sm^{-1} resulted in the best linear relationship between the measured and simulated evapotranspiration ($m = 0.9804$, $r^2 = 0.8698$; $m = 1.0523$, $r^2 = 0.9002$) (Table 5.5 and Figures 5.8 and 5.9). When back calculating the canopy resistance for summer at the reed site, the daily canopy resistance varied around 50 sm^{-1}, which provided the best fit between measured and simulated evapotranspiration (Figure 5.10).

The evapotranspiration simulated at the reed site during December, was accumulated over a 29-day period (Figure 5.11). A very close agreement was found between the measured (Bowen ratio evapotranspiration, BET) and the simulated (Penman-Monteith evapotranspiration, PMET (R_n,G_{sim})), with totals of 176.7 mm and 178 for BET and PMET (R_n,G_{sim}) respectively.

Table 5.5:

Statistical information of the relationship between the measured (Bowen ratio) (x) and simulated (canopy specific Penman-Monteith) (y) evapotranspiration.

	REEDS	FOREST
January	$y = 1.0523x + 0.0054$, $r^2 = 0.9002$ $r_c = 50\ sm^{-1}$	
May	$y = 0.9521x - 0.002$, $r^2 = 0.9317$ $r_c = 50\ sm^{-1}$ (DOY 139) BET = 4.83 mm/day PMET = 4.46 mm/day	
June	$y = 0.3377x + 0.009$, $r^2 = 0.9194$ $r_c = 50$ sm-1 (DOY 158 – Highly overestimating – back calculating suggest $rc \approx 50\ sm^{-1}$) $y = 0.4749x + 0.0019$, $r^2 = 0.902$ $r_c = 10$ sm-1 $y = 0.5224x + 0.0026$, $r^2 = 0.8874$ $r_c = 1$ sm-1	
September	$y = 1.0207x + 10.0105$, $r^2 = 0.8556$ $r_c = 50\ sm^{-1}$ (DOY 270)	$y = 1.0245x + 0.0445$, $r^2 = 0.7534$ $r_c = 30\ sm^{-1}$ questionable ??
October	$y = 0.9876x + 0.0121$, $r^2 = 0.8831$ $r_c = 30sm^{-1}$ DOY 282	$y = 1.0231x - 0.0059$, $r^2 = 0.8592$ $r_c = 100\ sm^{-1}$ DOY 267 to 304
December	$y = 0.9804x + 0.0023$, $r^2 = 0.8698$ $r_c = 50\ sm^{-1}$	
Winter	$r_c = 50\ sm^{-1}$	
Spring	$r_c = 30$ to $50\ sm^{-1}$	$r_c = 100\ sm^{-1}$
Summer	$r_c = 50\ sm^{-1}$	$r_c = 100\ sm^{-1}$

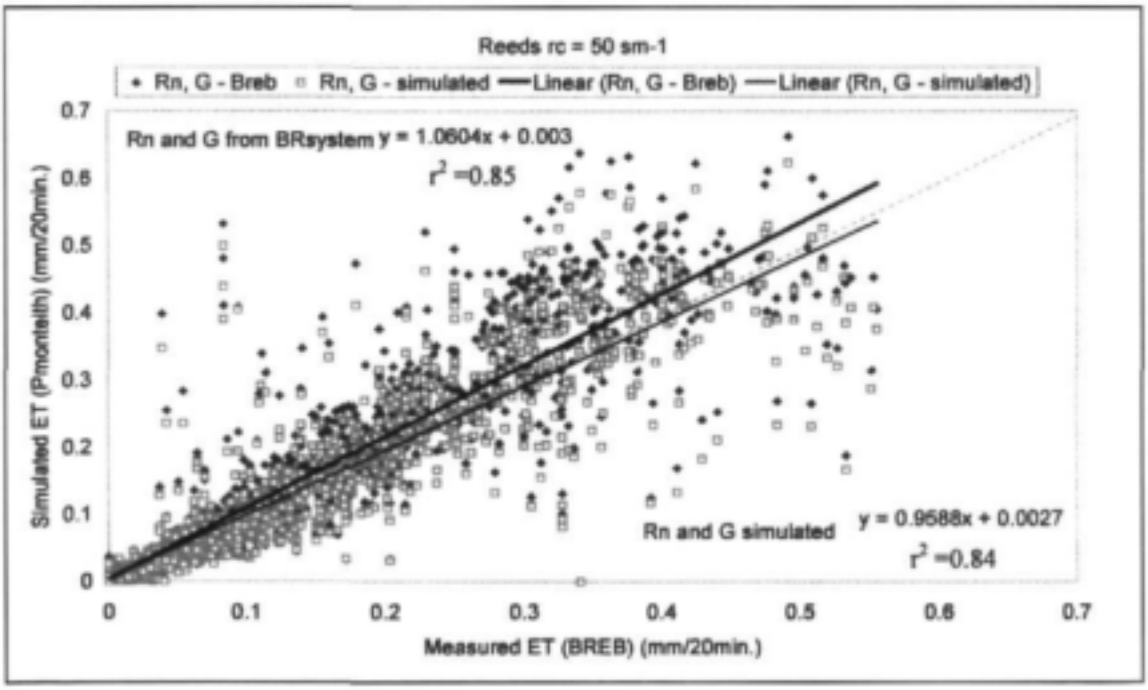

Figure 5.8: Bowen ratio (BREB) vs. canopy specific Penman-Monteith evapotranspiration (PMET) at the reed site

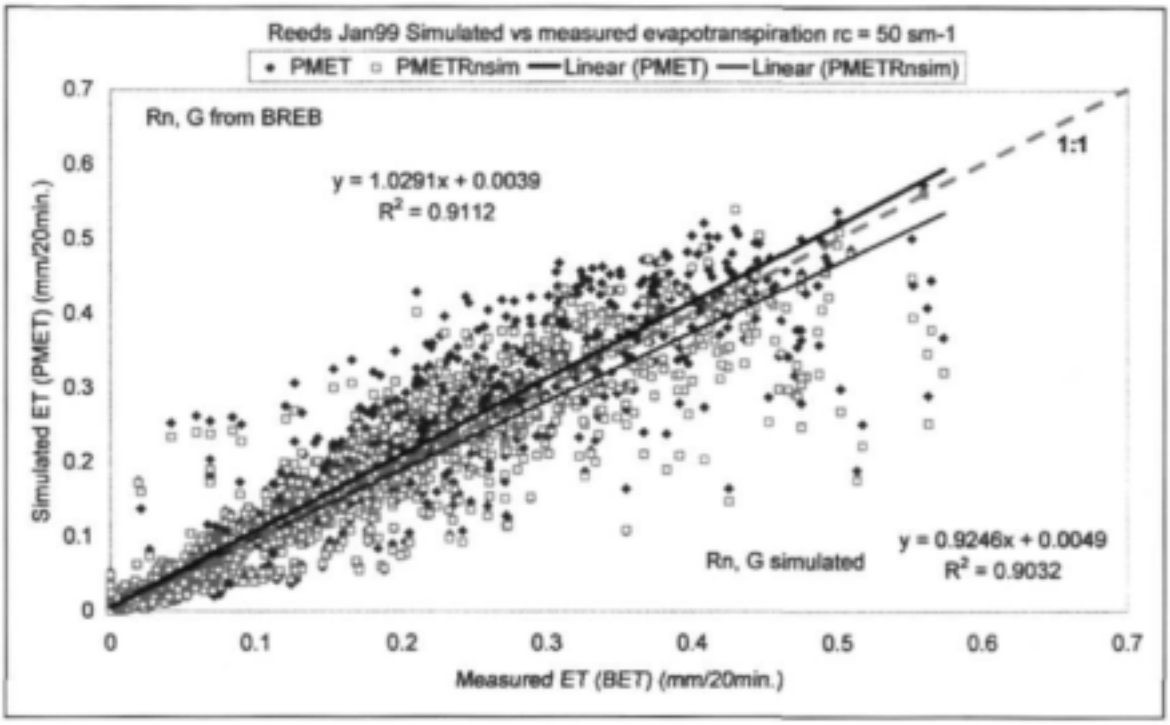

Figure 5.9: Bowen ratio (BET) vs. canopy specific Penman-Monteith (PMET) evapotranspiration at the reed site during January (30 days - summer)

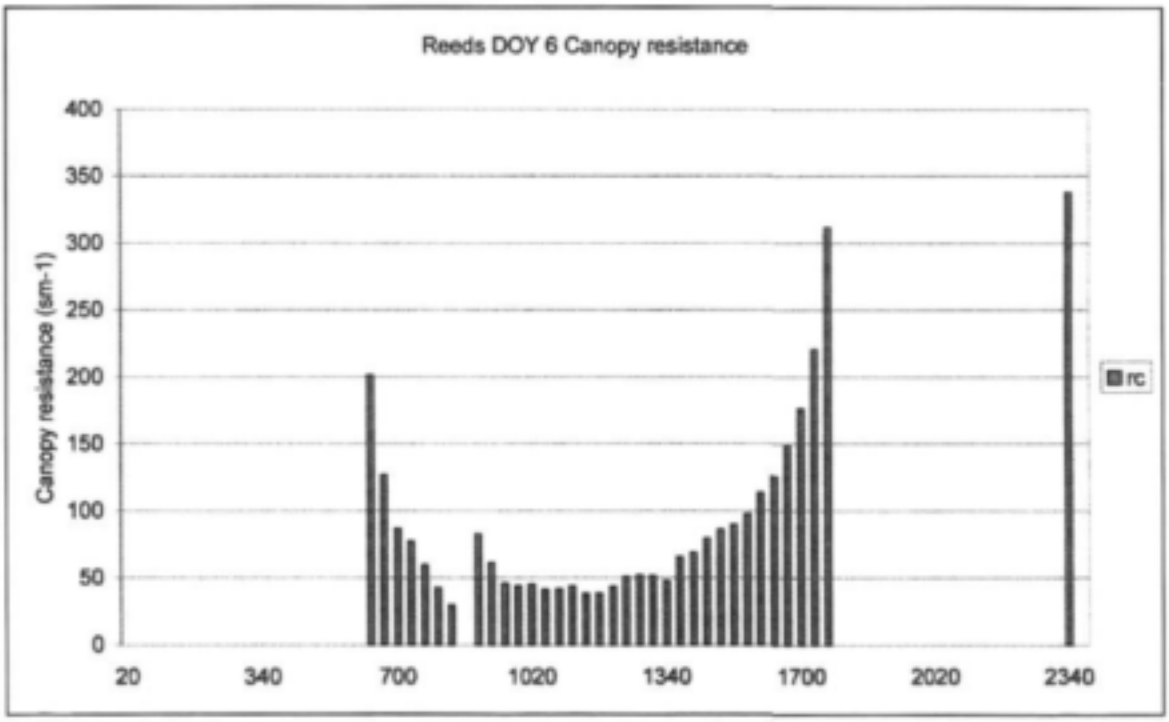

Figure 5.10: Canopy resistance back calculated from the Bowen ratio evapotranspiration data and Penman-Monteith equation during summer at the reed site

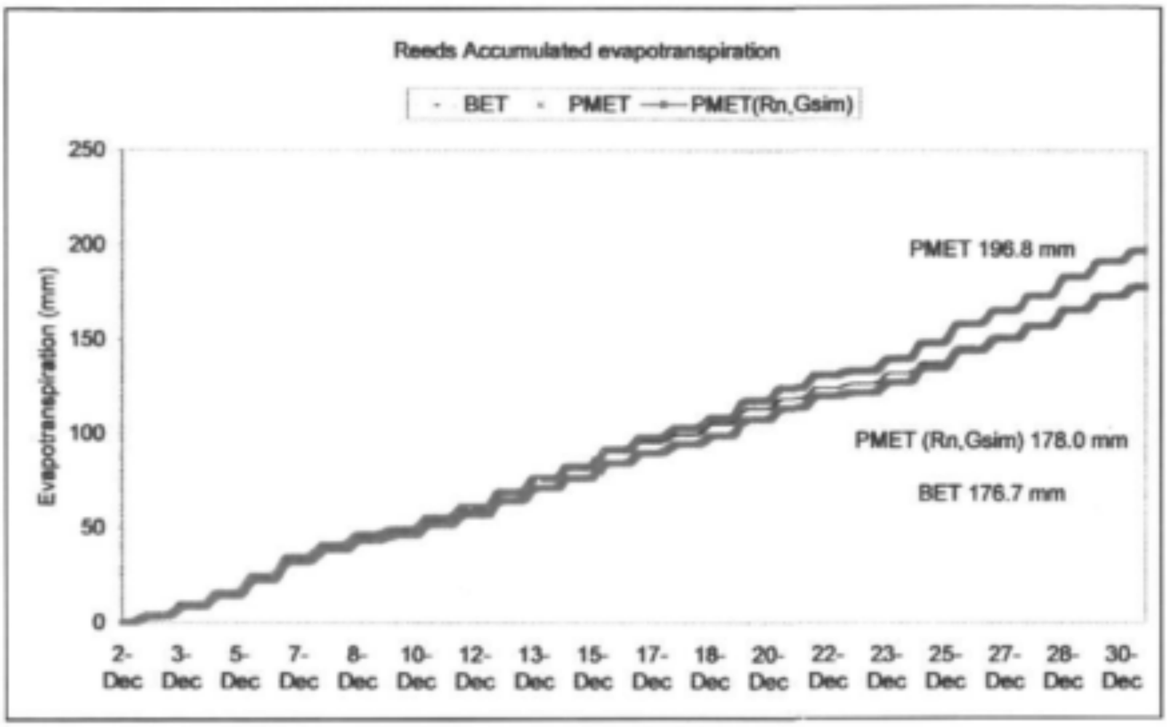

Figure 5.11: Accumulated simulated and measured evapotranspiration over a 29 day period in December

Toward the end of autumn (May) and during winter (June), the net radiation was lower and the soil heat flux density and canopy resistance higher than during summer. A statistically significant relationship was found between the simulated and measured evapotranspiration during autumn, using a canopy resistance of 50 sm^{-1} ($m = 0.95$, $r^2 = 0.93$) (DOY 139) (Table 5.5). However, a poor relationship ($m<<1$) was found between the simulated (canopy specific Penman-Monteith) and measured (Bowen ratio) evapotranspiration during winter, utilizing a canopy resistance of 50 sm^{-1} ($m = 0.34$, $r^2 = 0.90$) (Table 5.5). This relationship shows significant underestimating of evapotranspiration. The canopy resistance back calculated varied around 50 sm^{-1}. The poor relationship between the simulated and measured evapotranspiration may be due to the underestimation in the simulation of the net radiation and soil heat flux density (Tables 5.1 and 5.3).

During spring (DOY 270 and 282), the canopy resistance back calculated from the Bowen ratio estimates with the Penman-Monteith equation, varied between 20 sm^{-1} and 90 sm^{-1}. In the simulation of the evapotranspiration with the Penman-Monteith equation, a highly significant relationship was established using a canopy resistance 50 sm^{-1} (DOY 270) ($m = 1.02$, $r^2 = 0.86$) and on DOY 282 with a canopy resistance of 30 sm^{-1} ($m = 0.99$, $r^2 = 0.88$).

During spring, the accuracy of the simulation of evapotranspiration was tested by using the net radiation and simulated soil heat flux density, and by applying different canopy resistances. A decrease in the canopy resistance (r_c = 150 sm^{-1} to 100 sm^{-1}) resulted in a slope between the measured and simulated evapotranspiration approaching 1 (0.73 to m = 1.02), whereas the coefficient of determination did not change significantly (0.8619 to 0.8592) (Figure 5.12, Table 5.5).

The evapotranspiration values simulated at the reed (r_c = 50sm^{-1}) and forest (r_c = 100 sm^{-1}) sites were accumulated over a 31-day period (October). The accumulated evapotranspiration total is a mere 136 mm for the reeds and 117 mm for the forest, a difference of 19 mm, which equals to a daily average difference of 0.61 mm (Figure 5.13).

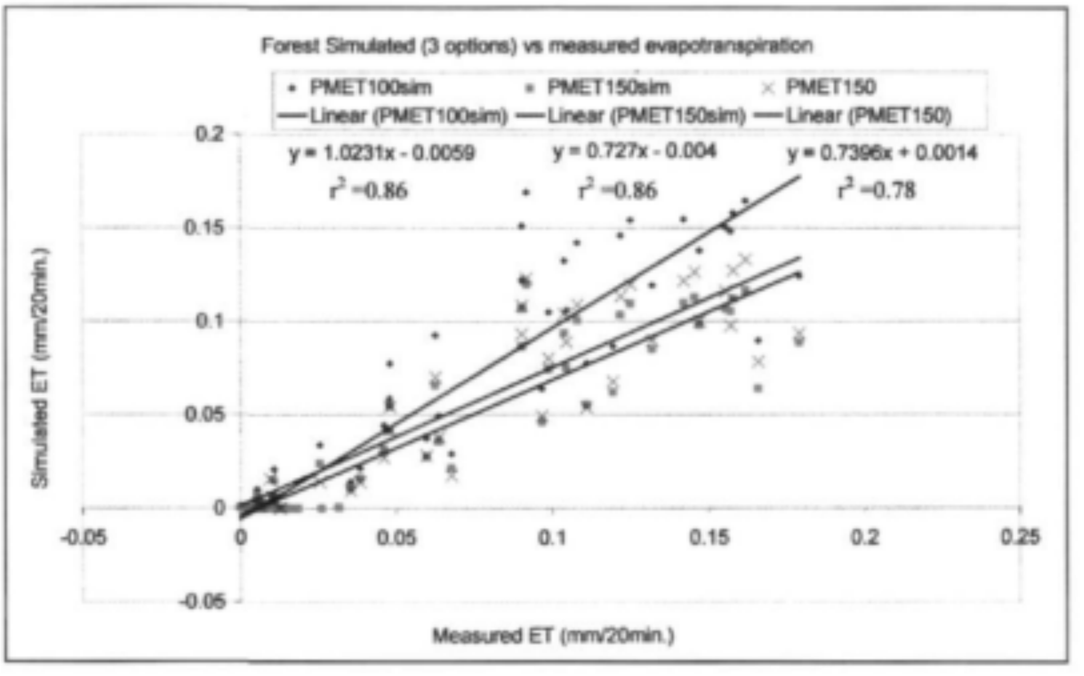

Figure 5.12: Bowen ratio (X) vs. canopy specific Penman-Monteith (Y) evaporation at the forest site during summer (DOY 267 to 304)

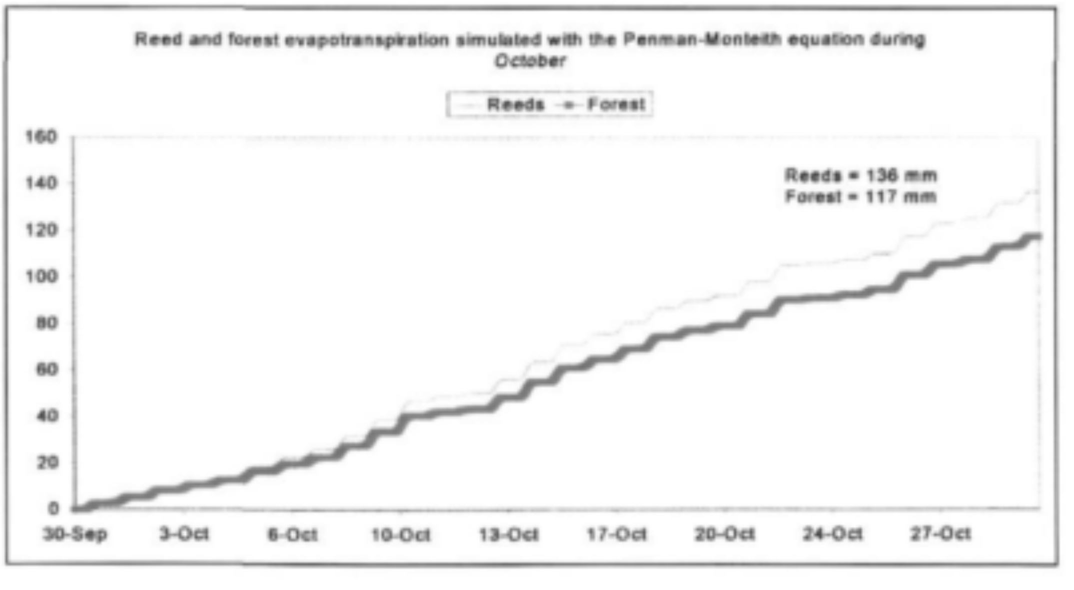

Figure 5.13: Accumulated Penman-Monteith evapotranspiration at the reed and forest sites for 31 days (October)

6. LOW FLOW VERIFICATION STUDY

6.1 The Sabie river riparian water balance

The length of the Sabie River in the Kruger National Park is 105 km and extends from Albasini trading station in the west to the Mozambique border in the east. The principal consumptive water users along this portion of the river include abstractions for irrigation between Albasini and Kruger Gate, abstractions for irrigation and domestic supply for communities within the KNP, animal consumption (negligible), and the focus of this report: evapotranspiration.

In the phase I project it was shown that evapotranspiration contributes significantly to consumptive water use. The long term (1960 to 1995) average Symons pan annual evaporation recorded at Skukuza was reported to be 1572 mm (4.3 mm day^{-1}). The riparian zone along the Sabie River is in places 500 m wide. Assuming a riparian zone of 3114 hectares in extent (data from Bredenkamp *et al*, 1991) and potential evaporation equal to S-pan evaporation, Birkhead *et al*., 1997, estimated a consumptive water use of 134 000 m^3 day^{-1} (1.54 m^3s^{-1}), thirteen times the water abstracted for domestic use within the KNP. Transmission losses from phase I (only 16 months data) ranged from 0.24 m^3s^{-1} to 0.43 m^3s^{-1} for mean monthly discharges during low flow periods.

The objective of this part of the study was to compare (verify) estimates of the total water use of the vegetation in the riparian zone using the evapotranspiration data from the previous section and to compare it with the actual flow losses between the Skukuza and Lower Sabie weirs.

6.2 Vegetation analysis

6.2.1 Study site

A length of the Sabie River within the boundaries of the Kruger National Park was identified. This began at the upstream Skukuza weir (X3H021) and extended approximately 55 km downstream to the Lower Sabie weir (X3H015) below Lower Sabie camp.

6.2.2 Method

Aerial photographs (scale 1:10 000) for this stretch of the river were obtained from the National Parks Board. For the purposes of the vegetation analysis only the central 60% of each photograph was utilised in order to eliminate distortion. An overhead transparency corresponding to the dimensions of the photograph was overlaid onto each photograph and only the area of river falling within the delineated zone was analysed.

A series of belt transects perpendicular to the flow direction and stretching from bank to bank within the riparian zone were used to analyse the vegetation composition along the river. Starting at the upstream weir, transects were marked off at 1 cm intervals on the photographs which corresponded to every 100 m on the ground. This resulted in a total of 556 transects between the two weirs. The start and end points of each transect (i.e. the northern and southern extremes of the riparian fringe) were estimated by eye and with the aid of a stereoscope and marked accordingly. The three-dimensional effect of the stereoscope enabled the banks of the river to be located as well as the differences between tall lush trees and the drier scrub on the flatter areas. The analysis of the vegetation composition along each transect was carried out by means of an overhead transparency, carrying a 1 mm x 1 mm grid, overlaid along the length of the transect beginning at the southern edge of the riparian zone and extending to the northern most point (Figure 6.1).

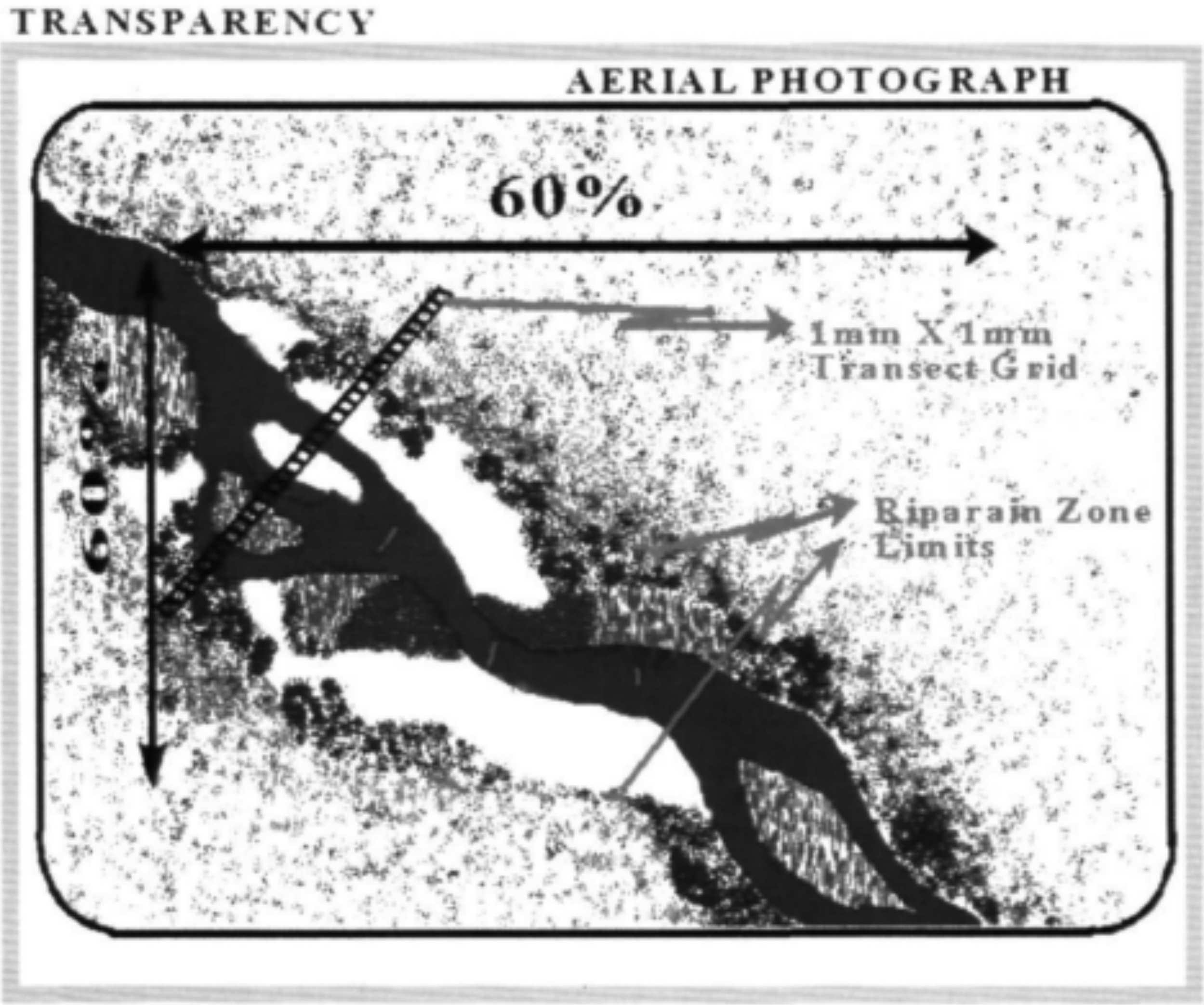

Figure 6.1: Graphical representation of the technique employed to analyse transects across the Sabie River

The predominant vegetation (± 50%) within each 1 mm x 1 mm grid cell was assigned to one of six categories, namely: forest, reeds, sand, water, scrub and rock. The data for each transect were entered into a spreadsheet using a different symbol to represent each category of cover, and totals for each category within each transect were obtained. These totals were subsequently scaled up to represent the region between transects. This simply involved multiplying the transect values by 10 to represent the 10 mm grid cells between each transect. The spatial distribution along the river together with the relative areas under each category of land cover is represented in Figure 6.2. Forests (511 ha - 38%) and reeds (297 ha - 22%) were the dominant vegetation types accounting for 60 % of the vegetation.

6.3 River gauging study

After identification of the length of the Sabie River to be utilised in this study (between the upstream and downstream weirs), eight years of flow data (1990-1998) for these weirs were analysed together with volumes of water abstracted for domestic and animal requirements (Gertenbach 1985 in Birkhead *et al.* 1977). Between the upstream Skukuza weir (X3H021) and the downstream Lower Sabie weir (X3H015), the Sand River joins the Sabie River as a tributary. The resultant additional flow into the Sabie River forms a significant component of the total volume and flow data for this addition were obtained from weir X3H008.

Transmission losses were estimated for the low flow period since this is the critical period in terms of water shortage. Although summer flows are equally important for determining the ecological reserve, the data were not reliable due to over-topping of the weirs, which caused regular loss of data.

Average transmission losses between the weirs in the low flow period (May to September) ranged from 0.26 $m^3 s^{-1}$ (0.68 million litres) in May to 0.41 $m^3 s^{-1}$ (1.06 million litres) in August at the end of the dry period (Figure 6.3). The results were similar to those reported in the previous study, where mean monthly transmission losses ranged from 0.26 to 0.49 $m^3 s^{-1}$.

Using the vegetation areas from Figure 6.2 and the water use of the reeds and trees as determined in this study, it was possible to calculate the expected losses due to the riparian vegetation (Figure 6.3). Open water losses were estimated using the Penman open water equation. In this exercise the tree transpiration rate was set at 2.5 and 3.1 mm day^{-1} for winter and summer respectively (see previous section). The reed transpiration was fixed according to the monthly means measured for the reed site. Scrub was not considered a component of the phreatic zone and both rock and sand were considered non-evaporating surfaces.

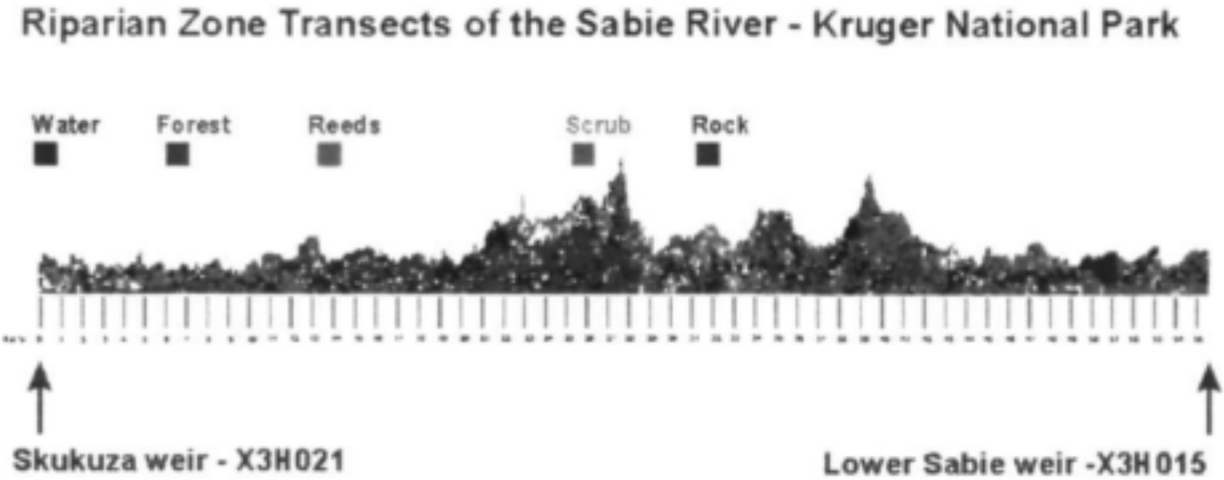

LAND COVER CATEGORY							
	Forest	Reeds	Sand	Water	Scrub	Rock	Total
Relative Cover (%)	38.38	22.02	11.88	14.38	11.64	1.71	100.00
Actual Area (ha)	511.9	293.7	158.4	191.8	155.2	22.8	1333.8

Figure 6.2: The distribution of riparian vegetation along a 60 km section of the Sabie River (from Skukuza to Lower Sabie).

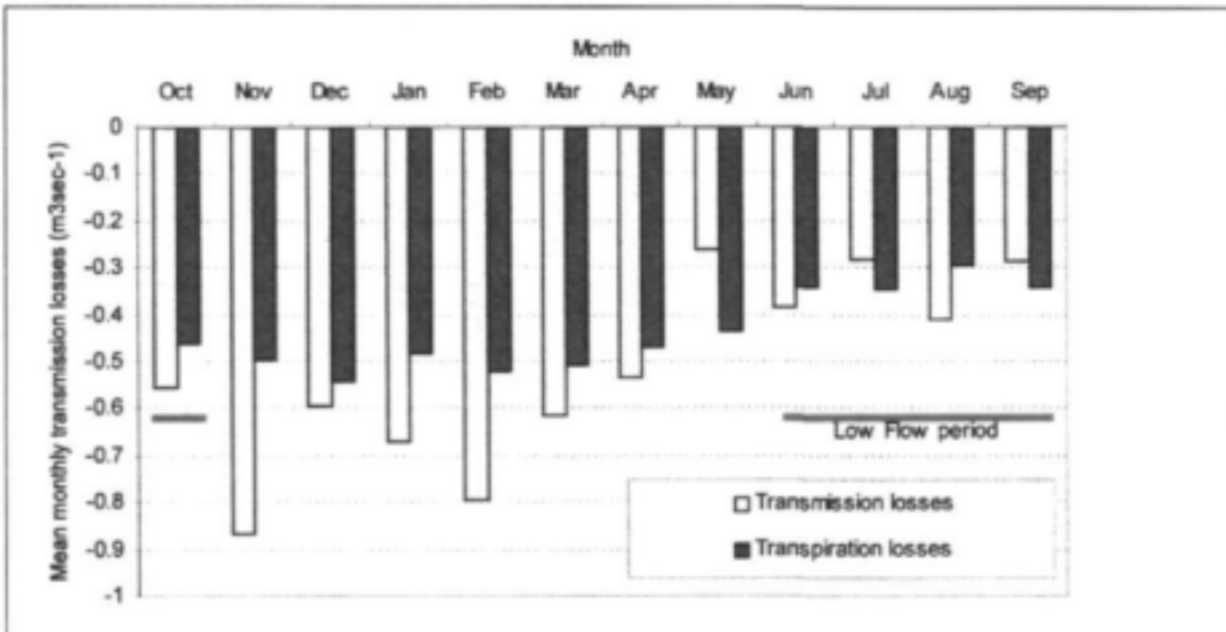

Figure 6.3: Mean monthly transmission losses and estimated riparian vegetation losses for a 55 km section of the Sabie River in the KNP.

One of the problems in gauging studies is the inherent inaccuracy involved in measuring stream flow from stage level for low discharges over gauging structures with wide crests. Nevertheless, in this study estimates of the water use of the vegetation for the low flow period (0.32 $m^3 s^{-1}$) were in close agreement with the values recorded from the gauging study (0.35 $m^3 s^{-1}$) (Figure 6.3).

Deviations between the monthly values were in the order of ±20% between June and September. This accuracy is acceptable since the transmission losses were estimated from three different weirs (i.e. some of the errors could be additive), abstractions were based on 1985 data (no recent data were available), and the gauging data were averages for the eight years prior to this study, compared with two seasons for the evapotranspiration data. The evapotranspiration losses were, however, consistent with the gauging data and lend credibility to the riparian evapotranspiration data collected in this study. Although gauging data are useful predictors of total transmission losses, they do not allow the individual components (vegetation, rock etc) to be estimated.

In the high flow period, the annual trend (monthly averages) in discharge from the Lower Sabie weir, together with the riparian transmission losses showed that the normal summer flow of 10 to 18 $m^3 s^{-1}$ was much greater than the maximum riparian water use of 0.54 $m^3 s^{-1}$ (December) (Figure 6.4). This can be contrasted to the low flow period when the water use of the vegetation represents a much higher proportional of the streamflow. The months of September and October appear to be the most critical, when the flow rate is still low (average = 3.4 $m^3 s^{-1}$) and the transmission losses are at their highest (0.48 $m^3 s^{-1}$). The flow rate would therefore be about 15% higher without the influence of the vegetation. These data support the observations from phase I, where it was concluded that transpiration during the low flow period declines much less than the river discharge rate, evapotranspiration from the riparian vegetation constituting a large proportion of the discharge through the winter months.

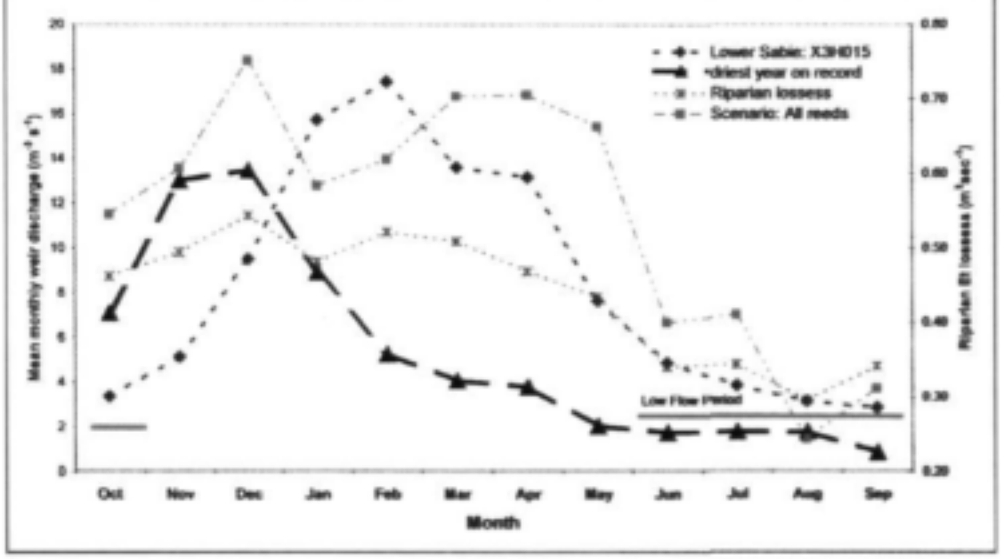

Figure 6.4 Stream discharge and transmission losses for a 60 km section of the Sabie River. Also shown is the impact on the transmission losses of converting all the forest to reeds.

One of the major concerns of managers within the KNP is the possible impact that increased sedimentation will have on the distribution of vegetation along rivers within the boundaries of the KNP. One scenario is that the area of reeds will increase at the expense of the forests. Large floods may also effect changes in the balance of reeds and trees. There are also large stretches of rivers outside the KNP, where destruction of riparian forests is resulting in a shift to more reed-dominated communities. This scenario was simulated by estimation of the riparian transpiration losses assuming that reed communities replaced all the forests. During the non-critical summer period the evapotranspiration losses due to this vegetation change increased by up to 50%. For example, in April the riparian evaporative loss increased from 0.47 to 0.71 $m^3 s^{-1}$. By contrast during the low flow months of August and September the evapotranspiration loss was less for the reed scenario than for the estimated real losses. This result is due to the higher tree than reed transpiration at this time of the year. These results illustrate how an understanding of the water use by different plant communities during the different seasons can be used for predicting transmission losses due to vegetation change.

In very dry years the riparian losses are the same order of magnitude as the streamflow. Thus any upstream landuse changes (i.e. increased agricultural activity) could result in no stream flow in the Sabie River. Such changes would ultimately impact negatively on the physical condition of the riparian forests through high levels of water stress. The incorporation of the knowledge obtained in this study on the seasonal evapotranspiration rates from the two major plant communities will ultimately give managers a more accurate estimate of required river flows for maintenance and/or determination of the ecological reserve. Such knowledge will need to be included into existing hydrological models.

7. DISCUSSION, LINKAGES TO RIVER MANAGEMENT AND CONCLUSIONS

7.1 Discussion

Bowen ratio evapotranspiration data provided direct, reliable estimates of evapotranspiration rates for the two dominant riparian communities growing along the Sabie River in the Kruger National Park. Not surprisingly, the results showed that regardless of season, the evapotranspiration flux was a significant term in the energy balance of both sites, accounting for more than 50% of the available energy. When expressed as a mass/depth of water using the simple conversion that 1 mm evaporation equals 2.45 MJ m^{-2} day^{-1}, it equates to summer daily averages of 4.8 mm day^{-1} and 3.1 mm day^{-1} at the reed and forest sites respectively. This is approximately 1 mm day^{-1} higher than the winter values for reeds and 0.6 mm day^{-1} for the forest site. Reed evapotranspiration therefore exceeded tree evapotranspiration for most of the study period. An important exception was during August and September (the critical low flow period) when the tree water use was greater than the reed water use, resulting from the water table dropping below the reed root zone (or possibly by physiological constraints imposed by the winter conditions). Reed transpiration at this time was less than 2 mm day^{-1}. The evapotranspiration rates of reeds, which are permanently inundated with water, may therefore be different. This is an area that requires further research.

In systems dominated by tall vegetation, the aerodynamically rough nature of the vegetation enhances convective fluxes, resulting in more efficient transport of latent and sensible heat fluxes away from the canopy (Price, 1994). When plants are adequately supplied with water, the evapotranspiration rates remain high, as the increased sensible heat fluxes increase air temperatures and vapour pressure deficits. This provides a positive feedback on evapotranspiration rates, which are only marginally offset by the weak canopy resistance. This applies to windy conditions. Our experience with working in the reed-bed community on hot days was that the conditions were often windless. Under such conditions the aerodynamic resistance would be high (low convective fluxes) and evapotranspiration reduced.

The dominant control on evapotranspiration rates was available energy, with a weak surface/vegetative resistance shown by a canopy resistance of < 50 s m^{-1}. On the elevated sand banks dominated by reeds, the water supply was therefore not limiting evapotranspiration until the end of the long dry winter period, when the plants would lose contact with the water table. In the braided stream channels, dominated by large trees it would appear that water supply was seldom, if ever limiting evapotranspiration. The conservative water use by the trees was therefore puzzling, as the trees were subjected to very high evaporative demands and were freely supplied with water.

There was little evidence in our data to suggest that advection significantly increased evapotranspiration through the movement of warmer, drier air flowing across the site from the drier surrounding areas. Thus the highest evapotranspiration rates recorded for the reeds (approximately 9.5 mm day^{-1}), were likely to be the maximum evapotranspiration rates for this community, given that measurements were conducted at times of the year that included annual maximum solar and net all-wave radiation (December). These evapotranspiration rates were similar to maximum rates recorded for sugar cane (8.6 mm day^{-1}), *Acacia mearnsii* (8.2 mm day^{-1}) and *Eucalyptus* trees (8.5 mm day^{-1}) (Burger, Everson and Savage 1999). The highest rates of evapotranspiration for the trees (approximately 4.5 mm day^{-1}) were recorded in mid-October and may not represent the highest rates possible, as full summer radiative conditions were not yet experienced. However, the average evapotranspiration rates in summer were likely to be reduced by the frequent occurrence of rainy and cloudy conditions.

During winter and spring the soil heat flux at the reed site served as a heat sink for approximately 20% of the net all wave radiation. This dropped to 10% in summer when there was increased shading from the full canopy. The contribution of the soil heat flux to reducing the available energy was therefore significant, and must be accounted for in models that use the energy balance approach.

Evapotranspiration from the reeds was strongly seasonal and varied from year to year. Therefore, it cannot be assumed that evapotranspiration rates have a consistent seasonal pattern of increase and decrease from year to year or that the magnitude of evapotranspiration for any given period is the same each year.

The micrometeorological measurements at the reed and forest sites showed the feasibility, and at the same time the difficulty in obtaining accurate measurements of evapotranspiration from these sites on the Sabie River. The limited area of the individual communities was the biggest constraint to applying conventional micrometeorological techniques. Fortunately, it was possible to find patches of the two most common cover classes (reeds and trees) that were sufficiently large in area to enable the development of accurate estimation of evapotranspiration. The Bowen ratio energy balance method worked reasonably well when evapotranspiration fluxes were fairly large, for example during the day over the reed community. The method had limitations when latent heat fluxes were low and humidity gradients small, as was often the case above the tall tree canopy.

The use of the eddy correlation technique was hampered by technical problems, which were exacerbated by the difficult access through the river channels. This was the first time that this technique had been attempted for routine monitoring in South Africa and many lessons were learnt. The loss of this equipment in the flood prevented the final testing of the equipment. The flood did, however, present the opportunity to invest in new equipment and new designs; such as the open path water vapour sensor, which will greatly facilitate the field use of this technically demanding technique. Further advances in science have led to the development of laser-based sensors (scintillometry), which have the ability to measure evapotranspiration from relatively small patches of vegetation over a set path, negating the need to be in the centre of the river. Such methodologies are expensive in terms of capital outlay (hundreds of thousands of Rands), but because of their efficiency (ease of setup, data analysis and maintenance costs) should be cheaper to operate than for example the eddy correlation technique, which would require access to the center of the river and will always be constrained by fetch limitations. The two techniques used in Phase I (Stem steady state heat energy balance and Heat Pulse Velocity techniques) are much cheaper (tens of thousands), but have limitations when applied to complex natural systems with many species, often with multi-stems, as found in the KNP. In addition, scaling-up from individual plants to whole canopies is problematic, leading to large errors. Perhaps more seriously, some of the theoretical assumptions of the HPV technique are unrealistic (a full description of these techniques can be found in Savage *et al.* 2000). Scintillometry therefore provides the way forward for quantifying the water use of riparian vegetation.

This study emphasized the complex interactions that underlie the evapotranspiration process, and highlighted the importance of using models that are able to account for these complex physical processes. The reed model developed in phase I of this project was shown to be an unrealistic predictor of reed evapotranspiration and should not be used for future predictions. In terms of modelling the latent heat flux in the Sabie River and other similar environments, either the Priestley-Taylor or Penman-Monteith methods yield the best results. The inclusion of seasonal specific canopy resistances and modelled available energy from relationships determined by this study, provides a model that yields excellent results yet is simple to use.

The results of the vegetation cover analysis showed that the forests (38%) and reeds (22%) were the dominant vegetation types accounting for 60 % of the area. Open water, rock and sand accounted for a further 28%. These data were used to scale up the evapotranspiration data for a 55 km section of the Sabie between the Kruger and Lower Sabie weirs. Comparisons of the total evaporation losses during the low flow period (0.32 $m^3 s^{-1}$) and gauging losses (0.35 $m^3 s^{-1}$) showed good agreement, and added validity to the evapotranspiration data. (3)

7.2 Linkages to river management

A great deal of effort and expense has been spent on obtaining an accurate estimate of the water use of the riparian vegetation in the Kruger National Park. The question arises as to how useful these data are and how they may best be put to good use? Clearly the objective of verification of the transpiration rates from the reeds has been met and the original reed model was shown to be an unrealistic description of the evapotranspiration processes within the reed community. The original conservative rates of transpiration from the trees were verified by this study, although the physiological reasons and physical processes remain an enigma.

In this study a more physically and universally accepted modelling approach was taken in comparison with the empirical approach of phase I. The canopy specific models for the reeds and trees were developed through an understanding of the energy balance of each community and its relationship to the well-known Penman-Monteith model. This will provide modellers with a more accurate approach to the calculation of the water requirements of similar riparian vegetation in southern Africa.

A major strategy of the Kruger National Parks Rivers Research Programme has been to "develop a consultative management process in which interactions between stakeholders, managers and researchers is facilitated by a Decision Support System" (Rogers and Bestbier 1997). A considerable effort has gone into developing a predictive modelling framework for understanding the consequences of management actions and system changes in general. It is within this framework that predictive tools such as hydrological models are required for linking into such Decision Support Systems. It is true to say that most of the vegetation dynamics of riparian forests are in some way linked to the hydrological cycle. In a system such as the Sabie River in the KNP most of the streamflow originates outside the Park in the high rainfall areas to the west. Evapotranspiration in the KNP is by far the most important loss of water from the soil and ground water reserves. In order to understand the links between vegetation dynamics and the hydrology of the river a basic understanding of the evaporative losses from the system is required. The National Water Act recognizes the need to provide water to ecologically sensitive areas through the recognition of the "ecological reserve" (White paper 1997). The law states "the ecological reserve must be determined for all or part of any significant water resources such as rivers, streams, wetlands, lakes, estuaries and groundwater". The Reserve must specify the quantity and quality of the water, which will maintain the resource in an ecologically healthy condition. This requirement of the National Water Act demands the accurate determination of the Reserve. This can only be achieved through an understanding of the hydrological and ecological links in riparian systems. Therefore rivers running through a broad landscape must be linked at the catchment scale. Catchment management provides a framework for integrating knowledge and perspectives of social and natural sciences into planning, policy and decision-making. Such an interdisciplinary framework is required to simultaneously address the socio-economic and environmental impacts of natural resource policy and management. While knowledge about the interactions between the biophysical processes and socio-economic issues in a watershed is essential for the long-term sustainability of both agricultural and natural systems, the mere generation of such knowledge is insufficient (Fulcher *et al.*, in press). The knowledge must be delivered to potential users or stakeholders in a way that maximizes its usefulness in catchment planning and management.

Long term ecological sustainability through the identification and setting of the ecological reserve can only be achieved by (i) increasing knowledge regarding the spatial and temporal interactions of ecological and hydrological processes within catchments and determining how these interactions are altered by changing land use or management practices at the catchment scale and (ii) developing decision support systems which make the knowledge accessible.

While integrated management is widely supported, the spatial information on socio-economic and bio-geophysical processes needed for comprehensive evaluation of integrated resource management plans is not readily accessible to local decision makers. Thus the challenge for ecologists, hydrologists and economists is to develop a user-friendly, interactive catchment management decision support system which identifies the relative contribution of sub-catchment areas to alternative land use activities and practices on water quantity, soil erosion, surface water quality and economics at the catchment scale. Future research in integrated catchment management should focus on the research and development of spatially explicit models (i.e. GIS based), which are capable of simulating the ecological and hydrological processes at the catchment scale for use as decision support systems for catchment planners, managers and stakeholders.

"Linkages" of this project to other projects/issues can be summarised as follows:

- Replacement of the transpiration component of the riparian water balance model developed by Birkhead *et al.* (1997) with canopy specific Penman-Monteith formulations.
- The extension/improvement of the results to other South African river systems where evaporation losses are considered important. An example is the Evaporation Losses from South African rivers study (McKenzie and Craig, 1999), where insufficient knowledge was available at the time to model reed evaporation along the Orange River, forcing the authors to assume that reed evapotranspiration was equal to open water evaporation.
- Determination of the ecological reserve: The KNPRRP was initiated to established the ecological water requirements of the rivers running through the KNP, so that they may be given due consideration in the planning and management of future resource developments. In a situation of competition between various sectors for a limited water resource, it is important for environmental requirements to be reliably established if equitable allocations are to be made. The procedures developed in this study will improve the basis for determining the consumptive water use of riparian vegetation.
- Integrated Catchment Management: Water resources development and management require an understanding of basic hydrologic processes and simulation at the catchment scale (thousands to tens of thousands of square kilometres). Recent advances in computer hardware and software and GIS/spatial analysis software have allowed large area simulation to become feasible. The information on the evapotranspiration of the dominant indigenous vegetation collected in this study will ultimately provide modellers with important inputs and data for the verification of these models.

The implementation of the above points falls outside the scope of this project and should be considered for future research. It is recommended that a workshop be held (outside the scope of this project), on how to further interpret the research results in terms of the "ecological reserve", by bringing all the results on the impact of the water use of vegetation together, and by developing a link to the operational management of rivers.

7.3 Conclusions

Anthropogenic changes upstream of the KNP have resulted in reduced winter base flows and concomitant increased stress levels amongst the natural river biota within the KNP. Effective management of these systems has been identified as an urgent priority in order to ensure the viability of these riverine systems (Birkhead *et al.* 1997). Birkhead *et al.* used an integrated research approach to determine the ecological reserve, but uncertainty in the reliability of the transpiration models for the trees and reeds led to recommendations for the verification of these models. The main objective of this project, the verification of previous transpiration measurements from reeds and trees in the Sabie River, was achieved using the Bowen ratio energy balance technique. The results have shown that the previously high reed evapotranspiration rates were unfounded. The canopy specific models developed in this study should rather be used to model the consumptive water use of the vegetation.

Evapotranspiration from the tree site was consistent with the previous research (phase I) where conservative tree evapotranspiration rates were found. However, the absolute daily evapotranspiration rates measured in this study (3.2 mm day^{-1}) exceeded that of the previous study (1.7 mm day^{-1}). Although the phase I model could be used for estimating transpiration, for consistency of approach and improved accuracy the site specific Penman–Monteith model should be adopted in the Riparian Water Balance Model.

Canopy specific models for the reeds and trees have been developed through an understanding of the energy balance of each community and its relationship to the well-known Penman-Monteith approach, providing a more accurate calculation of the water requirements of similar riparian vegetation in southern Africa. These canopy specific models, together with local climatic data and the area covered by each vegetation type, can be used to estimate the consumptive water use of similar riparian vegetation for any stretch of river.

Verification of the evapotranspiration estimates of this study was achieved by comparing the Bowen ratio estimates with transmission losses estimated through gauging studies. The gauging data were consistent with the evapotranspiration data collected in this project, confirming the validity of the evapotranspiration data.

REFERENCES

Baldocchi D and Meyers T (1998) On using eco-physiological, micrometeorological and biogeochemical theory to evaluate carbon dioxide, water vapor and trace gas fluxes over vegetation: a perspective *Agricultural and Forest Meteorology* 90 1-25

Bartholic JF Namken LN and Wiegand CL (1972) Aerial thermal scanner to determine temperatures of soils and of crop canopies differing in water stress *Agronomy Journal* 64 603-608

Birkhead AL Olbrich BW James CS and Rogers KH (1997) Developing an integrated approach to predicting water use of riparian vegetation *Water Research Commission Report No. K5/474/0/1.*

Bowen IS (1926) The ratio of heat losses by conduction and by evaporation from any water surface *Phys Rev* 27 779-787.

Bredenkamp GJ and Van Rooyen N (1991) A survey of the riparian vegetation of the Sabie River in the Kruger National Park *Ecotrust Pretoria South Africa.*

Broadhurst LJ Heritage GL van Niekerk, AW James CS and Rogers KH (1997) Translating hydrological output into local hydraulic conditions on the Sabie River, Kruger National Park *Water Research Commission Report* No. 474/2/96 volume 2 Water research commission, South Africa

Burger C Everson CS Savage MJ (1999) Comparative evaporation measurements above commercial forestry and sugarcane canopies in the Kwazulu-Natal midlands *Proceedings of Ninth South African National Hydrology Symposium 29-30 November 1999.*

Calder IR (1977) A model of transpiration and interception loss from spruce forest in Plynlimon, Central Wales *J Hydrol* 33 247-265.

Campbell GS (undated) On-line measurement of potential evapotranspiration with the Campbell Scientific automated weather station, *Application note by Campbell Scientific Inc.*, Department of Crop and Soil Sciences, Washington State University.

Everson CS (1995) Measurement of transpiration using Bowen ratio technology from plantation canopy surfaces, grassland, wheat and maize in the Natal midlands *CSIR Report no. FOR-DEA-924* 28 pp.

Fulcher C Prato T and Barnett Y (in press) Economic and environmental impact assessment using WAMADSS.

Gertenbach, WPD (1985) Beplanning van Waterbehoeftes van die NKW uit die Sabie Rivier. Internal Report No. NK/44.

Heritage GL van Niekerk AW and Moon BP (1995) Classifying bedrock influenced semi-arid river systems: extending the continuum concept *Proc. Int. Ass. Of Geomorphologists South East Asia Conf. On Geomorphology: Abstracts* June 1995 Singapore.

Kaimal JC and Businger JA (1963) A continuous wave sonic anemometer-thermometer *J. Appl. Meteorol.* 2 156-164.

Kaimal JC and Gaynor JE (1991) Another look at sonic anemometry *Boundary-Layer Meteorol.* 56 401-410.

Linacre ET (1976) Swamps p. 329-350 *In* Monteith JL (ed) Vegetation and the atmosphere, Volume 2 Case studies *Academic Press, Bristol, England.*

Mackenzie JA van Coller AL and Rogers KH (1999) Rule based modelling for management of riparian systems *WRC Report NO 813/1/99.*

McGlinchey MG and Inman-Bamber NG (1996) Predicting sugarcane water use with the Penman-Monteith equation *Evaporation and Irrigation Scheduling Proceedings of the International conference* Camp CR Sadler EJ and Yoder RE (Eds.) 592-598.

McKenzie RS and Craig AR (1999) Evaporation losses from South African rivers *WRC Report NO 638/1/99.*

Monteith JL (1973) Principles of environmental physics *Edward Arnold, London* 241 pp.

Monteith JL (1976) Vegetation and the Atmosphere *Volume II Case Studies Academic Press, London* 439 pp.

Monteith JL and Unsworth MH (1990) Principles of Environmental Physics 2nd ed. London Edward Arnold 291 pp.

Price JS (1994) Annual variability in summer evapotranspiration and water balance at a subarctic forest site *Nordic Hydrology* 25 331-334.

Rogers KH and Bestbier R (1997) Development of a protocol for the definition of the desired state of riverine systems in South Africa *Department of Environmental Affairs and Tourism, Pretoria South Africa.* Available at http://www.ccwr.ac.za/knprrp/index.html

Rosenberg NJ Blad BL and Verma SB (1983) MICROCLIMATE The Biological Environment 2nd ed. New York Wiley 495 pp.

Savage MJ Graham AND and Lightbody KE (2000) An investigation of the stem steady state heat energy balance technique in determining water use by trees *WRC Report NO 348/1/00.*

Slabbers PJ (1977) Surface roughness of crops and potential evapotranspiration *J Hydrol* 34 181-191 (Cited by Rosenberg *et al.*, 1993).

Stull RB (1988) An Introduction to Boundary Layer Meteorology Dordrecht Kluwer, 666 pp.

Unland HE Altaf M Harlow C Housse PR Garatuza-Payan J Scott P Sen OL and Schuttleworth WJ (1998) Evaporation from a riparian system in a semi-arid environment. Hydrol. Process. 12 527-542.

White paper on a national water policy for South Africa April 1997 *Department of Water Affairs and Forestry Pretoria South Africa.*

DATA STORAGE AND AVAILABILITY

1. NATURE OF THE DATA

The following data was captured in the execution of the project to determine the water use by reeds and trees in riparian environments.

1.1 Bowen ratio energy balance, eddy correlation and infra red thermometry data

The Bowen ratio energy balance data comprises both a complete set of weather station data together with the net radiation, temperature and humidity flux data necessary for the calculation of the latent heat flux of evaporation. This includes the soil heat flux density.

Bowen ratio evaporation is calculated from sampling conducted at 20 minute intervals. The raw data collected from the field is passed through several computational and rejection phases to provide a final spread sheet of 20 minute evaporation data.

These data records are stored, together with all site header data, in Excel worksheets as 20 minute, hourly and daily site evaporation.

Raw and processed data collected with the eddy correlation and infra red thermometry technique, are available for 20 minute periods.

2. STORAGE OF DATA

2.1 Processed data

All processed data has been catalogued and stored at Environmentek, CSIR, c/o Department of Agrometerorology, UNP, P/Bag X01, Scottsville, 3209.

2.2 Raw data

Raw data and data in various stages of compilation, has been stored as:
Bowen ratio, Eddy correlation and Infra-red thermometer data: Environmentek, CSIR, c/o Department of Agrometerorology, UNP, P/Bag X01, Scottsville, 3209. Contact persons: Dr. C.S. Everson, C. Jarmain and M.G. Gush.

These data are held on non-flexible diskette.

3. AVAILABILITY OF DATA

All data can be supplied to researchers and managers on non-flexible diskette. Data is the property of the Water Research Commission. Copies of the data have also been sent to the CCWR (Computing Centre for Water Research, %

University of Natal, Private Bag X1, Scottsville 3209 RSA) and the Kruger National Park Meta Database.

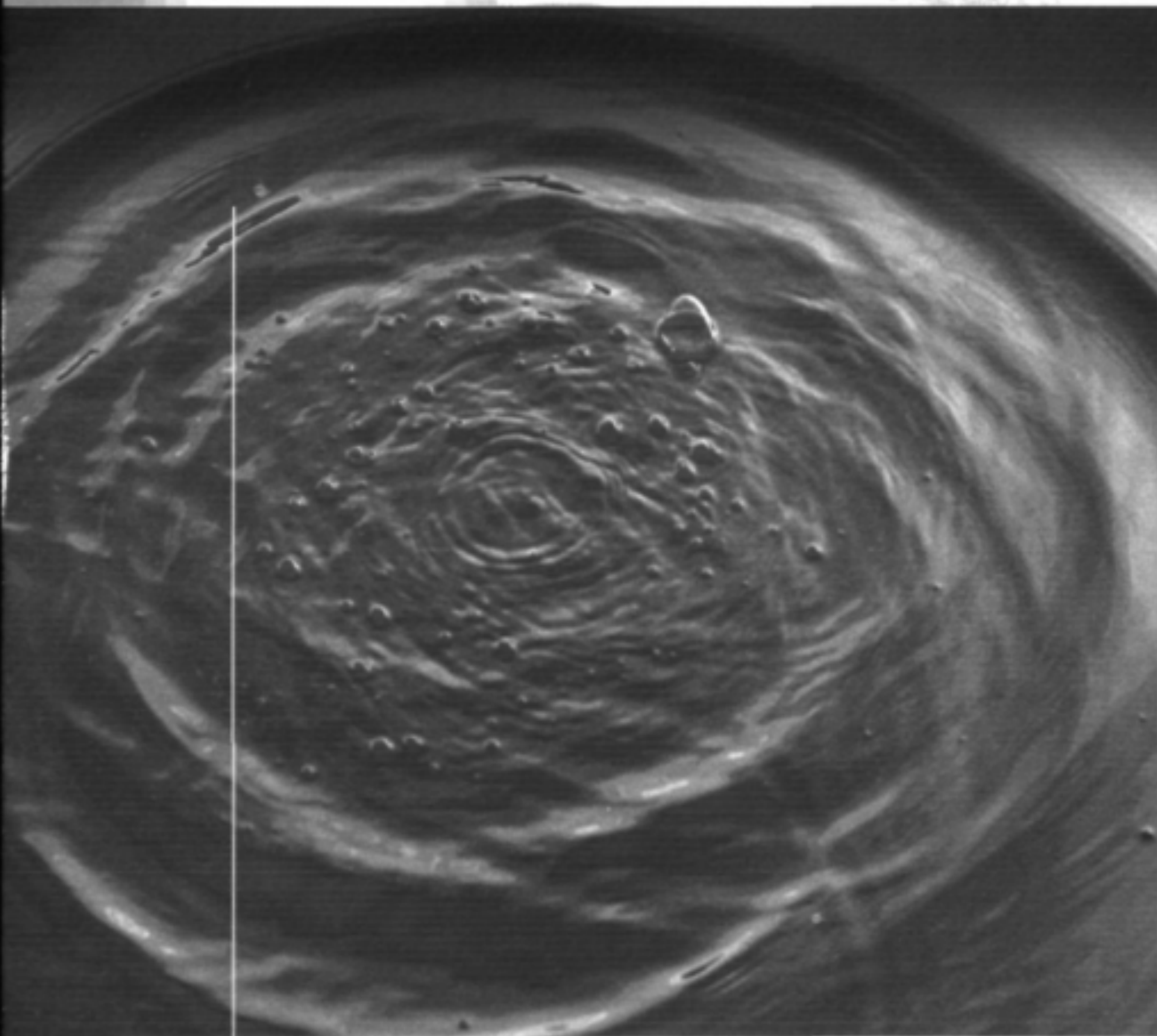

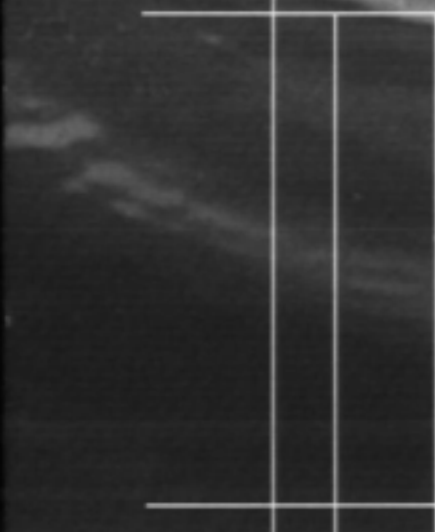

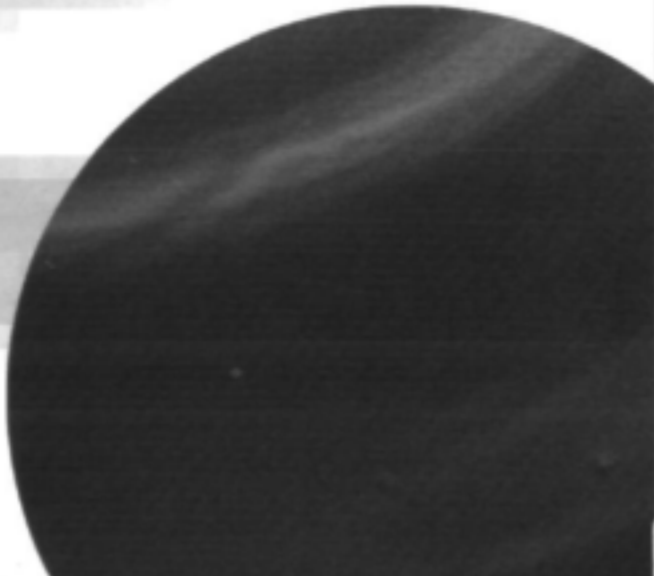

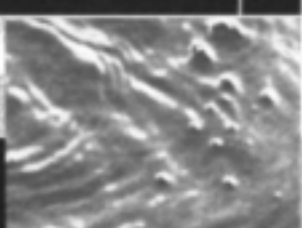

Water Research Commission
PO Box 824, Pretoria, 0001, South Africa
Tel: +27 12 330 0340, Fax: +27 12 331 2565
Web: http://www.wrc.org.za

1868457818